C51.17/12:990/2

Tech Notes

February 1990

PB90-925902

PENNSYLVANIA STATE UNIVERSITY
FEB 21 1990
DOCUMENTS COLLECTION
U.S. Depository Copy

Technology fact sheets from Federal laboratories

NTIS

U.S. DEPARTMENT OF COMMERCE
National Technical Information Service
Center for the Utilization of Federal Technology

The Complete Guide to U.S. and State Government Business Help

For New and Growing Businesses

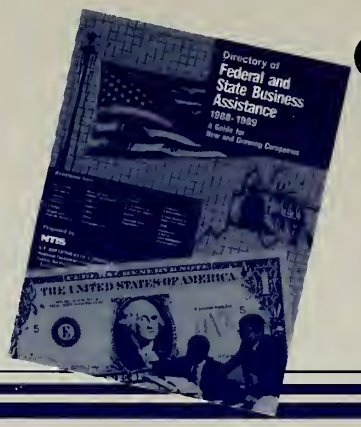

SECOND BIG EDITION!

Directory of Federal & State Business Assistance– A Guide for New and Growing Companies.

Your guide to sources of financing, technical information, planning and management know-how, procurement, and marketing assistance. Order this book today!

Describes 180 Federal and more than 500 State Programs

You get the information you need to directly contact hundreds of Federal and State sources of business assistance:

- Full summary of services offered
- Telephone number
- Mailing address
- Eligibility requirements (if any)

Take advantage of these programs designed to help U.S. businesses compete effectively in domestic and international markets.

Some of the programs listed:

Dept. of Commerce Export Licensing

Bureau of Labor Statistics Prices and Living Conditions Office

Federal Grant Data Center

Small Business Answer Desk

Florida Product Innovation Center

Iowa Small Business Loan Program

Michigan Biotechnology Institute

New York Direct Loan Program

You'll learn:

- How to get funding for your company's R&D
- Which states provide venture money
- How to take advantage of free export assistance
- What Federal and State contacts offer free management and procurement consulting
- Where to get mail lists of potential overseas business buyers
- Where to find evaluation of energy-related inventions or engineering help
- How to get help in selecting a site for your manufacturing plant
- Where to find customized economic impact statistics

and much more.

Federal Offices Want to Work with You

The 180 Federal entries selected for inclusion are arranged by agency. Discover sources of help in exporting, patent licensing, procurement, locating wage information, obtaining loan guarantees, finding marketing information, plus much more. A handy index lets you quickly locate just the Federal resources you need.

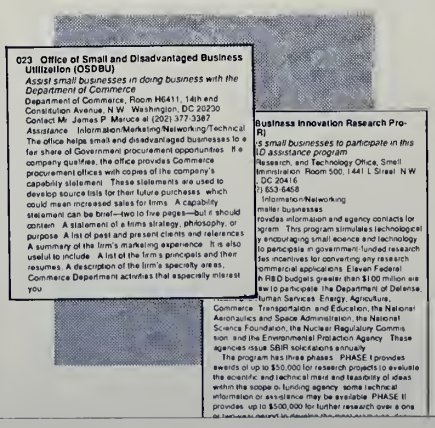
023 Office of Small and Disadvantaged Business Utilization (OSDBU)
Assist small businesses in doing business with the Department of Commerce
Department of Commerce, Room H6411, 14th and Constitution Avenue, N.W., Washington, DC 20230
Contact: Mr. James P. Maruca at (202) 377-3387
Assistance: Information/Marketing/Networking/Technical
The office helps small and disadvantaged businesses to a fair share of Government procurement opportunities. It e... company qualifies, the office provides Commerce procurement offices with copies of the company's capability statement. These statements are used to develop source lists for their future purchases, which could mean increased sales for firms. A capability statement can be brief—two to five pages—but it should contain: A statement of a firm's strategy, philosophy, or purpose. A list of past and present clients and references. A summary of the firm's marketing experience. It is also useful to include: A list of the firm's principals and their resumes. A description of the firm's specialty areas, Commerce Department activities that especially interest you.

Business Innovation Research Pro... (R)
...s small businesses to participate in this ...D assistance program
...Research, and Technology Office, Small ...inistration, Room 500, 1441 L Street N.W. ..., DC 20416 ...) 653-6458
...Information/Networking
...maller businesses
...rovides information and agency contacts for ...gram. This program stimulates technological ...y encouraging small science and technology ...to participate in government-funded research ...ties incentives for converting any research ...ommercial applications. Eleven Federal ...h R&D budgets greater than $100 million are ...ire to participate: the Department of Defense, ...Human Services, Energy, Agriculture, Commerce, Transportation, and Education, the National Aeronautics and Space Administration, the National Science Foundation, the Nuclear Regulatory Commission, and the Environmental Protection Agency. These agencies issue SBIR solicitations annually.
The program has three phases. PHASE I provides awards of up to $50,000 for research projects to evaluate the scientific and technical merit and feasibility of ideas within the scope o... funding agency. some technical information or assistance may be available. PHASE II provides up to $500,000 for further research over a one ...

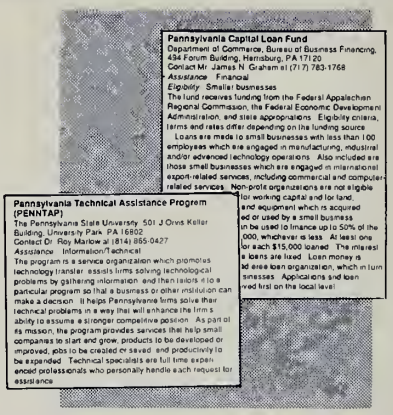
Pennsylvania Capital Loan Fund
Department of Commerce, Bureau of Business Financing, 484 Forum Building, Harrisburg, PA 17120
Contact: Mr. James N. Graham at (717) 783-1768
Assistance: Financial
Eligibility: Smaller businesses
The fund receives funding from the Federal Appalachian Regional Commission, the Federal Economic Development Administration, and state appropriations. Eligibility criteria, terms and rates differ depending on the funding source.
Loans are made to small businesses with less than 100 employees which are engaged in manufacturing, industrial and/or advanced technology operations. Also included are those small businesses which are engaged in international export-related services, including commercial and computer-related services. Non-profit organizations are not eligible...
...for working capital and for land, ...and equipment which is acquired ...ed or used by a small business ...n be used to finance up to 50% of the ...000, whichever is less. At least one ...or each $15,000 loaned. The interest ...e loans are fixed. Loan money is ...ed area loan organization, which in turn ...sinesses. Applications and loan ...ved first on the local level.

Pennsylvania Technical Assistance Program (PENNTAP)
The Pennsylvania State University, 501 J. Orvis Keller Building, University Park, PA 16802
Contact: Dr. Roy Marlow at (814) 865-0427
Assistance: Information/Technical
The program is a service organization which promotes technology transfer, assists firms solving technological problems by gathering information and then tailors it to a particular program so that a business or other institution can make a decision. It helps Pennsylvania firms solve their technical problems in a way that will enhance the firm's ability to assume a stronger competitive position. As part of its mission, the program provides services that help small companies to start and grow, products to be developed or improved, jobs to be created or saved, and productivity to be expanded. Technical specialists are full time, experienced professionals who personally handle each request for assistance.

States Want to Assist Your Business

States know that strong businesses mean a strong economy. Services described include venture financing, planning help, product marketing, employee training, exporting assistance, site location, technology development, and technical and management information.

Every effort has been taken to make this Directory a valuable working resource to assist the growth of your company.

TO ORDER:

ASK FOR the ***Directory of Federal & State Business Assistance – A Guide for New and Growing Companies.*** (180 pp. ISBN 0-934213-10-0). Reference order number PB88-101977/ABH. The price is $29 plus $3 for handling.

CALL (703) 487-4650 and use your American Express, VISA, MasterCard, or NTIS deposit account.

Or send a check payable to the

National Technical Information Service
U.S. DEPARTMENT OF COMMERCE
Springfield, VA 22161.

Tech Notes

Highlighting Selected U.S. Government Technology & Resources

February 1990

Contents

Agriculture & Food 116
Computers 121
Electrotechnology 129
Energy 143
Engineering 146
Environmental Science & Technology 169
Manufacturing, Machinery & Tools 170
Materials 182
Medicine & Biology 191
Natural Resources Technology & Engineering 199
Physical Sciences 201
Transportation & Components 211

Published monthly by the National Technical Information Service (NTIS), Tech Notes bring together individual one- to two-page fact sheets prepared by Federal agencies, their laboratories, or contractors. These fact sheets highlight current Federal technology determined to have commercial or practical application. Topics cover new processes, materials, techniques, software, instrumentation, and resources.

Some of the current sources are the Department of the Navy, Department of the Army, NASA, Department of Energy, Environmental Protection Agency, Department of the Interior, and the Department of Agriculture.

Special assistance is provided by the Federal Laboratory Consortium.

Change of address or questions concerning subscriptions should be sent to:
Subscriptions Department
National Technical Information Service
Springfield, VA 22161
(703) 487-4630

Suggestions, comments, or questions concerning Tech Notes should be directed to:
Tech Notes Editor
Room 300B F
National Technical Information Service
Springfield, VA 22161
(703) 487-4805

How to Use Tech Notes

Every Tech Notes fact sheet lists a source for additional information. The source of this information may be a special support package from the originating agency, a personal contact, a licensing opportunity, or a backup report available from NTIS.

Each fact sheet also is perforated to allow for easy removal for those subscribers who may wish to keep a special fact sheet file or route to others in their organization

Sources of Further Backup Information

Below are two representative examples of how each Tech Note fact sheet provides you with a source of further information. In most cases, this information is provided directly by the agency or its laboratory.

However, there are cases where NTIS is the source for backup documentation. In these cases, use the order form at the end.

Examples:

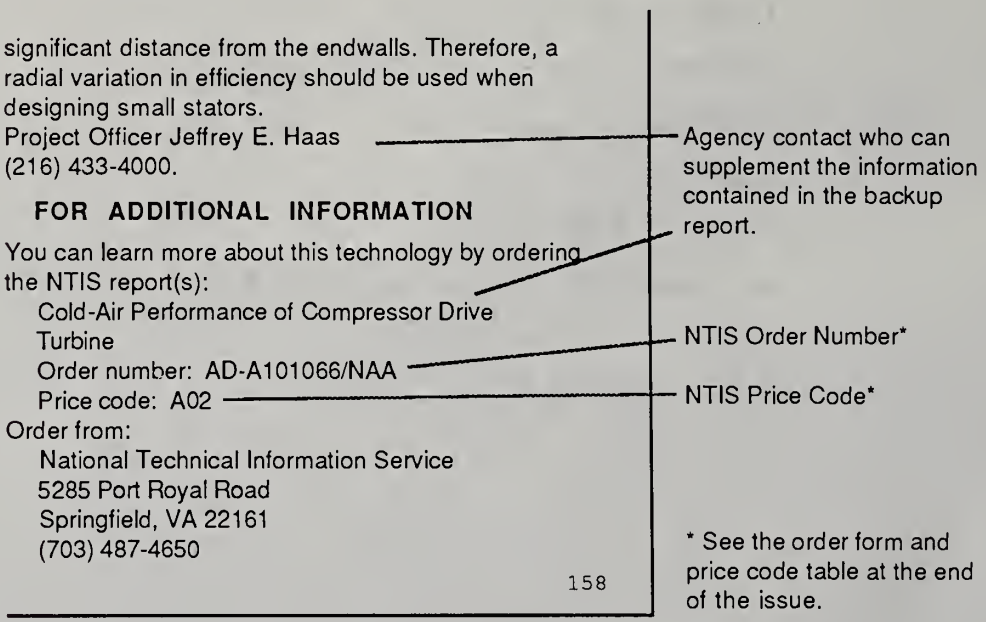
significant distance from the endwalls. Therefore, a radial variation in efficiency should be used when designing small stators.
Project Officer Jeffrey E. Haas
(216) 433-4000.
FOR ADDITIONAL INFORMATION
You can learn more about this technology by ordering the NTIS report(s):
Cold-Air Performance of Compressor Drive Turbine
Order number: AD-A101066/NAA
Price code: A02
Order from:
National Technical Information Service
5285 Port Royal Road
Springfield, VA 22161
(703) 487-4650
158
Agency contact who can supplement the information contained in the backup report.
NTIS Order Number*
NTIS Price Code*
* See the order form and price code table at the end of the issue.

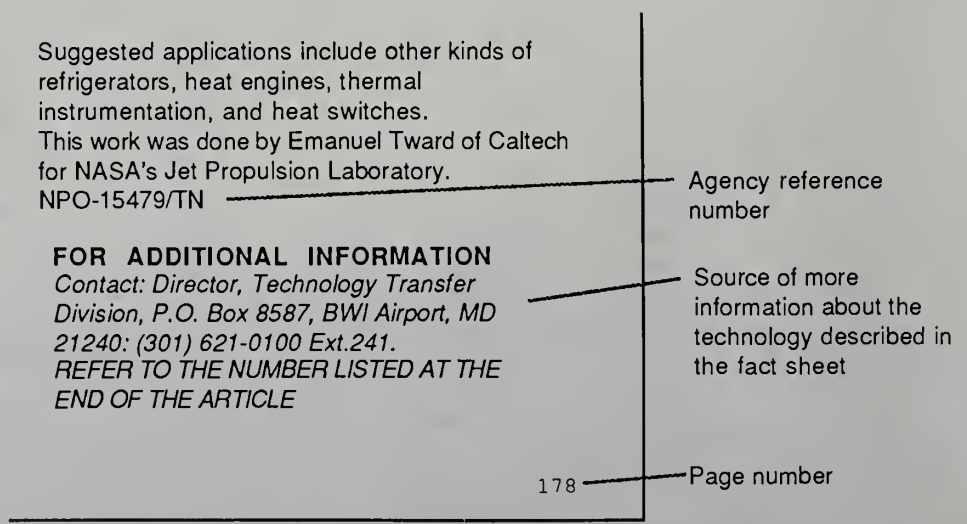
Suggested applications include other kinds of refrigerators, heat engines, thermal instrumentation, and heat switches.
This work was done by Emanuel Tward of Caltech for NASA's Jet Propulsion Laboratory.
NPO-15479/TN
FOR ADDITIONAL INFORMATION
Contact: Director, Technology Transfer Division, P.O. Box 8587, BWI Airport, MD 21240: (301) 621-0100 Ext.241.
REFER TO THE NUMBER LISTED AT THE END OF THE ARTICLE
178
Agency reference number
Source of more information about the technology described in the fact sheet
Page number

Tech Notes Title List for February 1990

Agriculture & Food

0116 Genes Blasted into Cells

0117 Kenaf Tops Equal High-Quality Hay

0118 Mechanical Fruit Harvester (Licensing Opportunity)

0119 Less Pickleworm Pesticide

Testing & Instrumentation

0120 New Material Will Help Gauge Cholesterol in Eggs

Computers

0121 Data Acquisition & Reduction Processor System

0122 Heterojunction-Diode Transistor EBS (Electron-Beam Semiconductor) Amplifier (Licensing Opportunity)

0123 Dynamic Transfers of Tasks Among Computers—An allocation scheme would give jobs to idle computers. (Licensing Opportunity)

0124 Network-Control Algorithm—Channels are allocated optimally to links in a multilink, multinode network.

Software

0125 Transportable Instructional Support System

0126 Simulating Scenes in Outer Space—Scientifically accurate simulations are generated quickly.

Testing & Instrumentation

0127 Device for Inspection of Materials by Eddy Current (Licensing Opportunity)

0128 Method of Measuring Magnetic Effects Due to Eddy Currents (Licensing Opportunity)

Electrotechnology

0129 Digital 8-DPSK Modem for Trellis-Coded Communication—Signal-processing elements are realized largely in software.

0130 Exciter for X-Band Transmitter and Receiver—Design and performance are described.

0131 Eye-Safe Lidar—Experimental solid-state systems may find use in meteorology.

0132 Integrated Semiconductor/Optical Information Processors—Optical, electro-optical, and electronic devices would be integrated into three-dimensional structures. (Licensing Opportunity)

0133 Making a Circular-Harmonic Filter—An optical image-correlating system is made rotationally invariant.

0134 Healing Voids in Interconnections in Integrated Circuits—A seemingly harsh treatment fills voids (cracks) in aluminum conductors. (Licensing Opportunity)

0135 Multiplying Video Mixer—Transparent or opaque overlays can be put on background images.

0136 Piezoelectrostatic Generator—High voltage is generated by compact, lightweight equipment. (Licensing Opportunity)

0137 Real-Time Optimization of Receiver Bandwidth—Estimates of signal and noise spectra enhance the reception of weak signals.

0138 Reflection Oscillators Containing Series-Resonant Crystals—Transistors operate beyond their normal rated frequencies. (Licensing Opportunity)

0139 Robotic Vision Would Combine Optics and Microwaves—Information on the shapes of objects would be more complete. (Licensing Opportunity)

0140 SEU in an Advanced Bipolar Integrated Circuit—Vulnerability to SEU varies with size and applied current.

0141 Vector Adaptive/Predictive Encoding of Speech—Vector quantization enhances the quality of digitally transmitted speech.

Testing & Instrumentation

0142 Demodulation Circuit for AC Motor Current Signature Analysis (Licensing Opportunity)

Other Items of Interest

0196 Biomedical Telectrodes—Compact transmitters would eliminate the need for wires to monitors.

0208 Digital/Optical Conversion Module (Licensing Opportunity)

Energy

0143 Occupant Evaluation of Commercial Office Lighting

0144 Lightweight Nickel Composite Electrode

0145 Protecting Fuel Cells from Drowning—Water in the fuel is extracted before it reaches the cells.

Engineering

0146 Linear Harmonic Analysis of Free-Piston Stirling Engines

0147 Seven-Effect Absorption Chiller using Three Refrigeration Circuits (Licensing Opportunity)

0148 Reliability Studies for Compressed-Gas-Insulated Apparatus

0149 Sodium Sulfide/Ferrous Sulfate Treatment Process (Licensing Opportunity)

0150 'Standard Crack' Helps Detect Metal Fatigue in Aircraft

0151 Portland Cement Clinker Materials Available

0152 Triple-Effect Absorption Chiller using Two Refrigeration Circuits (Licensing Opportunity)

Engineering (Cont.)

0153 Adaptive Control for Cooperative Dual Robot Arms—Simple control strategies are derived from control strategies for single arms. (Licensing Opportunity)

0154 Analysis of Straight and Wavy Annular Seals—Rotordynamic coefficients are derived. (Licensing Opportunity)

0155 Adherent Thermal Barrier for Combustion Chamber—An unusual fabrication process progresses from the inside outward.

0156 Bearing-Bypass Loading on Bolted Composite Joints—An unexpected interaction between the effects of bypass and bearing loads is reported.

0157 Mathematical Models of Turbulence in Transonic Flow—Predictions of several models are compared with measurements of a well-documented flow.

0158 Mechanical Device Traces Parabolas—Continuous curves are generated and points located with ease.

0159 Ozone/Ultraviolet-Photo-Oxidation Reactor—Hydrazines are precessed more thoroughly into harmless substances.

0160 Numerical Simulation of Turbine Rotor/Stator Interaction—Unsteady effects in flows are studied.

0161 Rapidly-Indexing Incremental-Angle Encoder—The absolute position can be determined after rotation through a small angle.

0162 Silver Ink for Jet Printing—There are no silver particles to foul the printing head.

0163 Tamper-Resistant Secure Disposal Container—A closure device shuts the container when it is tipped on its front, back, or sides.

0164 Using NASTRAN to Analyze Vibrations of Rotor Blades—Nonlinear and linear analyses are combined.

Software

0165 Computing Stress, Stability, and Vibration of Shells—Complicated, branched shells of revolution are analyzed by a finite-difference energy method.

Testing & Instrumentation

0166 Measuring Airflow with Digital Holographic Interferometry—Pressures on surfaces of airfoils are computed from interference fringes.

0167 Diode-Laser Doppler Velocimeter—Features include ruggedness and compactness (Licensing Opportunity)

0168 Multiple-Boundary-Condition Vibration Tests—Experiments build confidence in this emerging technique. (Licensing Opportunity)

Other Items of Interest

0171 New Calibration System Halves Gage Block Errors

0190 Predicting the Propagation of Cracks—Safe operating lives of components of structures can be estimated.

Environmental Science & Technology

0169 High Energy Lithium Battery

Other Items of Interest

0149 Sodium Sulfide/Ferrous Sulfate Treatment Process (Licensing Opportunity)

0153 Adaptive Control for Cooperative Dual Robot Arms—Simple control strategies are derived from control strategies for single arms. (Licensing Opportunity)

0154 Analysis of Straight and Wavy Annular Seals—Rotordynamic coefficients are derived. (Licensing Opportunity)

Manufacturing, Machinery & Tools

0170 Optical Spectral Radiometric/Laser Reflectance System for Weld Pool Surface Temperature Measurement

0171 New Calibration System Halves Gage Block Errors

0172 Arc-Light Reflector for Television Weld Monitoring—Light is spread more evenly over the image area. (Licensing Opportunity)

0173 Expansion Valve with Temperature-Sensitive Flow Regulation—A variable-area orifice adjusts the flow of cryogenic vapor.

0174 Improving a Remote Manipulator—The latest parameters, tools, adaptations, and software are documented.

0175 Intelligent Welding Controller—A control system would adapt to changing design requirements and operating conditions.

0176 Making Internal Molds of Long, Curved Tubes—Mold material is carried to an internal weld joint and removed after an impression is taken.

0177 Making Jointless Dual-Diameter Tubes—Welds between sections that have different diameters are eliminated.

0178 Making Large Composite Vessels Without Autoclaves—Differential thermal expansion provides the requisite pressure.

0179 Robotic Tool for Tightening and Cutting—The tool can be used in the assembly of truss structures.

0180 Roller Bearings Survive Loss of Oil Supply—A ring holds a small emergency supply of oil.

0181 Spray Deflector for Water-Jet Machining—A cheap disk shields expensive parts from erosion. (Licensing Opportunity)

Materials

0182 Examination of the Shot Peening Process

0183 'Next-Generation' Scintillation Material Discovered

0184 Non-Chromate Surface Preparation of Aluminum

0185 Superplastic Forming of Al-Li Alloys

0186 Dynamic Delamination Buckling in Composite Laminates—A finite-element computer program performs a linear buckling analysis at each time step.

0187 Bonding Gauges to Carbon/Carbon Composites—Thermal-expansion properties are modified to prevent bonds from failing. (Licensing Opportunity)

0188 Making Polymeric Microspheres—A combination of advanced techniques yields uniform particles for biomedical applications. (Licensing Opportunity)

0189 Screen-Printed $YBa_2Cu_3O_{7-x}$ Films on Alumina—Superconducting films are made in a relatively simple process.

0190 Predicting the Propagation of Cracks—Safe operating lives of components of structures can be estimated.

Other Items of Interest

0134 Healing Voids in Interconnections in Integrated Circuits—A seemingly harsh treatment fills voids (cracks) in aluminum conductors. (Licensing Opportunity)

0156 Bearing-Bypass Loading on Bolted Composite Joints—An unexpected interaction between the effects of bypass and bearing loads is reported.

0195 Non-Toxic Acids are the Basis for a New Class of Cements

0205 Fluid Properties of Lennard-Jones Mixtures

0209 HRXRP-5 High-Resolution X-Ray Microprobe

Medicine & Biology

0191 Animal Disease Diagnostic and Investigative Laboratory

0192 Animal Resources Diagnostic and Investigative Laboratory

0193 Dexter—A Finger-Spelling Hand

0194 Animal Resource Support for Biomedical Research

0195 Non-Toxic Acids are the Basis for a New Class of Cements

0196 Biomedical Telectrodes—Compact transmitters would eliminate the need for wires to monitors.

0197 Cleaning Animal's Cages with Little Water—Freezing and thawing may save energy and time.

Testing & Instrumentation

0198 Radiolabeling Technique for Early Cancer Detection (Licensing Opportunity)

Other Items of Interest

0120 New Material Will Help Gauge Cholesterol in Eggs

0131 Eye-Safe Lidar—Experimental solid-state systems may find use in meteorology.

Natural Resources Technology & Engineering

0199 Fractal Geometry Harnessed to Aid Mining Petroleum Work

0200 Very-Long-Baseline Interferometry Using Cheap Satellites—Celestial radiation below 25 MHz, heretofore inaccessible, could yield new insights.

Physical Sciences

0201 Algorithm Estimates Microwave Water-Vapor Delay—Accuracy equals or exceeds that of conventional linear algorithms.

0202 Algorithm for Hypersonic Flow in Chemical Equilibrium—An improved shock-capturing scheme is mathematically stable. (Licensing Opportunity)

0203 Hollow-Cathode Source Generates Plasma—Exposure to air and moisture does not degrade performance

0204 Survey of Cooling Techniques—Methods of maintaining electronics at the best operating temperatures are reviewed.

Software

0205 Fluid Properties of Lennard-Jones Mixtures

0206 Gaussian-Beam Laser-Resonator Program—Radii of laser beams are calculated as functions of position.

Testing & Instrumentation

0207 Digital Count Rate Meter with Logarithmic Scale (Licensing Opportunity)

0208 Digital/Optical Conversion Module (Licensing Opportunity)

0209 HRXRP-5 High-Resolution X-Ray Microprobe

0210 Standard Method for Radiation Tests of Liquids—Three vials are used.

Other Items of Interest

0158 Mechanical Device Traces Parabolas—Continuous curves are generated and points located with ease.

0159 Ozone/Ultraviolet-Photo-Oxidation Reactor—Hydrazines are precessed more thoroughly into harmless substances.

Transportation & Components

0211 Digital Video Measurements of Wing Deflections in a Wind Tunnel—Solid-state cameras and a computer-controlled image-acquisition system measure deformations of wind-tunnel models.

Agriculture & Food

0116 Genes Blasted into Cells

0117 Kenaf Tops Equal High-Quality Hay

0118 Mechanical Fruit Harvester (Licensing Opportunity)

0119 Less Pickleworm Pesticide

Testing & Instrumentation

0120 New Material Will Help Gauge Cholesterol in Eggs

Genes Blasted into Cells

Genes carried on tiny pellets that race into plants at nearly 1,000 miles an hour may carry useful new traits to crops of the future. The pellets are metal particles so small that they resemble a fine powder. They're propelled by a gene gun or "bioblaster," biotechnology's new assault weapon on recalcitrant plants that stubbornly refuse to accept new genes.

The resisting plants unfortunately include several of our main food crops—corn, wheat, rice, and other plants that belong to a class called monocots. They are typically immune to tactics that have worked successfully with tomato, tobacco, and other species in the class known as dicots.

The amenable dicots, for example, are readily infected in nature by a bacterium *(Agrobacterium tumefaciens)*. Scientists can manipulate the bacterium so that it carries new genes into the dicots. But the bacterium isn't as helpful with cereal crops because it's generally unable to infect them.

These typically difficult-to-engineer grains are the target of research geneticist Michael E. Fromm and research microbiologist Theodore M. Klein of the Agricultural Research Service/University of California Plant Gene Expression Center in Albany, California.

The researchers estimate that they're only a year or two away from getting corn to accept new genes using the gene gun method. They're using the gun developed in 1983 by Cornell University researchers John C. Sanford, Edward D. Wolf, Nelson K. Allen, and Klein, who was then at Cornell.

The technique Fromm and Klein use is basically the same as that which researchers in some 20 labs throughout the United States, Europe, and Canada are following to genetically engineer target organisms with the bioblaster.

Klein and Fromm start by mixing sample genes with millions of tungsten particles, coating the particles with the genetic material (DNA). That mixture—a dark-grey soup—goes inside a small white plastic cylinder, which in turn is positioned in the path of the gene gun's .22-caliber blank cartridge.

With the push of a button, the gun's electrical firing pin hits the cartridge, setting off the gunpowder. The force of the exploding gunpowder sends the plastic cylinder down the gene gun's barrel and into a steel plate. The plate stops the cylinder, but its contents—the genes and tungsten mixture—escape, shooting out through a small hole in the plate and crashing into the leaf, stems, embryos, or cells waiting in the petri dish below.

A vacuum pump (connected by hose to the gun) sucks air out of the chamber that the particles move through so that they can travel with little resistance, gaining the momentum they must have in order to punch through the tough cell wall and the cell's inner lining (membrane).

The particles are so small that they

JACK DYKINGA

JACK DYKINGA

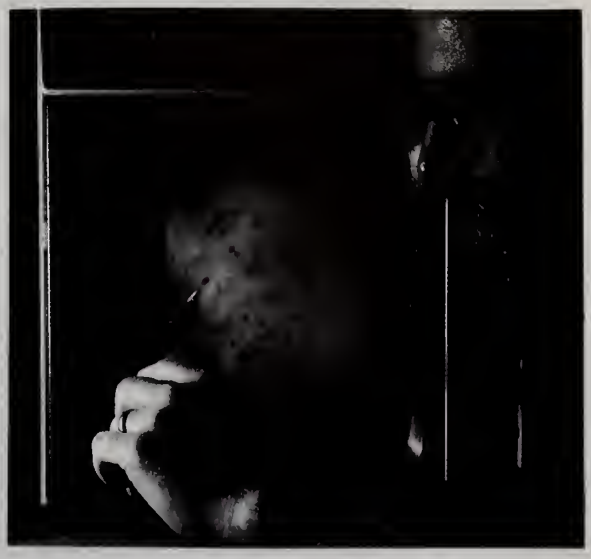

JACK DYKINGA

From left: microbiologist Theodore Klein uses a pipette to place the gene-and-tungsten mixture that will be blasted into plant cells within the gene gun (background). The .22 caliber cartridges are of the type used in standard construction nail guns. Geneticist Michael Fromm examines a projected slide that shows tissue from a kernel of maize after bombardment by gene gun microprojectiles. Red spots represent cells that have taken up the new gene. (K-3090-12) (K-3090-4) (K-3091-2)

need all the velocity they can get. Often they are 10 or more times smaller than the cells they'll pierce.

The process needs fine-tuning, says Klein. For example, although many thousands of cells are penetrated simultaneously—an important time-saver—others may be untouched. And not every cell that is bombarded will accept the gene as part of its own genetic material.

Nevertheless, Fromm predicts that particle bombardment will become "one of the most useful techniques for genetic engineering of plants."

One reason: the technology is unusually versatile. Cornell's Sanford says it has been used successfully to deliver new genes into organisms ranging from yeast to algae to "higher plants" as well as to animal and human cells.

And that list now includes tobacco, a plant often used in laboratory tests. In 1988, Klein and Fromm were the first to use the 45-pound bioblaster to genetically engineer that crop, using sample or "marker" genes. Success in such experiments requires that the healthy, fertile plants growing from bits of bombarded tissue have the new gene or genes actively working inside.

Another good reason for keeping the apparatus in the molecular biologist's arsenal is that mutations, unwanted in some research yet almost unavoidable with many genetic engineering approaches, are infrequent with the bioblaster.

Further, the process uses intact cells. With monocots, it's easier to produce plants from these cells than from protoplasts (cells that have had their outer wall stripped away). Yet some genetic engineering techniques rely on protoplasts.

Electroporation is one example: that process uses an electric current to briefly create a tiny opening in the protoplast's membrane so that genes can enter.

And the microprojectile technique requires only very small amounts of genetic material—a real advantage for most scientists.

Sanford says the particle gun idea came about after his unsuccessful attempts to use lasers to create a cell wall opening genes could slip through. "People kept telling me I should go see Ed Wolf," says Sanford of his co-inventor. A professor of electrical engineering at Cornell, Wolf is best known for his work with particle beams—the kind used for such precision tasks as etching miniature circuits for computers.

It was good advice. Less than a year after Sanford and Wolf first began tossing ideas back and forth, they filed a patent application for the particle bombardment process and gene gun device. They describe the technology as a linking of biology and ballistics, or "biolistics."

Scientists at Agracetus, an agricultural biotechnology company in Madison, Wisconsin, are using a similar approach. The process has "worked with every plant we've tried," says an enthusiastic Winston J. Brill, vice-president for research and development.

Agracetus scientists scored what was apparently a genetic engineering "first" in 1988 when they used the particle bombardment process to transfer genes into soybean plants.

These successes and others have encouraged biotechnologists who are now working to exploit the microprojectile technology. In a very short time biolistics has become one of genetic engineering's most powerful weapons.

Theodore M. Klein and Michael E. Fromm are with the USDA-ARS/UC Berkeley Plant Gene Expression Center, 800 Buchanan Street, Albany, CA 94710 (415) 559-5908. ◆

Gene Transfers With a Bioblaster

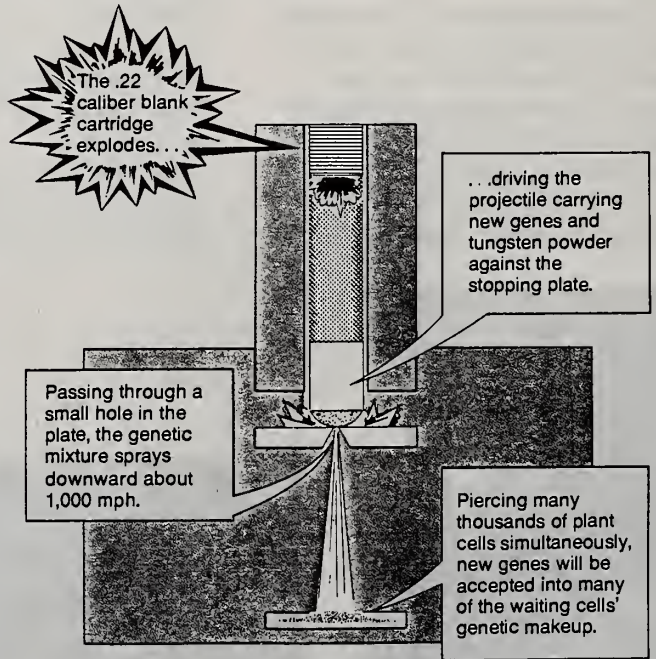
The .22 caliber blank cartridge explodes. . .
. . .driving the projectile carrying new genes and tungsten powder against the stopping plate.
Passing through a small hole in the plate, the genetic mixture sprays downward about 1,000 mph.
Piercing many thousands of plant cells simultaneously, new genes will be accepted into many of the waiting cells' genetic makeup.

Kenaf Tops Equal High-Quality Hay

The same tropical plant that may provide backing for your dining room rug and newsprint for your morning paper could also help grow your dinner steak, scientists say.

The plant is kenaf, or *Hibiscus cannabinus*. It looks like bamboo and is considered an important contender against jute from Southeast Asia as a source of rope and fiber.

It's also being seriously considered as a source of roughage and protein for cattle and sheep. The upper 2 to 3 feet of the plant, normally left to rot in the fields when kenaf is harvested for fiber, can be ground into a feed ingredient with digestibility equal to that of high-quality hay.

Kenaf also has a crude protein content ranging from 15 to 22 percent depending on the part of the plant used.

"We're going to try feeding it to animals as a protein supplement," says William A. Phillips, an animal scientist at ARS' Forage and Livestock Research unit at El Reno, Oklahoma. "We expect a digestibility of 65 to 70 percent, which is very good, about the same as alfalfa." The next question is, will animals eat the stuff?

"We planted about 2 acres of kenaf last May," Phillips says. "We harvested some at 80 days of growth and fed the whole plant to six lambs. They ate the leaves and leaf stems but didn't want to eat the stalks.

"However, if you increased the plant density per acre, the stalks would be smaller. The ideal plant population would be 80,000 to 100,000 plants per

(Photo by David Nance, courtesy of USDA/CSRS)

A prototype harvester cuts mature kenaf in the lower Rio Grande Valley of Texas. It was developed cooperatively by USDA and private industry. (Photo by David Nance, courtesy of USDA/CSRS)

acre, and we only had about 30,000.

Even with only 30,000 plants per acre, Phillips and his fellow researchers collected about 500 pounds of dry matter per acre of kenaf.

"If you're raising kenaf for some other purpose, this would give you another crop to sell," he notes. "The tops could be worth $20 to $30, based on the value of comparable alfalfa hay."

If the whole plant is used as forage, the kenaf producer may be able to get two crops per growing season, Phillips says.

"When you harvest the first time, if you leave 4 or 5 inches of stubble, depending on available moisture you can get a second crop," he says. "Where you cut the first stalk, it usually comes back as more than one plant, and you can harvest again in 60 to 70 days."

"Depending on market prices, it may be more advantageous to harvest kenaf as feed. If we have a kenaf industry develop for fiber, the tops could be harvested for a whole second crop."—

William A. Phillips is in USDA-ARS Forage and Livestock Research, P.O. Box 1199, El Reno, OK 73036 (405) 262-5291. ◆

Mechanical Fruit Harvester

A new invention that mechanically harvests small fruits may reduce a grower's picking costs and improve the quality of the harvest.

This device could also give the processing industry access to the new, thornless blackberries that have been an instant success in the fresh markets.

"Most fruit for fresh-market consumption is now hand-picked," says ARS engineer Donald L. Peterson. "Small-fruit growers face multiple problems in harvesting their crops. Not only is hand labor expensive, but there is no guarantee that qualified laborers will be available when they're critically needed."

To remedy these problems, Peterson, working at the Appalachian Fruit Research Station in Kearneysville, West Virginia, designed a new spiked-drum shaker. The device, attached to a mechanical harvester, shakes the vines just enough to remove the fruit with minimum damage to both fruit and vines.

As the harvester moves between the rows, the drum gently shakes each cane, relieving it of ripened fruit.

The device consists of a stationary frame and oscillating arms that support rod panels. Several flexible nylon spikes, radially spaced at equal angles, extend from the rod panels. In motion, the spikes resemble small Ferris wheels minus the bucket seats. It's the steady swinging of the spikes that seems to be the secret of the shaker's success.

"We can easily position the shaker for most types of trellises that growers use: V-shaped, T-shaped, or conventional vertical-trellis shape," he says. "It has fewer moving parts than other shakers and is effective because it delivers more uniform force and acceleration—ideal for harvesting blackberries."

Mechanical harvesting could help develop a new processing market. To increase harvest efficiency, Peterson is working with horticulturist Fumiomi

Engineer David Peterson watches his spiked-drum shaker as it traverses a row of blackberry bushes at the Appalachian Fruit Research Station, Kearneysville, West Virginia. (K 2949-6)

Takeda to integrate improved growing practices with the ability to machine harvest.

Although this harvester was specifically designed for thornless blackberries, Peterson says he hopes to use it on other crops that grow on prickly vines, such as raspberries, or on blueberries and other small fruits.

ARS introduced the first thornless varieties, Smoothstem and Thornfree, in 1966.

For technical information about this patent, contact Donald L. Peterson, USDA-ARS, Appalachian Fruit Research Station, Rte. 2, Box 45, Kearneysville, WV 25430 (304) 725-3451. Patent application serial No. 07/229,877, "Shaking Mechanism for Fruit Harvesting." ◆

FOR ADDITIONAL INFORMATION: Inquiries concerning rights for commercial use of this invention should be addressed to: Office of Federal Patent Licensing, Center for the Utilization of Federal Technology, Room 304, NTIS, Springfield, VA 22161; (703)487-4738. Refer to Patent Application 07/229,877/TN.

Research Technology
Agricultural Research Service
U.S. Department of Agriculture

Less Pickleworm Pesticide

A box trap and a pheromone synthesized by ARS scientists may help farmers cut their pesticide war on pickleworms almost in half.

A major insect problem, pickleworms follow spring north each year to lay eggs in the 50,000 acres of cucumbers in North and South Carolina. As summer progresses, the insect becomes a problem in states farther north.

The adult pickleworm moths lay eggs in the fields. Larvae hatch and eat their way into young cucumbers.

Growers start spraying their fields with potent pesticides almost every week for the moths' 6- to 7-week season as soon as the nighttime temperature reaches 60°F—the temperature the moths follow north. Whether they actually see any pickleworms or not makes no difference. Once the temperature reaches the critical point, the growers spray.

Why the worm witch hunt? It's because pickle packers will refuse to accept a truckload of cucumbers if they notice even one with a pickleworm hole. (Understandably enough—imagine biting into a pickle and finding...)

FRED WITTE

Pickleworm moth (K-1550-6)

But Agricultural Research Service entomologist Kent D. Elsey of the U.S. Vegetable Laboratory in Charleston, South Carolina, plans to end the blitzkrieg approach to crop protection. Elsey devised a warning system so that farmers need apply pesticides only when there are actually pickleworms in the fields.

A pheromone—a naturally produced scent that attracts—is placed inside 3-foot-square box traps out in the fields. The male moths following the pheromone scent fly into the boxes and become trapped inside.

"Once the adult pickleworm moths start appearing in the traps, it is time to begin spraying" Elsey says.

The pheromone, which moths produce naturally, was synthesized by Jerome A. Klun, of the Chemical Ecology Laboratory at the Beltsville Agricultural Research Center in Beltsville, Maryland.

"It takes very little of the pheromone to bait each trap—just a tiny amount on a bit of rubber about the size of a pencil eraser, and it lasts about a week," Elsey says.

In recent trials, using the traps to monitor for the presence of moths, Elsey was able to control the pickleworm with about half the number of sprayings.

"Some years pickleworms don't appear at all, and in those years growers could avoid any spraying for them if a monitoring system like this were in place," Elsey says.

Some day Elsey envisions a line of traps that extension agents or others could check and then send out appropriate warnings or all clears—kind of an early warning line against pickleworms.

Kent D. Elsey is with the U.S. Vegetable Laboratory, 2875 Savannah Highway, Charleston, SC 29407 (803) 556-0840. ◆

NIST Technology Update

National Institute of Standards & Technology
(Formerly the National Bureau of Standards)
U.S. Department of Commerce, Gaithersburg, MD 20899

New Material Will Help Gauge Cholesterol in Eggs

Researchers involved in studies of cholesterol amounts in eggs and other foods should find a new NIST standard reference material (SRM) helpful. It is a bottled set containing samples of dried whole egg powder certified to have a cholesterol concentration of 19.0 milligrams per gram, plus or minus 0.2 mg/g. Because eggs are significant sources of dietary cholesterol intake, the SRM can help researchers produce accurate data on how much cholesterol is present in egg samples. Laboratories can use the NIST materials to develop cholesterol-measuring methods or to validate existing techniques.

FOR ADDITIONAL INFORMATION: The SRM consists of three capped glass bottles, each containing 8 grams of dried whole egg powder. It is available for $95 from the Office of Standard Reference Materials, NIST, B311 Chemistry Bldg., Gaithersburg, MD. 20899; telephone: (301)975-6776.

Computers

0121 Data Acquisition & Reduction Processor System

0122 Heterojunction-Diode Transistor EBS (Electron-Beam Semiconductor) Amplifier (Licensing Opportunity)

0123 Dynamic Transfers of Tasks Among Computers—An allocation scheme would give jobs to idle computers. (Licensing Opportunity)

0124 Network-Control Algorithm—Channels are allocated optimally to links in a multilink, multinode network.

Software

0125 Transportable Instructional Support System

0126 Simulating Scenes in Outer Space—Scientifically accurate simulations are generated quickly.

Testing & Instrumentation

0127 Device for Inspection of Materials by Eddy Current (Licensing Opportunity)

0128 Method of Measuring Magnetic Effects Due to Eddy Currents (Licensing Opportunity)

U.S. Navy Fact Sheet

Data Acquisition & Reduction Processor System

This technology provides a means of evaluating and debugging computer software (and hardware) through the capture, time-tagging, display, and reduction of parallel data words from multiple asynchronous digital data sources with provisions for irregular sampling rates for the data from each source. Time-tagging allows time correlation of multiple asynchronous data sources over long time periods. Operator selected criteria reduce in real-time the volume of data captured. Developed for use with the Performance monitor Interface (PMI) of the AN/UYK-43 computer. Current implementation limits system to eight 32-bit data sources.

It also can be adapted to any paralleled digital data source (32 bits maximum in current hardware) which accompanies the data with a data sampling clock signal that does not exceed 6.67MHz (limited by current hardware implementation).

Its advantages are that time correlation of data from multiple asynchronous sources. Real-time data quantity reduction. Large data sample storage space (1M words per data input in current implementation). Data captured from one or more sources can control data capture from one or more other sources.

FOR ADDITIONAL INFORMATION: For information on licensing of this subject, contact the Naval Surface Warfare Center, Mr. Ramsey D. Johnson, Code D211, Naval Surface Weapons Center, Silver Spring, MD 20903.

Heterojunction-Diode Transistor EBS (Electron-Beam Semiconductor) Amplifier

The amplifier has been proposed for EBS technology to improve the state-of the art by increasing the current handling capability, extending the frequency of operation, and increasing the bandwidth. EBS technology is based on an electron beam, with energies near 10 keV, which is modulated and aimed at a target array, make of semiconductor devices. The incident electron beam produces substantial current gain in the semiconductor devices, on the order of 10^3 in silicon p-n junctions. The proposal is to use heterojunction devices, by epitaxially growing two different materials having identical crystalline lattice, structures, different fundamental energy bandgaps and different impurity types of different concentrations. These devices are proposed in both the modulating and amplification portions of the EBS devices. By replacing silicon p-n junctions, which are currently used, with heterojunction devices made of either p-AlGaAs/n-GaAs or p-InP/n-InGaAs, the combinations of properties assures greater out currents, higher frequency modulation and increased bandwidths.

This is a proposed device, which needs to be demonstrated. However, the material technology is her (1989) and similar devices developed for different purposes clearly show the potential for these devices for EBS technology is there.

PATENT STATUS: The patent is currently being reviewed for public or private sector use. United States Patent Number: 4,410,903 Oct 18, 1983.

PUBLICATIONS: This was a spin off of other work, the references are listed below. More details are included in the patent disclosure.

H. Morkoc et al, "A Study of High-Speed Normally Off and Normally on Al0.5Ga0.5As Heterojunction Gate GaAs FETs (JHET)," IEEE Transaction on Electron Devices, ED-25 (6) 1978, pp. 609-27.

S. Umebachi et al, "A New Heterojunction Gate GaAS FET, "IEEE Transaction on Electron Devices, ED-22, 1976, pp. 613-4.

J. C. Campbell et al, "High Sensitivity InP/InGaAs Heterojunction Phototransistor," Electronics Letts., 16, 1980, pp. 713-4.

J. C. Campbell et al, "InP/InGaAs Heterojunction Phototransistors," IEEE J. Quant. Electron. QE-17, 1981, pp. 264-9.

FOR ADDITIONAL INFORMATION: C. M. HANSON, Code 561, Naval Ocean Systems Center, San Diego, CA 92152-5000; (619)553-5242.

NASA Tech Brief
National Aeronautics and Space Administration
NASA's Jet Propulsion Laboratory, Pasadena, California

Licensing Opportunity

Dynamic Transfers of Tasks Among Computers

An allocation scheme would give jobs to idle computers.

A distributed computer system consists of several computers with the same or different processing capabilities, connected together by a network. In such a distributed multicomputer system, there is a probability that one of the computer stations will be idle while another computer station will have more than one job waiting in the queue for service. We call this probability the imbalance probability. A high imbalance probability typically implies poor system performance. By reallocating queued jobs to idle or lightly loaded stations, a reduction in system response time can be expected. This technique is called load sharing and is one of the main focuses of this paper.

An ideal resource-sharing algorithm should have the following characteristics:

1. Dynamics: The load distribution can adapt to rapid system load changes.
2. Decentralized: Each processor determines, on its own, whether to process a job locally or send the job to some other station for processing. There is no need for a central dispatcher. Since the central dispatcher is not required, the problem of a single point of failure is eliminated.
3. Heterogeneous: The computer stations need not have the same processing power.

The proposed enhanced receiver-initiated dynamic algorithm (ERIDA) for resource sharing fulfills all the above criteria.

When a job finishes service and leaves a station in this new algorithm, the station checks the workload indicator by dividing the queue length by the service rate. If the workload indicator is below a certain low threshold level, the lightly loaded station initiates a search for the busiest station. If the workload indicator of the busiest station is above certain high threshold, a job from that busy station is transferred to the lightly loaded station. Thus, the ERIDA provides a method that balances the workload among hosts, resulting in an improvement in the response time and throughput performance of the total system.

The ERIDA adjusts dynamically to the traffic load of each station. When the workload indicator of every station is greater than a certain threshold level, the algorithm generates no overhead — an important advantage.

In a homogeneous 20-node system, service stations have the same service rates, and the arrival rates at each station are also assumed to be equal. The approximate ERIDA queueing model is validated by a GPSS/PC (general-purpose simulation system/personal computer) simulation. The comparison of results from the average response time generated by the approximate queueing model and the results from the simulation excercise are shown in the figure. This figure shows that the results from the approximate queueing models are very close to the simulation results.

Comparing the ERIDA to a non-achieveable centralized resource-sharing system (M/M/10), the figure shows that the ERIDA performance is worse than the centralized M/M/10 system. The inefficiency of the ERIDA can be illustrated by the following scenario: If one of the stations finishes the jobs in its queue and sees that all the other stations are not heavily loaded, this station will go to relinquish and remain idle until either another local job arrives or until wakeup timeout. This idle station will not be able to share the load with any other stations that become overloaded during its relinquish period. For this system configuration, we can conclude that a centralized resource-sharing scheme provides the best performance, since no job will wait if any station is idle. However, this centralized scheme is typically not practical for implementing on a distributed system.

In the same figure, the results of the ERIDA are compared against the case without load sharing, i.e., the case of multiple independent M/M/1 queues. The average response time is always improved

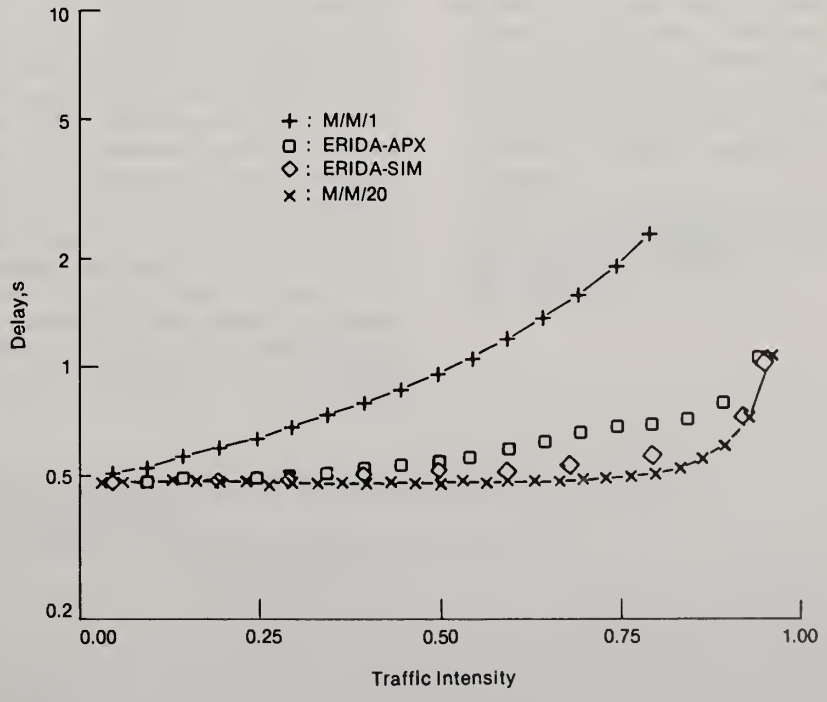

Average Response Time Comparison among ERIDA DIT (ERIDA-APX: □), ERIDA simulation (ERIDA-SIM: ◇), centralized (M/M/20: X) and an independent system (M/M/1: +), each operating in a 20-server homogeneous system.

when the ERIDA resource-sharing scheme is applied. Obviously, the independent M/M/1 queue system is inefficient, since there may be jobs queued up in front of one of the stations when the other one is idle.

This work was done by Howard T. Liu of Caltech and John A. Silvester of the University of Southern California for **NASA's Jet Propulsion Laboratory**.

This invention is owned by NASA, and a patent application has been filed. Inquiries concerning nonexclusive or exclusive license for its commercial development should be addressed to the Patent Counsel, NASA Resident Office-JPL.
NPO-17197/TN

Jet Propulsion Lab.
NASA Resident Office
Technology Utilization Officer: Gordon S. Chapman
Mail Stop 180-801
4800 Oak Grove Drive
Pasadena, CA 91109
(818) 354-4849
Patent Counsel: Paul F. McCaul
Mail Code 180-801
4800 Oak Grove Drive
Pasadena, CA 91109
(818) 354-2734
Technology Utilization Mgr. for JPL: Norman L. Chalfin
Mail Stop 156-211
4800 Oak Grove Drive
Pasadena, CA 91109
(818) 354-2240

FOR ADDITIONAL INFORMATION: *Contact: Director, Technology Transfer Division, P.O. Box 8757, BWI Airport, MD 21240; (301) 621-0100 Ext. 241*
REFER TO THE NUMBER LISTED AT THE END OF THIS ARTICLE

NASA Tech Brief
National Aeronautics and Space Administration
NASA's Jet Propulsion Laboratory, Pasadena, California

Network-Control Algorithm

Channels are allocated optimally to links in a multilink, multinode network.

An algorithm has been developed for the optimal routing of packets of data along the links of a multilink, multinode digital communication network. The algorithm is iterative and converges to a cost-optimal assignment that is independent of the initial assignment.

The network is assumed to have an arbitrary topology, in which each node is connected to several other nodes through full-duplex-multichannel links (see example figure). The problem is to determine the link route between originating and destination nodes and the number of channels for packet-switched traffic along the route that minimize the cost, subject to the constraints imposed by the maximum average allowable network delay.

To simplify the analysis, the cost of initial setup, the propagation delay on each link, and the processing delay at each node are neglected. The cost of using each half duplex link is assumed to be proportional to the number of channels used in that link: This assumption assures the convexity of the cost function, which in turn assures that the iterative optimization process leads to a global optimum.

The algorithm begins with the selection of an initial feasible flow vector, which characterizes the link route and the flow. The gradient of the cost function in the flow-vector space is then computed and used to find the shortest path. A flow-deviation subalgorithm is then used to find the next iteration of the feasible flow vector that minimizes the cost function. If the fraction of the user demand that satisfies this flow vector can be increased, it is increased, and the resulting cost function is evaluated. The foregoing steps are repeated until the decrements of the cost function at an iteration become arbitrarily small, indicating the attainment of the global optimum. The number of channels in each link is then assigned according to the resulting flow vector.

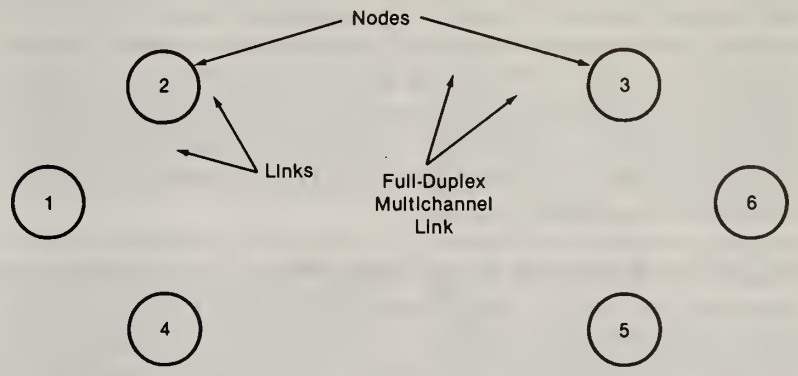

Each Node Is Connected to other nodes through links, each containing a number of two-way (one way at a time) channels. The algorithm assigns channels according to message traffic leaving and arriving at each node.

The algorithm depends in part on the assumption that the number of channels in a link can be treated as a continuous variable. This assumption may not be applicable where the number of channels is small, in which case integer programming can be used to determine the number of channels. The algorithm can also be modified to take account of different priorities among the packets belonging to different users by using different delay constraints or imposing additional penalties via the cost function.

This work was done by Hak-Wai Chan and Tsun-Yee Yan of Caltech for **NASA's Jet Propulsion Laboratory.**
NPO-17505/TN

FOR ADDITIONAL INFORMATION: *Contact: Director, Technology Transfer Division, P.O. Box 8757, BWI Airport, MD 21240; (301) 621-0100 Ext. 241*
REFER TO THE NUMBER LISTED AT THE END OF THIS ARTICLE

U.S. Air Force Fact Sheet

Transportable Instructional Support System

The Instructional Support System (ISS) provides a standardized, transportable software package for support of computer-based training (CBT) throughout the DoD. ISS Is a CBT system that supports both computer-assisted instruction (CAI) and computer-managed instruction(CMI). Written in Ada, a standard high-order language designed to minimize hardware dependence, ISS is transportable across a wide range of computer systems, ranging from mini to microcomputers. In addition, ISS is developed in modular components, enabling users to select only those capabilities required to support their specific training requirements. The functional requirements of the ISS were based on the capabilities of the Advanced Instructional System (AIS). The AIS was a large scale CBT system which integrated CAI within the context of CMI and provided support for operational training and a testbed for training research and development. In addition to the AIS capabilities, an analysis of major DoD training systems was made to determine additional capabilities required in ISS. Recent updates include rehosting the ISS to the Zenith 248 microcomputer under the MS-DOS operating system, creation of a MicroCMI capability, incorporation of a videodisc capability on micro, mini and mainframe-based systems and incorporation of a networking capability on the micro-based system.

Acceptance testing was conducted by AFHRL/ID and Strategic Air Command (SAC) personnel and an operational test and evaluation was conducted by SAC at Dyess AFB, Texas. SAC used the ISS to develop, deliver and manage 170 hours of B-1B aircrew training. ISS runs on the Digital Equipment Corporation Vax family of computers, ranging from a MicroVAX II to a Vax 8650 under the VMS operating system. It can be rehosted to additional systems with the modification of 2000-5000 lines of assembly code. Currently, AFSC is in the process of establishing a System Program Office at the Human Systems Division at Brooks AFB, TX for a two year period, where the ISS will undergo full scale development. Plans are underway to transition the ISS to the Standard Systems Center at Gunter AFB, AL for long term support requirements.

The ISS is currently being demonstrated in the Air Force, Department of Defense and other government agencies. SAC is using the ISS to develop and deliver instructional materials on B-1B aircrew training and manage and assess student progress. AFSC's System Acquisition School at Brooks AFB, TX is using the ISS to develop and deliver systems acquisition training. In addition to these organizations, ISS is the core of two major training systems, ATC's General Imagery Intelligence Training System at Goodfellow AFB, TX and AFSC's Advanced On-the-Job Training System at Bergstrom AFB, TX. Other potential applications are AFSC's School of Aerospace Medicine (Brooks AFB, TX), SAC's B-1B main operating base support (Carswell AFB, TX), ATC's Advanced Training System (Brooks AFB, TX) and AFIT's introduction of exportable courses (Wright-Patterson AFB, OH).

The ISS is a work made for hire under a government contract which vests copyright ownership in McDonnell-Douglas Astronautics Corporation and grants the government a copyright license to use, duplicate or disclose the ISS in while or in port, in any manner and for any purpose whatsoever, and to have or permit others to do so.

A technical report on ISS is currently in publication. Other available publications include AFHRL-TR-85-53, Instructional Support System (AD-A166-776), the ISS Functional Description and brochures entitled "ISS: An Overview for Managers", "ISS: An Overview for Instructional Personnel" and "Conquering the Training Challenges of Tomorrow with Computer-Based Training".

FOR ADDITIONAL INFORMATION: For additional information, contact either Ms. Barbara Eaton or Mr. Bill Hawks, AFHRL/IDC, Brooks AFB, TX 78235-5601; (512)536-2242. The AFHRL Office of Research and Technology Application (ORTA) focal point is Mr. Douglas E. Blair, AFHRL/PRT, Brooks AFB, TX 78235-5601; (512)536-3426.

Simulating Scenes In Outer Space

Scientifically accurate simulations are generated quickly.

The Multimission Interactive Picture Planner, MIP, is a computer program for scientifically accurate and fast, three-dimensional animation of scenes in deep space. MIP is also versatile, reasonably comprehensive, and portable, and runs on microcomputers. New techniques were developed to perform rapidly the calculations and transformations necessary to animate scenes in scientifically accurate three-dimensional space. At the same time, portability is maintained, inasmuch as the transformations and clipping have been written in FORTRAN 77 code. MIP was primarily designed to handle Voyager, Galileo, and the Space Telescope. It can, however, be adapted to handle other missions.

The simulated scene includes a rotating body (usually a planet), any natural satellites, a spacecraft, the Sun, stars, descriptive labeling, and field-of-view boxes. The central body and natural satellites are triaxial wire-frame representations with terminators, limbs, and landmarks. Hidden lines are removed for the central body and natural satellites, but not for the scene as a whole, so that bodies can be seen behind one another. The program has considerable flexibility in its step time, observer position, viewed object, field of view, and the like. Most parameters can be changed from the keyboard while the simulation is running.

When MIP is executed, it asks the user for a control file, which should be prepared before execution. The control file identifies which mission MIP should simulate, the star-catalog files, the ephemerides files to be used, the central body, landmarks, and other constants. The control file also describes the fields of view. Control files are included to simulate the Voyager 1 encounter with Jupiter and the passage of the Giotto spacecraft by Halley's comet. Data are included for Voyager 1 and 2 (all six planetary encounters) and Giotto.

MIP comes in IBM PC or compatible format, including a working example. It requires 512K of random-access memory, a CGA or compatible graphics adapter, and DOS 2.0 or higher. However, the program is primarily designed to be ported and configured on a wide variety of computers. Users must supply their own graphics primitives to clear the screen, change the color, and connect two-dimensional points with straight lines. Also, the users must tie in the graphics primitives along with their ephemeris readers. MIP does everything else, including clipping. MIP was developed in 1988.

This program was written by John D. Callahan of Caltech for **NASA's Jet Propulsion Laboratory**.
NPO-17246/TN

FOR ADDITIONAL INFORMATION

CONTACT:
COSMIC®
112 Barrow Hall
University of Georgia
Athens, GA 30602
(404) 542-3265

U.S. Navy Fact Sheet

Licensing Opportunity

Device for Inspection of Materials by Eddy Current

The technology solves the problem of using eddy current methods to inspect materials which are conductive only in the circumferential direction and where both circumferential and axial resolution of the detected anomaly is required. The device comprises an encircling coil transmitter and a receiver. When applied to filament wound carbon fiber reinforced composites, the transmitter induces eddy current flow in the circumferentially wound fibers. The receiver detects localized variations in this current flow which may be due to fiber breakage or to variations in fiber density. The receiver may be a U-shaped eddy current probe, or possibly a Hall probe, or a SQUID. The device can be used for the inspection of any component which has conductivity in the circumferential direction; conduction paths need not be limited to this direction.

Its main advantages provides is that it provides for the eddy current inspection of components which could not be inspected with the same degree of defect resolution by existing eddy current coils and coil combinations.

The method can be applied with modified laboratory instruments. The technology is ready for design of a commercial instrument. Capitalization costs would be low.

FOR ADDITIONAL INFORMATION: For information on licensing of this subject, contact the Naval Surface Warfare Center, Mr. Ramsey D. Johnson, Code D211, Naval Surface Weapons Center, Silver Spring, MD 20903-5000.

Method of Measuring Magnetic Effects Due to Eddy Currents

This invention relates to the measurement of magnetic effects due to eddy currents, but more specifically, the present invention relates to a discrete-time method of measuring the magnetic effects due to eddy currents induced into conductive material by sinusoidally time-varying magnetic fields.

Magnetic effects due to eddy currents can be measured by applying a large sinusoidally varying magnetic field to the conductive material being measured. This applied field induces an alternating current in the conducitve material which in turn induces an alternating magnetic field that is ninety degrees out of phase with the applied field and at the same frequency.

A previous method used to measure eddy current effects required cancellation of the applied field by using an analog signal to drive a "compensation coil" would around the measurement magnetometer. This signal was derived from the current being used to produce the applied field and passed through a "compensation circuit" consisting of an amplifier and phase shifter. The amplitude and phase of the compensation signal were manually adjusted so as to cancel the applied field as the measurement magnetometer.

In test facilities where it is desired to use over one hundred measurement sensors, for example, the manual adjustment of all compensation circuits becomes a difficult and time-consuming task. In addition, variation in the values of analog components of the compensation circuit due to temperature and aging cause a loss of applied field cancellation, requiring that all compensation circuits be adjusted before every test.

The objects of this invention are to: (1) eliminate the necessity of having to manually cancel or compensate, in measuring the magnetic effects due to eddy currents, the component of the applied field as the measurement sensor or sensors before an accurate measurement can be made; (2) use digital signal processing to, inter alia, avoid the short and long term noise problems normally caused by the need to apply large magnetic fields in the measurement method; (3) decrease measurement time by eliminating all time consuming manual adjustments and replace them with a fast, computer-implemented linear least-mean-squared (LMS) estimation, in an improved manner.

FOR ADDITIONAL INFORMATION: For information on licensing of this subject, contact the Naval Surface Warfare Center, Mr. Ramsey D. Johnson, Code D211, Naval Surface Weapons Center, Silver Spring, MD 20903.

Electrotechnology

0129 Digital 8-DPSK Modem for Trellis-Coded Communication—Signal-processing elements are realized largely in software.

0130 Exciter for X-Band Transmitter and Receiver—Design and performance are described.

0131 Eye-Safe Lidar—Experimental solid-state systems may find use in meteorology.

0132 Integrated Semiconductor/Optical Information Processors—Optical, electro-optical, and electronic devices would be integrated into three-dimensional structures. (Licensing Opportunity)

0133 Making a Circular-Harmonic Filter—An optical image-correlating system is made rotationally invariant.

0134 Healing Voids in Interconnections in Integrated Circuits—A seemingly harsh treatment fills voids (cracks) in aluminum conductors. (Licensing Opportunity)

0135 Multiplying Video Mixer—Transparent or opaque overlays can be put on background images.

0136 Piezoelectrostatic Generator—High voltage is generated by compact, lightweight equipment. (Licensing Opportunity)

0137 Real-Time Optimization of Receiver Bandwidth—Estimates of signal and noise spectra enhance the reception of weak signals.

0138 Reflection Oscillators Containing Series-Resonant Crystals—Transistors operate beyond their normal rated frequencies. (Licensing Opportunity)

0139 Robotic Vision Would Combine Optics and Microwaves—Information on the shapes of objects would be more complete. (Licensing Opportunity)

0140 SEU in an Advanced Bipolar Integrated Circuit—Vulnerability to SEU varies with size and applied current.

0141 Vector Adaptive/Predictive Encoding of Speech—Vector quantization enhances the quality of digitally transmitted speech.

Testing & Instrumentation

0142 Demodulation Circuit for AC Motor Current Signature Analysis (Licensing Opportunity)

Other Items of Interest

0196 Biomedical Telectrodes—Compact transmitters would eliminate the need for wires to monitors.

0208 Digital/Optical Conversion Module (Licensing Opportunity)

NASA Tech Brief
National Aeronautics and Space Administration
NASA's Jet Propulsion Laboratory, Pasadena, California

Licensing Opportunity

Digital 8-DPSK Modem for Trellis-Coded Communication

Signal-processing elements are realized largely in software.

A digital real-time modem processes octuple differential-phase-shift-keyed (8-DPSK) trellis-coded modulation. The modem is intended for use in communicating data at a rate up to 4.8 kb/s in a land-mobile satellite channel (Rician fading) of 5-kHz bandwidth at a carrier frequency of 1 to 2 GHz. Other communication systems that might benefit from this type of modem include land mobile (without satellites), paging, digitized voice, and frequency-modulation subcarrier data broadcasting.

The modem includes digital signal processors, each programmed to execute a different function. The flexibility afforded by basing the system largely on software enables both rapid realization of design and refinement via changes in algorithms. In keeping with this approach, the signal processors are constructed on general-purpose circuit boards, the central element of each of which is a commercially available digital signal-processing chip.

Each board has two 4K × 16-bit word spaces for program and data memory. In addition, the program memory is switchable between operation as a random-access memory for development and as an electrically programmable read-only memory for final placement of the algorithm. Additional circuitry supports five dedicated 16-bit parallel input/output ports (two input and three output). Three levels of hardware interruption are accessible.

The modulator and demodulator (see figure) are partitioned into two distinct systems under separate asynchronous control by an external controller. The multiprocessor design is greatly simplified by following a pipelined approach. Taken separately, the flow of signals for either the modulator or demodulator can essentially be viewed as feedforward for both control and data signals. This results in simple interfaces between boards and provides an effective architecture for mitigating the effects of the fading channel. Data are passed in parallel fashion sequentially from board to board on an interruption basis.

The modulator consists of a single circuit board, a clock unit (shared with the demodulator), and two digital-to-analog subsystems. The clock unit provides clock signals locked to frequencies of 4.8 and 28.8 kHz. The 4.8-kHz clock is used to transfer the raw data to be transmitted from the external terminal processor to the modulator, while the 28.8-kHz clock is used to transfer data from the modulator circuit board to the digital-to-analog subsystems. Each digital-to-analog subsystem consists of a 12-bit digital-to-analog converter and a 4-kHz low-pass filter.

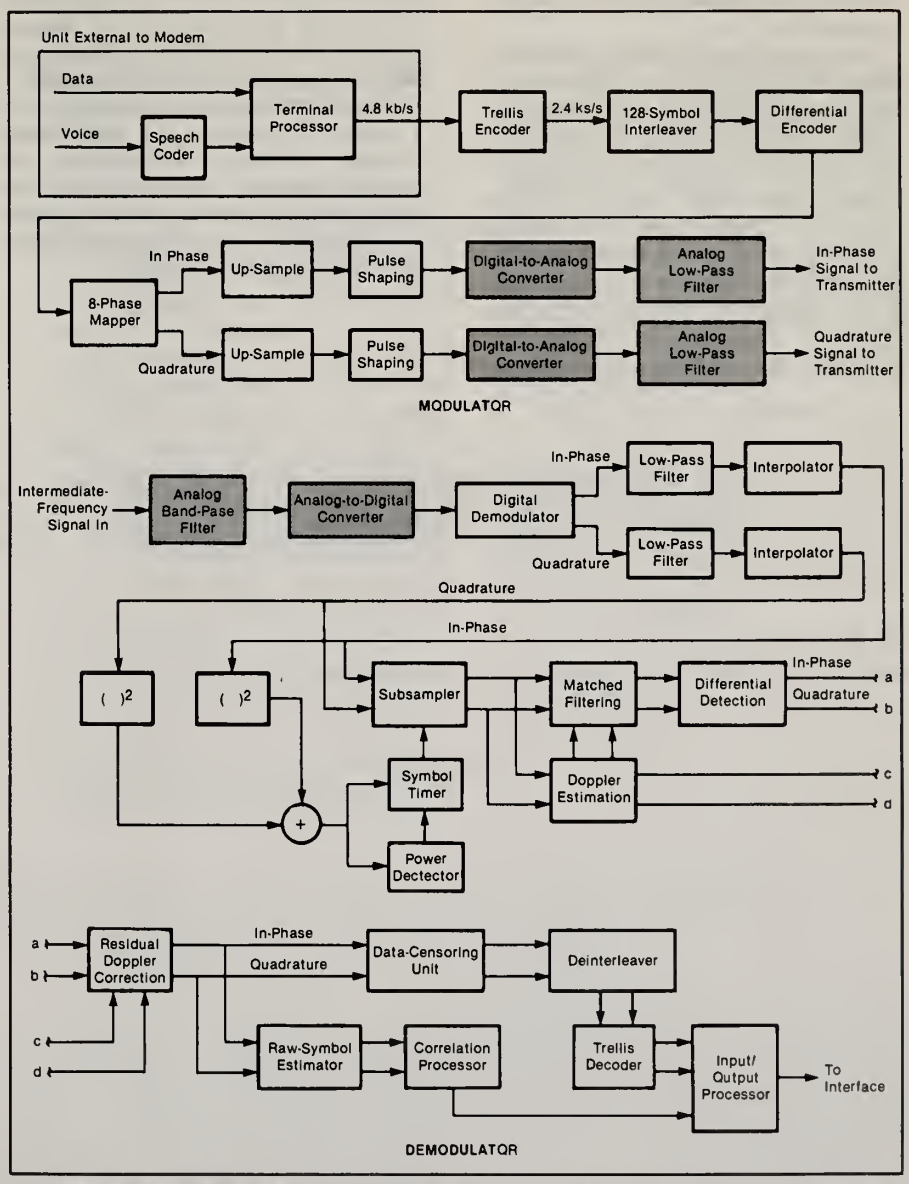

The Modulator and Demodulator contain digital signal processors that perform the modem functions. The design is flexible in that functions can be altered via software.

The demodulator consists of an analog-to-digital subsystem, six circuit boards, and two clock units. The analog-to-digital subsystem consists of a 40-kHz-wide bandpass filter centered at 28.8 kHz, followed by a 12-bit analog-to-digital converter. The first clock unit (common with the modulator) provides a clock signal at 18.432 MHz, which is divided down by the analog-to-

digital subsystem to the 115.2 kHz sampling frequency. The second clock unit, also run from the 18.432-MHz signal, is the 4.8-kHz jitter clock used to transfer data from the demodulator to the terminal processor. The phase of the jitter-clock signal can be advanced or retarded by the demodulator to the timing derived from the incoming data.

This power- and bandwidth-efficient modem incorporates many novel features. Among these features are the modulation scheme and the feedforward architecture that have been optimized to combat the effects of the fading channel. The 100-percent root raised cosine pulse shaping employed has the unique feature of two intersymbol interference-free points per symbol. These two points per symbol are utilized for a data-derived Doppler estimator and matched filtering and contribute to the robustness of the data-derived symbol timing, which has zero data-induced timing variance at these points. This modem has been successfully tested and evaluated in both laboratory and field experiments, including a recent full-scale satellite experiment. In all cases, the modem has performed within 1 dB of theory.

This work was done by T.C. Jedrey, N.E. Lay, and W. Rafferty of Caltech for **NASA's Jet Propulsion Laboratory.**

This invention is owned by NASA, and a patent application has been filed. Inquiries concerning nonexclusive or exclusive license for its commercial development should be addressed to the Patent Counsel, NASA Resident Office-JPL. Refer to NPO-17578/TN.

Jet Propulsion Lab.
NASA Resident Office
Technology Utilization Officer: Gordon S. Chapman
Mail Stop 180-801
4800 Oak Grove Drive
Pasadena, CA 91109
(818) 354-4849
Patent Counsel: Paul F. McCaul
Mail Code 180-801
4800 Oak Grove Drive
Pasadena, CA 91109
(818) 354-2734
Technology Utilization Mgr. for JPL: Norman L. Chalfin
Mail Stop 156-211
4800 Oak Grove Drive
Pasadena, CA 91109
(818) 354-2240

FOR ADDITIONAL INFORMATION: *Contact: Director, Technology Transfer Division, P.O. Box 8757, BWI Airport, MD 21240; (301) 621-0100 Ext. 241*
REFER TO THE NUMBER LISTED AT THE END OF THIS ARTICLE

NASA Tech Brief
National Aeronautics and
Space Administration

Exciter for X-Band Transmitter and Receiver

Design and performance are described.

A report describes a developmental X-band exciter for the X-band uplink subsystem of the Deep Space Network. The X-band transmitter-exciting signal is expected to have a fractional frequency stability of 5.2×10^{-15} during a 1,000-second integration period. The exciter also generates coherent test signals for the S- and X-band Block III translator of the Deep Space Network, a Doppler-reference signal for the associated Doppler-extractor system, the first-local-oscillator signal for the associated receiver, and a reference signal for the associated ranging subsystem.

The main transmitter-exciting signal is generated by a heterodyne principle often used to stabilize output frequencies; a stable higher frequency is added to a less-stable lower frequency so that the resultant fractional stability is close to that of the more stable source. In this case, the higher-frequency input signal at 6,500 MHz is obtained by multiplying by 65 the frequency of a 100-MHz input reference signal from a hydrogen maser. The lower-frequency input signal at 690 MHz is obtained by multiplying by 16 the frequency of a portion of a 43.125-MHz signal from a synthesizer.

The two input signals are mixed and band-pass filtered to produce a signal at the transmitter-exciting frequency of 7,190 MHz. This signal is amplified, then fed through X-band command and ranging phase modulators and a radio-frequency relay to an output terminal.

Before multiplication, the portion of the 43.125-MHz signal used to generate the exciter output is passed through a voltage-controlled phase shifter, which is part of the overall-phase-control loop that reduces the variations in phase of the transmitted signal due to changes in temperature, voltages, and characteristics of components. The other portion of the raw 43.125-MHz input is multiplied directly and added to the 6,500-MHz signal to generate an unmodulated 7,190-MHz reference signal for use in the phase detector of the phase-control loop.

The coherent S- and X-band test signals and the local-oscillator, Doppler-reference, and ranging-subsystem-reference signals are generated from the inputs and outputs of the main exciter by various combinations of frequency multiplication, mixing, addition, and subtraction. Other engineering details described in the report include the physical configuration of the components and subsystems, stabilization of temperature, controlling and monitoring circuits, the distribution of the Doppler-reference signal, and the Doppler-signal-extracting system.

Tests of the prototype exciter show that the controlling and monitoring and internal phase-correcting loops perform according to the applicable design criteria. Measurements of the stability of the frequency and of the single-sideband noise spectral density of the transmitter-exciting signal are to be made subsequently.

This work was done by Carl E. Johns of Caltech for **NASA's Jet Propulsion Laboratory**.
NPO-17261/TN

FOR ADDITIONAL INFORMATION: *Contact: Director, Technology Transfer Division, P.O. Box 8757, BWI Airport, MD 21240; (301) 621-0100 Ext. 241*
REFER TO THE NUMBER LISTED AT THE END OF THIS ARTICLE

NASA Tech Brief
National Aeronautics and Space Administration

NASA's Jet Propulsion Laboratory, Pasadena, California

Eye-Safe Lidar

Experimental solid-state systems may find use in meteorology.

A laser infrared radar (lidar) undergoing development is harmless to human eyes, consists almost entirely of solid-state components, and offers high range resolution. The lidar operates at a wavelength of about 2 μm. If the radiation from such a device strikes an eye, it is almost completely absorbed by the cornea without causing damage (provided that the lidar is sufficiently distant and suitably low in power or pulse energy), even if aimed directly at the eye. The 2-μm lidar is intended for remote Doppler measurements of winds and differential-absorption measurements of concentrations of gases in the atmosphere.

The lidar includes a continuous-wave ring-laser oscillator pumped by a semiconductor laser diode. A multipass slab laser amplifier is pumped by a flashlamp, which is the only major non-solid-state component. Diodes cannot yet provide the intense light needed by a laser power amplifier. Even here, however, laser-diode pumping is likely to be feasible in the future. Laser-diode pumps have efficiencies of 35 to 40 percent. The use of laser-diode pumping offers high overall efficiency (approaching 15 percent) and long lifetime (approaching 20,000 h). Furthermore, the solid-state laser medium allows energy to be stored and radiation to be amplified in volumes large enough to generate 100 W average power.

The output of the oscillator passes through a permanent-magnet optical isolator. An acousto-optical device gates the continuous wave and imposes 40 MHz of frequency modulation (see figure). The power amplifier converts the gated, modulated signal into high-power pulses. A paraboloidal mirror in a telescope launches the pulses into space. The mirror collects reflected pulses, and a single-mode optical fiber carries them to a single-mode optical-fiber coupler, where the reflection signal is combined with the transmitter signal or the signal from another local oscillator. The output of the coupler is fed to a photodiode, which converts the output optical signal into an electrical signal for processing.

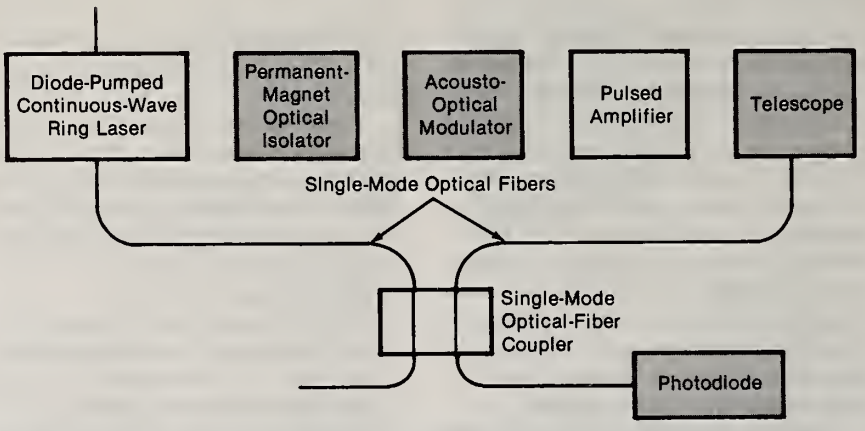

Continuous-Wave Light from a laser oscillator is amplified and modulated for transmission from a telescope. A small portion — about 1 mW — of the output of the oscillator is fed to a single-mode fiber coupler, where it mixes with return pulses.

In experiments, an yttrium aluminum garnet (YAG) laser doped with thulium and holmium produced continuous-wave light at 2 μm. The Tm:Ho:YAG laser requires a minimum pump power of 4.4 mW at the diode-laser wavelength of 0.782 μm. The thulium ions absorb the pump radiation efficiently and transfer it to the holmium ions without radiation. This laser works at a slope efficiency (2-μm output divided by the excess of the 0.782-μm pump input over the threshold) of 19 percent. Work continues on the Tm:Ho:YAG laser in the effort to attain single-mode oscillation.

Meanwhile, the lidar system has been demonstrated with a neodymium-doped YAG laser as the continuous-wave oscillator. This device produces light at 1.064 μm — not an eye-safe wavelength. Nevertheless, the demonstration showed that the system can coherently detect scattered laser radiation from clouds and from atmospheric aerosols.

This work was done by Robert L. Byer of Stanford University for **NASA's Jet Propulsion Laboratory.**
NOP-17464/TN

FOR ADDITIONAL INFORMATION: *Contact: Director, Technology Transfer Division, P.O. Box 8757, BWI Airport, MD 21240; (301) 621-0100 Ext. 241*
REFER TO THE NUMBER LISTED AT THE END OF THIS ARTICLE

NASA Tech Brief
National Aeronautics and Space Administration

Licensing Opportunity

NASA's Jet Propulsion Laboratory, Pasadena, California

Integrated Semiconductor/Optical Information Processors

Optical, electro-optical, and electronic devices would be integrated into three-dimensional structures.

Optical information processors of a proposed new type would be made of integrated three-dimensional devices that would include optical, electro-optical, and electronic devices. The integration would be achieved by a combination and extension of advanced semiconductor (integrated-circuit) and integrated-optics technology. The development of the new processors could lead to the miniaturization of sophisticated optical information-processing systems.

The figure illustrates the concept of an integrated device that would perform matrix•vector multiplication. This device would combine two separate components of a previously demonstrated system for matrix•vector multiplication: an electrically-addressable spatial light modulator that generated the light-and-dark matrix pattern, and a thin chip of GaAs, in which the multiplication was performed by degenerate four-wave mixing via the photorefractive effect. In the integrated device, the spatial light modulator would be fabricated on the surface of the chip.

Because the photorefractive portion of the device would constitute an all-optical processor, its inputs and control signals would have to be spatially modulated beams of light, which could be generated by other optical processors or by the electrically addressable spatial light modulator on its surface. Several types of spatial light modulators could satisfy the requirements for speed (a frame rate ⩾ 1,000 Hz) and compatibility with lasers that have wavelengths suited to the photorefractive effect. The logical choice for integration is semiconductor spatial light modulators on semiconductor processors. Candidate superlattice spatial light modulators of this type include GaInAs/GaAs, GaInAs/InP, and HgCdTe/CdTe.

The simplistic approach to integration is to miniaturize the established components, but this is not likely to exploit the full potential of the new concept. A more promising approach would be to use holographic patterns generated by computers and electron-beam lithography to make

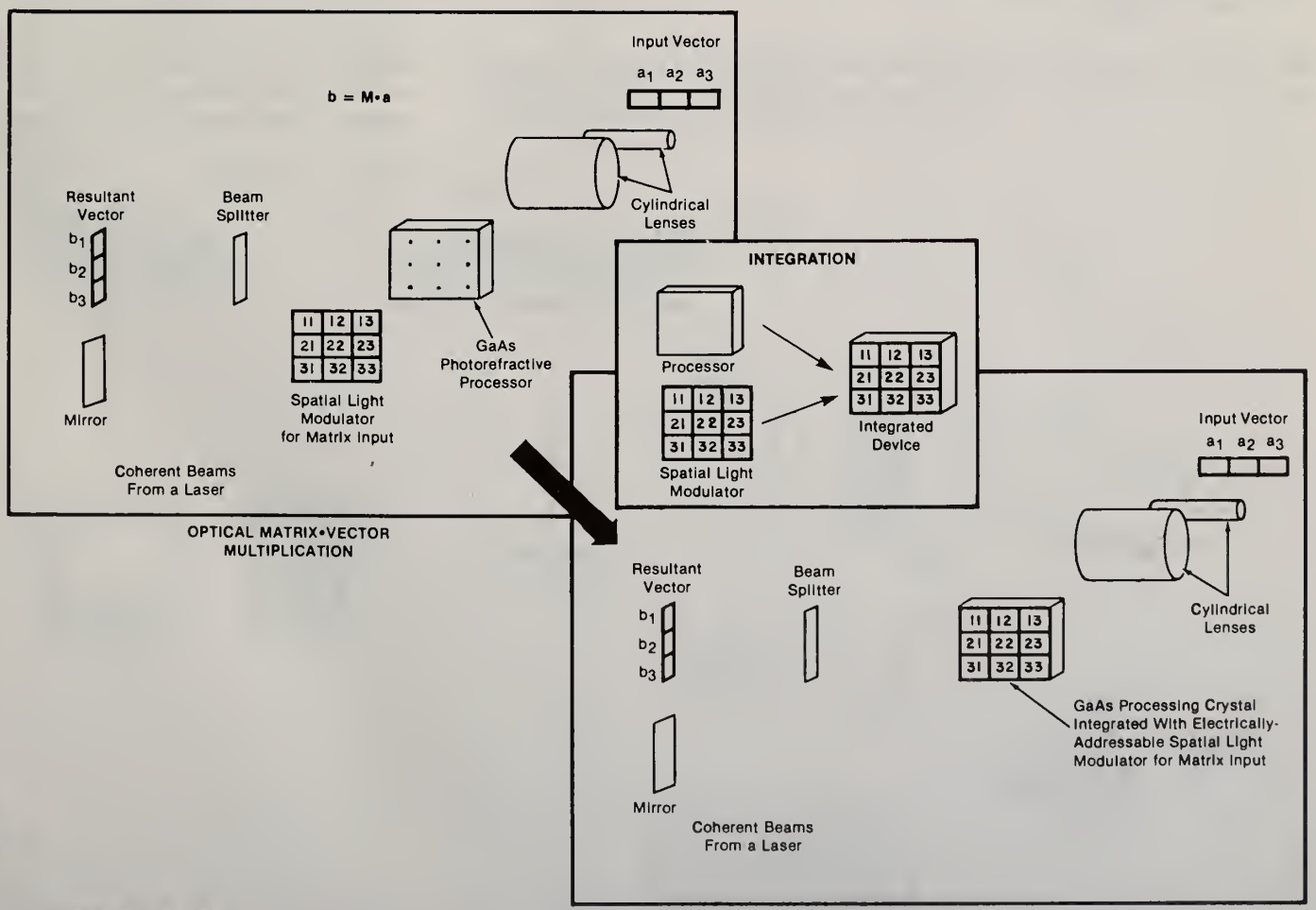

An **Integrated Device** has been proposed to perform the functions of two separate devices in a previous optical matrix•vector multiplier.

holographic patterns on surfaces and interfaces. These patterns could not only provide the functions of conventional optical components but could also create novel applications.

This work was done by Li-Jen Cheng of Caltech for **NASA's Jet Propulsion Laboratory.**

In accordance with Public Law 96-517, the contractor has elected to retain title to this invention. Inquiries concerning rights for its commercial use should be addressed to

Edward Ansell
Director of Patents and Licensing
Mail Stop 301-6
California Institute of Technology
1201 East California Boulevard
Pasadena, CA 91125

Refer to NPO-17533/TN.

Jet Propulsion Lab.
NASA Resident Office
Technology Utilization Officer: Gordon S. Chapman
Mail Stop 180-801
4800 Oak Grove Drive
Pasadena, CA 91109
(818) 354-4849
Patent Counsel: Paul F. McCaul
Mail Code 180-801
4800 Oak Grove Drive
Pasadena, CA 91109
(818) 354-2734
Technology Utilization Mgr. for JPL: Norman L. Chalfin
Mail Stop 156-211
4800 Oak Grove Drive
Pasadena, CA 91109
(818) 354-2240

NASA Tech Brief
National Aeronautics and Space Administration
NASA's Jet Propulsion Laboratory, Pasadena, California

Making a Circular-Harmonic Filter

An optical image-correlating system is made rotationally invariant.

An experiment has shown that a circular-harmonic filter can be generated optically. Such a filter could be used in an optical image-recognition system that is based on the correlation between the target (the image to be recognized) and a matched spatial filter. In addition to the usual invariance under translation of the target, the circular harmonic filter is invariant under rotation of the target; that is, the peak intensity of the illumination at the origin of the correlation plane does not vary when the target is rotated about the optical axis.

The target for this study is a 36-sector spoke-wheel binary pattern. The real part of the fundamental component of the pattern (which is the 36th circular harmonic), plus a constant bias to provide for the recording of negative amplitudes, is generated by computer and recorded on photographic film (see Figure 1). The imaginary part is the same as the real part, but rotated 2.5°, this angle being a quarter

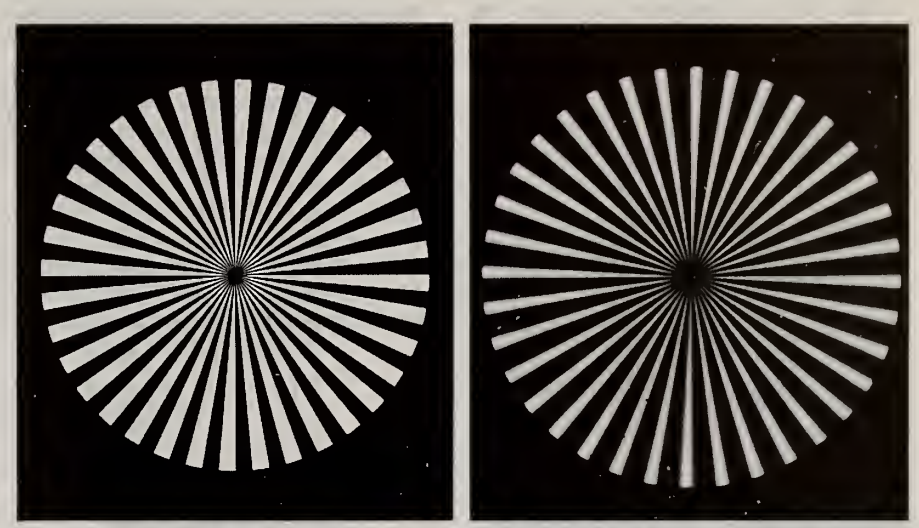

Figure 1. This **Spoke-Wheel-Pattern Target** is decomposed into the real part and the imaginary part (not shown) of its fundamental circular-harmonic component. The real and imaginary parts are used to make the circular-harmonic filter.

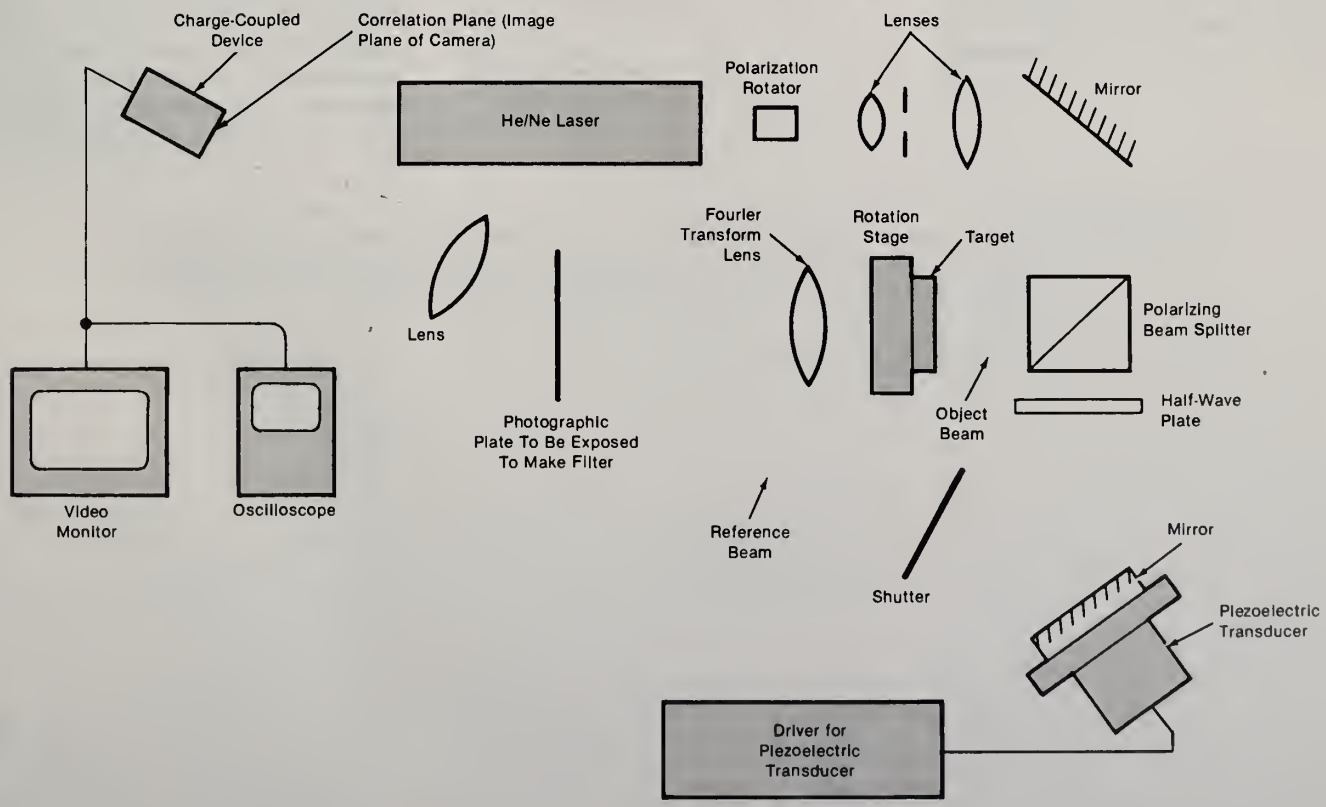

Figure 2. This **Holographic Apparatus** is used to make the circular-harmonic filter and to perform correlation tests.

period of the 36th circular harmonic.

The filter is a hologram made by a phase-shifted-double-exposure procedure in the apparatus shown in Figure 2. A laser beam is split into an object beam and a reference beam. The object beam passes through the target mounted on a rotation stage and is focused onto the holographic plate that is to become the filter. The reference beam is reflected from a mirror on a piezoelectric transducer through the holographic plate at an angle, where it interferes with the object beam to generate the hologram.

During the first exposure, the piezoelectric transducer is turned off, and the function recorded in the hologram is the Fourier transform of the real part of the circular-harmonic filter. During the second exposure, the piezoelectric transducer is turned on to shift the phase of the reference beam 90°, and the target is rotated 2.5° to record the Fourier transform of the imaginary part of the circular-harmonic filter.

To perform a correlation test, the reference beam is blocked by a shutter. The image to be correlated with the target is placed in the rotation stage. Correlation or the lack thereof is observed as a bright spot or the lack of a bright spot, respectively, at the center of the test image. In the experiment, the correlation was performed with the target itself. The brightness of the correlation spot was found to be invariant under both rotation and translation of the target, as expected.

This work was done by Yeou Yen Cheng of Caltech for **NASA's Jet Propulsion Laboratory.**
NPO-17263/TN

FOR ADDITIONAL INFORMATION: *Contact: Director, Technology Transfer Division, P.O. Box 8757, BWI Airport, MD 21240; (301) 621-0100 Ext. 241*

REFER TO THE NUMBER LISTED AT THE END OF THIS ARTICLE

NASA Tech Brief
National Aeronautics and Space Administration
NASA's Jet Propulsion Laboratory, Pasadena, California

Licensing Opportunity

Healing Voids in Interconnections in Integrated Circuits

A seemingly harsh treatment fills voids (cracks) in aluminum conductors.

An unusual heat treatment heals voids (cracks) in aluminum interconnections on integrated circuits (IC's). The voids (cracks) have been attributed to such causes as mismatched thermal expansion and precipitation of silicon in the aluminum conductors during the processing of IC wafers and the packaging of IC chips. The treatment consists of heating an IC to a temperature between 200 °C and 400 °C, holding it at that temperature, and then plunging the IC immediately into liquid nitrogen.

Ordinarily, one would expect such a treatment to start voids (cracks) or make them longer. Indeed, the treatment was first tried in the effort to inflict further damage during a study of voiding (cracking) in aluminum interconnection in random-access-memory IC's. Researchers had hoped that further damage would lead to a capability to estimate growth kinetics. To their surprise, the treatment healed the interconnects (see figure).

In the new treatment, the high temperature is necessary but not the critical step and can range from 200 to 400 °C, which is speculated to depend on the temperature used to deposit aluminum in manufacture. A typical holding time at the evaluated temperature is 30 minutes. The critical step is the rapid cooling in liquid nitrogen.

This work was done by Edward F. Cuddihy, Russell A. Lawton, and Thomas Gavin of Caltech for **NASA's Jet Propulsion Laboratory.**

This invention is owned by NASA, and a patent application has been filed. Inquiries concerning nonexclusive or exclusive license for its commercial development should be addressed to the Patent Counsel, NASA's Resident Office-JPL. Refer to NPO-17678/TN.

Jet Propulsion Lab.
NASA Resident Office
Technology Utilization Officer: Gordon S. Chapman
Mail Stop 180-801
4800 Oak Grove Drive
Pasadena, CA 91109
(818) 354-4849
Patent Counsel: Paul F. McCaul
Mail Code 180-801
4800 Oak Grove Drive
Pasadena, CA 91109
(818) 354-2734
Technology Utilization Mgr. for JPL: Norman L. Chalfin
Mail Stop 156-211
4800 Oak Grove Drive
Pasadena, CA 91109
(818) 354-2240

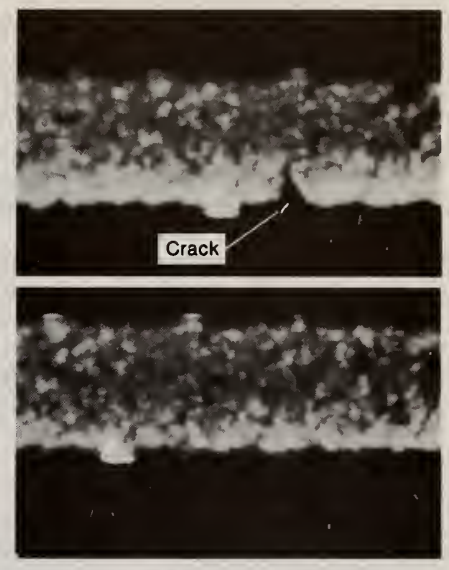

Two Voids (Cracks) can be observed on opposite sides of an aluminum interconnection. After the thermal treatment, the voids (cracks) have disappeared. The aluminum line is 7 μm wide. The pictures appear slightly fuzzy because the aluminum interconnection is being photographed through a glassivation layer that is on top of the aluminum.

FOR ADDITIONAL INFORMATION: *Contact: Director, Technology Transfer Division, P.O. Box 8757, BWI Airport, MD 21240; (301) 621-0100 Ext. 241*
REFER TO THE NUMBER LISTED AT THE END OF THIS ARTICLE

NASA Tech Brief
National Aeronautics and Space Administration
NASA's Jet Propulsion Laboratory, Pasadena, California

Multiplying Video Mixer

Transparent or opaque overlays can be put on background images.

A video mixing circuit places a transparent overlay image on all or a portion of the normal image (denoted here as the "background" image) on a television screen. The overlay might be computer-generated graphics, text, or another image. If additional circuitry is included, the overlay can also be made opaque.

The circuit is a multiplying mixer. In a full-color television system, one such mixer would be needed for each of the three primary colors, and the multiplicity of mixers would provide great flexibility in the choice of contrasts, components of the overlay in different colors, intensities, and degrees of transparency or opacity.

The background video brightness signal is fed into one input terminal of the circuit, while the overlay brightness signal is fed into the other input terminal (see figure). The amplitude of the background brightness signal is thus modulated by the overlay brightness signal, resulting in a video image in which the background image appears as though viewed through the overlay.

The additional circuitry (not shown in detail) would provide a choice of transparent or opaque overlays. In the transparent mode, the mixer would function as described above. In the opaque mode, the additional circuitry would replace the background-image brightness signal with an auxiliary full-brightness signal in the overlay region. Thus, the overlay image would be a full-brightness image modulated by the overlay video signal and would contain no background image at all; that is, the overlay would appear opaque.

This work was done by Neil W. Heckt of Boeing Aerospace Co. for **NASA's Jet Propulsion Laboratory.**
NPO-17332/TN

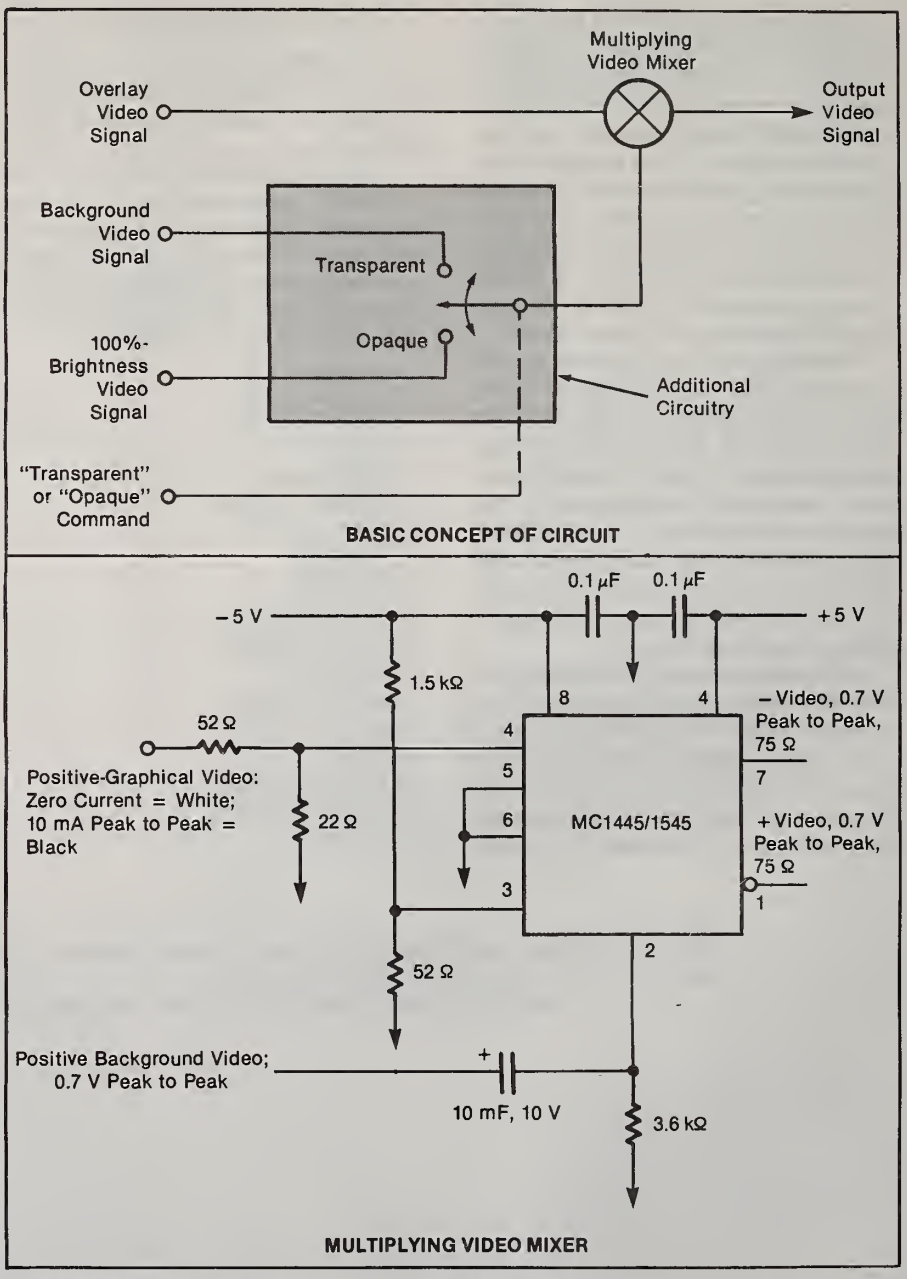

The **Multiplying Video Mixer**, combined with the additional circuitry, would place transparent or opaque overlay images on normal (background) video images.

FOR ADDITIONAL INFORMATION: *Contact: Director, Technology Transfer Division, P.O. Box 8757, BWI Airport, MD 21240; (301) 621-0100 Ext. 241*
REFER TO THE NUMBER LISTED AT THE END OF THIS ARTICLE

NASA Tech Brief
National Aeronautics and Space Administration
Marshall Space Flight Center, Alabama

Licensing Opportunity

Piezoelectrostatic Generator

High voltage is generated by compact, lightweight equipment.

An improved variable-capacitance electrostatic generator puts out high pulsed direct (in effect, rectified alternating) voltages at currents greater than those usually obtainable from electrostatic generators. The generator is light in weight and relatively compact because it relies on the piezoelectric effect to convert mechanical energy directly into electrical energy and contains neither transformers nor bulky high-voltage rectifiers. Unlike some other variable-capacitance electrostatic generators, the piezoelectrostatic generator requires neither an external power supply to charge, nor a vacuum to insulate, its electrodes.

The heart of the piezoelectrostatic generator is a stator composed of multiple piezoelectrostatic capacitive elements shaped somewhat like slices of pie (see Figure 1). Each element contains two piezoceramic strips connected in series between two outer electrodes, insulated from the electrodes by two dielectric strips. The elements are mounted in cantilever configuration and connected in parallel to combine the piezoelectric currents generated in all of them.

An alternating axial force tending to bend the piezoceramic elements is applied to the inner tips of the elements; for example, by supplying a sinusoidal voltage through diodes to alternate solenoidal actuators as shown in Figure 2. By the piezoelectric effect, the bending stresses induce electric charges on the opposite faces of the elements.

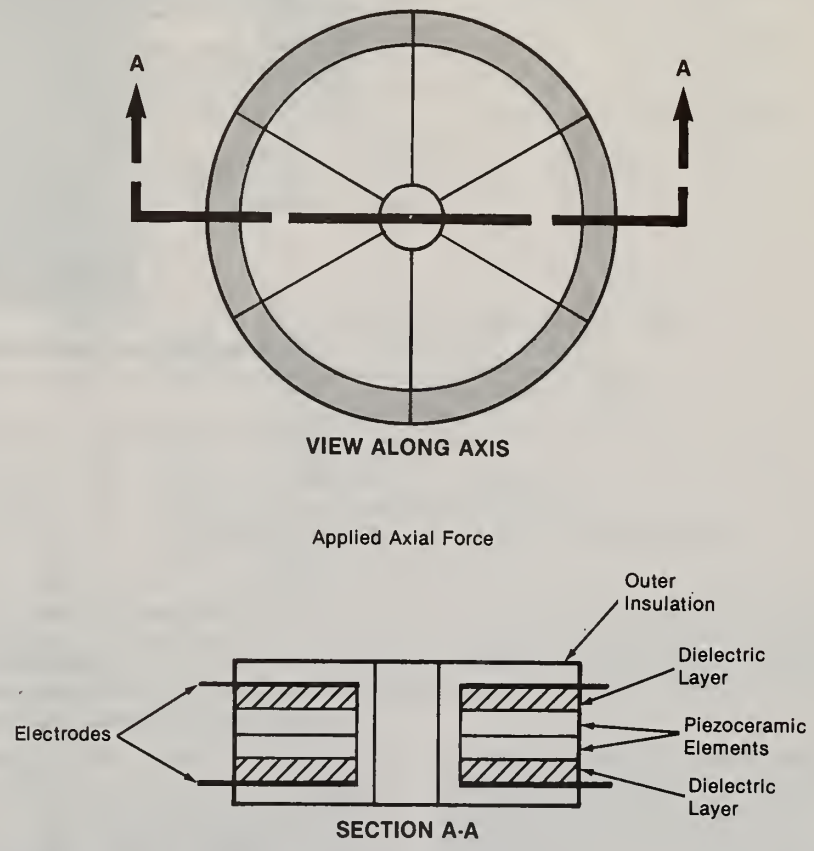

Figure 1. **Piezoelectrostatic Elements** are, in effect, capacitors that generate their own voltages when stressed. They are connected in parallel and cyclically stressed at their inner tips to produce electricity.

While the bending force rises from zero to maximum during the first half of each half cycle, diodes and switches synchronized with the applied-force signal short-circuit the electrodes together to allow electric charges to flow between them and balance the charges on the piezoceramic elements. When the stator reaches maximum flexure, the maximum charge has been stored in the electrodes. The electrodes are then disconnected from each other, and then the stator is allowed to relax. By the piezoelectric effect, this causes a change in the charge on the faces of the elements, which in turn causes a high-voltage pulse as the electrodes discharge through the load.

The voltage achievable by short-circuiting during bending is greater than that achievable by sending current to the load during the entire cycle. This is because of the increase in electric permeability of the piezoceramic with an increase in stress. The net result is that the capacitance of the elements decreases during relaxation while some of the charge induced during bending is retained, so that the voltage due to the remaining charge in the elements is increased.

This work was done by Glen A. Robertson of **Marshall Space Flight Center.**

Inquiries concerning rights for the commercial use of this invention should be addressed to the Patent Counsel, Marshall Space Flight Center. Refer to MFS-28298/TN.

George C. Marshall Space Flight Center
Technology Utilization Officer: Ismail Akbay
Code AT01
Marshall Space Flight Center,
AL 35812
(205) 544-2223
Patent Counsel: Leon D. Wofford, Jr.
Mail Code CC01
Marshall Space Flight Center,
AL 35812
(205) 544-0024

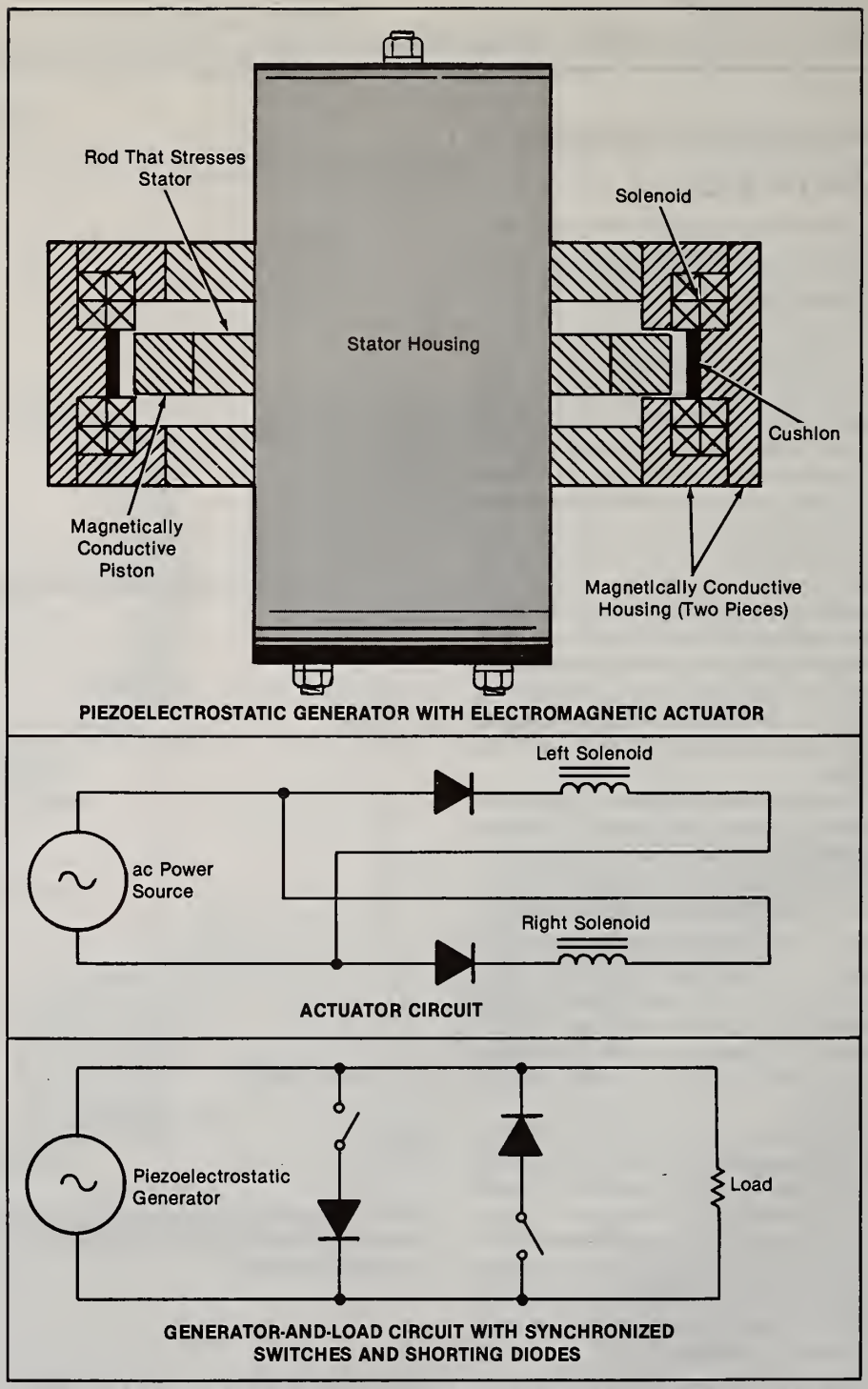

Figure 2. An **Electromagnetic Actuator** includes two opposing solenoidal electromagnets, which apply alternating axial stress to the multiple-element piezoelectrostatic stator shown in Figure 1. The electronic switches in the circuit shown at the bottom are synchronized with the applied force.

NASA Tech Brief
National Aeronautics and Space Administration
NASA's Jet Propulsion Laboratory, Pasadena, California

Real-Time Optimization of Receiver Bandwidth

Estimates of signal and noise spectra enhance the reception of weak signals.

A digital signal-processing subsystem continually seeks the optimum bandwidth for the digital carrier-tracking phase-locked loop (see figure) in a receiver of weak subcarrier-phase-modulated telemetry signals. The optimum bandwidth is defined here as the one that minimizes the steady-state root-mean-square (rms) phase error within the loop. It is typically wide enough to enable the receiver to track out phase jitter in the received carrier signal, yet narrow enough to limit the entry of thermal noise into the loop. Although the subsystem is intended specifically for the reception of signals from the *Pioneer 10* spacecraft, the principle of real-time optimization of bandwidth can be adapted to other situations to enhance the reception of weak signals that might otherwise be "buried" in noise.

The determination of the optimum bandwidth is based on the spectral densities of the additive receiver noise and of the components of the phase signal in the output of the phase detector in the phase-locked loop. Estimates of the spectrum are first obtained by applying fast Fourier transforms to the output of the phase detector. Given a knowledge of the transfer function of the closed phase-locked loop, the subsystem uses the data from the transforms to estimate the phase spectrum, the noise spectrum of the receiver, and the power of the received carrier signal. The optimum bandwidth is then calculated from these estimated components.

The success of this technique depends in part on the correctness of the mathematical model of the phase noise, because any real-time characterization of the phase can assist in reception. In the original application, the significant components of phase noise are generated by the transmitter, propagation of the signal (including the effects of motion, the Sun, and the atmosphere), and the voltage-controlled oscillator in the receiver. Analytic expressions for the optimum bandwidth have been derived for phase-noise spectral densities proportional to $f^{-\alpha}$ (where f = frequency), a model often quoted in the literature. For oscillator phase spectra at low frequencies, one can use $\alpha = 3$, while the effect of solar scintillation can be represented by $\alpha = 8/3$.

The value of the technique was demonstrated in the application to *Pioneer 10*. Loop bandwidths and minimum carrier-to-noise ratios for which tracking could be done were estimated for various operating conditions. It was found that the minimum signals that can be tracked are 5 to 15 dB below those that can be tracked by current receivers. This improvement is accomplished by the use of bandwidths of 0.1 to 1.0 Hz, in contrast with the 3-Hz bandwidth in current use.

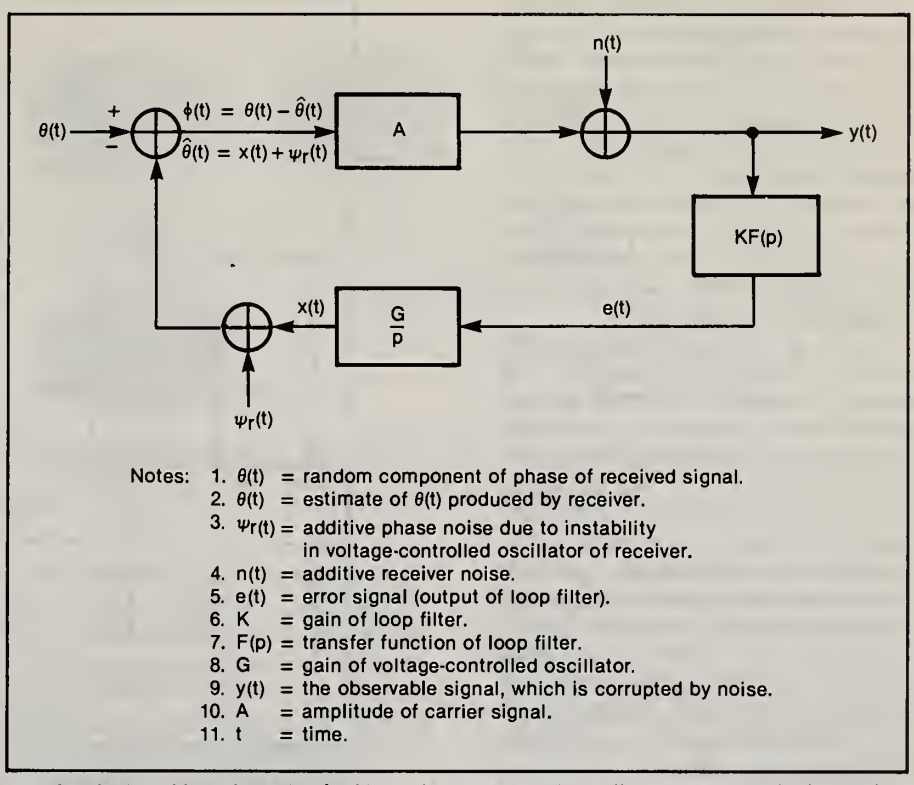

Notes:
1. $\theta(t)$ = random component of phase of received signal.
2. $\theta(t)$ = estimate of $\theta(t)$ produced by receiver.
3. $\psi_r(t)$ = additive phase noise due to instability in voltage-controlled oscillator of receiver.
4. n(t) = additive receiver noise.
5. e(t) = error signal (output of loop filter).
6. K = gain of loop filter.
7. F(p) = transfer function of loop filter.
8. G = gain of voltage-controlled oscillator.
9. y(t) = the observable signal, which is corrupted by noise.
10. A = amplitude of carrier signal.
11. t = time.

The **Carrier-Tracking Phase-Locked Loop** is represented by a linear mathematical model at small rms phase errors. The loop continuously generates estimates $\hat{\theta}(t)$ of the received phase $\theta(t)$. The bandwidth (in effect, the scale of the complex-frequency variable p) can be optimized to minimize the rms phase error.

This work was done by V.A. Vilnrotter, W.J. Hurd, and D.H. Brown of Caltech for **NASA's Jet Propulsion Laboratory.**
NPO-17400/TN

FOR ADDITIONAL INFORMATION: *Contact: Director, Technology Transfer Division, P.O. Box 8757, BWI Airport, MD 21240; (301) 621-0100 Ext. 241*
REFER TO THE NUMBER LISTED AT THE END OF THIS ARTICLE

NASA Tech Brief
National Aeronautics and Space Administration

Licensing Opportunity

Goddard Space Flight Center, Greenbelt, Maryland

Reflection Oscillators Containing Series-Resonant Crystals

Transistors operate beyond their normal rated frequencies.

A crystal-controlled transistor reflection oscillator is easily tunable and stable, consumes little power, and costs less than do other types of oscillators that operate at the same frequencies. This unusual combination of features is made possible by a design concept that includes operation of the transistor well beyond the 3-dB frequency of its current-versus-frequency curve. The concept takes advantage of newly available crystals that resonate at frequencies up to about 1 GHz.

The top of the figure shows a bipolar-transistor version of the oscillator. The emitter of transistor Q is connected with variable (tuning) capacitor C_1 and series-resonant crystal X. The emitter is also connected to ground through bias resistor R_1. The base is connected to the parallel combination of inductor L and capacitor C_3 through dc-blocking capacitor C_4 and is forward-biased with respect to the emitter by resistors R_3 and R_4. Impedance Z could be the 220-Ω resistor shown or any small impedance that enables the extraction of the output signal through coupling capacitor C_2. If Z is a tuned circuit, it is tuned to the frequency of the crystal.

The circuit shown at the bottom of the figure is approximately equivalent, at the frequencies of interest, to the circuit shown above and can be used to determine the conditions for oscillation. The analysis of this circuit shows that the input admittance at the base includes a negative conductance and a parallel capacitive susceptance reflected from C_1 and X on the emitter side. The conditions for oscillation (zero net conductance and zero net susceptance) are approximated by

$$\frac{1}{j\omega L} + j\omega C_3 + j\omega C_1(1 + \omega_t R_x C_1) \quad \frac{\omega^2}{\omega_t^2} = 0$$

from which

$$\frac{1}{\omega L} - \omega C_3 - \omega C_1 (1 + \omega_t R_x C_1) = 0$$

and $$Y_L - \omega^2 C_1 / \omega_t = 0$$

where ω = the angular frequency of oscillation; $\omega_t = 2\pi f_t$; R_x = the series resistance of the crystal at resonance; and Y_L = the admittance related to the total losses in the base circuit, including both the losses in inductor L and the losses in resistors R_3 and R_4.

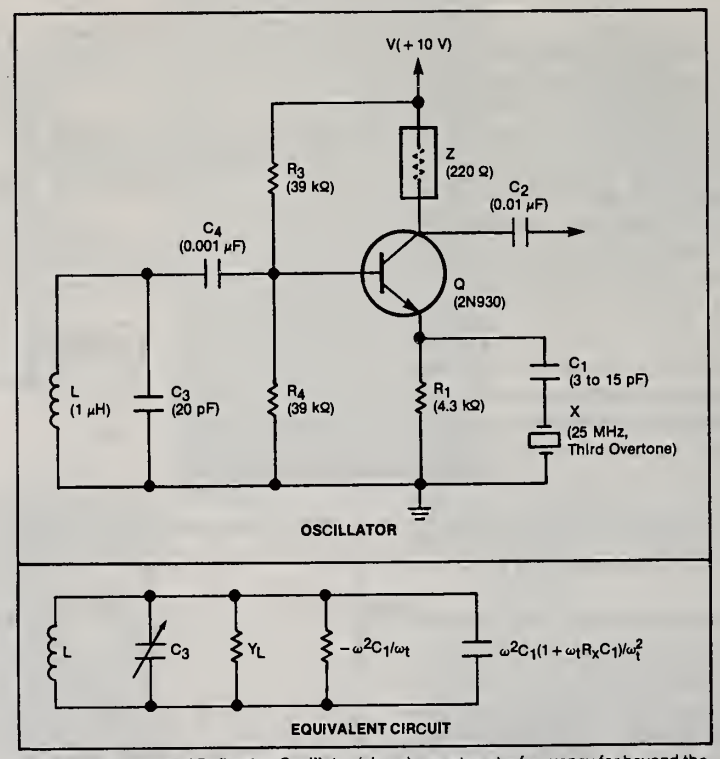

The **Crystal-Controlled Reflection Oscillator** (above) operates at a frequency far beyond the usual 3-dB rolloff frequency of the transistor. The components shown here are only representative. The equivalent circuit (below) is used to analyze the conditions of oscillation.

The second equation shows that the parallel combination of R_3 and R_4 must be selected to provide an amount of positive conductance that balances part of the negative conductance reflected from the emitter side at the frequency of oscillation. Alternatively, one can consider the oscillation to take place at the frequency for which this condition is satisfied. An approximate solution of the first equation is

$$\omega^2 = 1/L(C_3 + C_1/4)$$

This is useful in determining the approximate frequency of oscillation and the major elements that determine that frequency.

This work was done by Leonard E. Kleinberg of **Goddard Space Flight Center.**

This invention is owned by NASA, and a patent application has been filed. Inquiries concerning nonexclusive or exclusive license for its commercial development should be addressed to the Patent Counsel, Goddard Space Flight Center. Refer to GSC-13173/TN.

Goddard Space Flight Center
Technology Utilization Officer: Donald S. Friedman
Mail Code 702.1
Greenbelt, MD 20771
(301) 286-6242
Patent Counsel:
R. Dennis Marchant
Mail Code 204
Greenbelt, MD 20771
(301) 286-7351

NASA Tech Brief
National Aeronautics and Space Administration
Lyndon B. Johnson Space Center, Houston, Texas

Licensing Opportunity

Robotic Vision Would Combine Optics and Microwaves

Information on the shapes of objects would be more complete.

A conceptual robotic-vision system would process the data from both microwave and visible-wavelength sensors. The concept, called "fusion of sensors," would yield better information on the shapes of some objects than could be obtained from one type of sensor alone. For example, when a shiny, metallic object is illuminated by the Sun or a point light source against a dark background, specular reflections from points or lines on the object can overload the visible-light sensors, thereby effectively obscuring the view of less-reflective parts. In such a case, the specular reflections could be used to locate the object, while information about the gross features and orientation of the object might still be obtained by analyzing the scattering of microwaves from its surface.

The proposed robotic-vision system would fuse data from television images with polarized low-resolution radar-scattering cross sections. Using an iterative procedure, the system would generate successive approximations to the shape of the target by minimizing the differences between the observed radar returns and the radar returns that would be observed if the object were characterized by a computed scattering transfer matrix.

Assuming that the object is a perfect electrical conductor, the scattering of microwaves can be calculated by numerical integration of terms involving phased vector surface-current densities as functions of a set of parameters that describe the surface. In one version of the iterative procedure (see figure), the surface currents would be found from an initial estimate of the surface from visual data, then used to make an initial estimate of the radar scattering. The computed and actual scattering data would then be compared, and the differences would be used to refine the parameters of the surface from the initial estimate. The process would be repeated until the visible and microwave-derived estimates of the surface converged.

In a proposed test of the system, radar cross sections would be obtained from various surfaces at various frequencies and attitudes. Each surface should be smooth, contain at most one specular point, and be easy to model on a computer. The surface should be covered with a conductive material of thickness much greater than its skin depth at the microwave frequency of interest. Target shapes that lend themselves most readily to this type of investigation include spheres, ellipsoids, paraboloids, and hyperboloids.

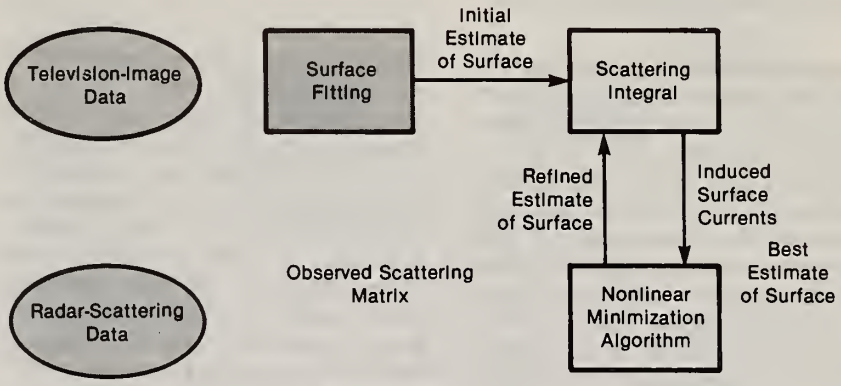

The **Robotic-Vision System** would integrate the information from television and radar images to reconstruct a three-dimensional image of the object.

This work was done by Kuma Krishen of **Johnson Space Center** *and Scott Shaw and Rui J.P. deFigueiredo of Rice University.*

This invention is owned by NASA, and a patent application has been filed. Inquiries concerning nonexclusive or exclusive license for its commercial development should be addressed to the Patent Counsel, Johnson Space Center. Refer to MCS-21334/TN.

Lyndon B. Johnson Space Center
Technology Utilization Officer: Dean C. Glenn
Mail Code IC-4
Houston, TX 77058
(713) 483-3809
Patent Counsel: Edward K. Fein
Mail Code AL3
Houston, TX 77058
(713) 483-4871

FOR ADDITIONAL INFORMATION: *Contact: Director, Technology Transfer Division, P.O. Box 8757, BWI Airport, MD 21240; (301) 621-0100 Ext. 241*
REFER TO THE NUMBER LISTED AT THE END OF THIS ARTICLE

NASA Tech Brief
National Aeronautics and
Space Administration

SEU in an Advanced Bipolar Integrated Circuit

Vulnerability to SEU varies with size and applied current.

A report summarizes an investigation of single-event upsets (SEU) (changes in logic states caused by cosmic rays and the like) in a bipolar integrated-circuit set of flip-flops (memory cells). The device to be tested was made by the advanced digital bipolar silicon process of Honeywell, Inc. The device was a circuit chip containing 4 cells: a minimum-geometry cell (linear scale 1×) and 3 cells of linear scale 2×, 4×, and 10× (areal scales of 1×, 4×, 16×, and 100×, respectively). The emitter areas ranged from 2 square microns for the minimum geometry (IX) device to 200 square microns for the 10× device. This construction enabled the study of the effect of size on SEU behavior. In addition, each cell was externally biased so that the effect of bias current (or, equivalently, power) on SEU behavior could be studied.

In one series of tests, the device was irradiated with 250-MeV bromine ions. The resulting data show that these high-stopping-power ions result in the collection of charge far in excess of the critical charge for SEU (Q_C). This is manifested by the large SEU cross sections in excess of the areas of the buried layers in the device. This behavior indicates that even ion tracks that hit in the substrate area surrounding the buried layer area can cause SEU by the diffusion of charge to the junctions of the substrate and buried layers.

As the cell current (I_{CELL}) was increased above 40 μA, the SEU cross sections of the 1× and 2× cells decreased, as expected, due to the increase in Q_C. However, the cross sections of the 4× and 10× cells increased for I_{CELL} above 80 μA on account of the saturation of the large transistors, which caused the response times to increase, thereby allowing ion-generated charge to be collected by diffusion for a longer time.

Another series of tests involved irradiation with 150-MeV iron ions. The most striking feature of the data from these tests was a dramatic decrease in the SEU cross section of the 10× cell at increasing values of I_{CELL} above 65 μA. At I_{CELL} below 65 μA, the SEU cross section of the 10× cell approached the area of the buried layer. This indicates that any ion track that intersects the junction of the buried layer and the substrate will cause SEU. As I_{CELL} is increased, ion tracks must inject charge into the base or the emitter as well as the substrate/buried-layer junctions to cause SEU. The SEU cross section continues to decrease to less than one-tenth the emitter area at I_{CELL} = 200 μA. In the 1×, 2×, and 4× cells, the SEU cross sections decreased slightly with increasing I_{CELL}, their values converging on the areas of the buried layer for each device.

A third series of tests was conducted with 100-MeV oxygen ions. SEU was not observed in the 10× cell. The other cells exhibited decreases in the sensitivity to SEU with increasing I_{CELL}. The SEU cross section of each device fell sharply with increasing I_{CELL} above 50, 100, and 150 μA in the 4×, 2×, and 1× cells, respectively.

The results of this study provide important information for the optimal design of devices fabricated using a buried-layer bipolar process that must operate in heavy-ion SEU environments. Designers can use this information to provide required levels of suppression of SEU in specific applications via combinations of size and/or cell-current (or power) scaling.

This work was done by John A. Zoutendyk and Elaine C. Secrest of Caltech and Dale F. Berndt of Honeywell, Inc., for **NASA's Jet Propulsion Laboratory**. *"Increasing Resistance of Bipolar IC's to Radiation-Induced SEU's by Increasing Power."*
NPO-17553/TN

FOR ADDITIONAL INFORMATION: *Contact: Director, Technology Transfer Division, P.O. Box 8757, BWI Airport, MD 21240; (301) 621-0100 Ext. 241*
REFER TO THE NUMBER LISTED AT THE END OF THIS ARTICLE

NASA Tech Brief
National Aeronautics and Space Administration
NASA's Jet Propulsion Laboratory, Pasadena, California

Vector Adaptive/Predictive Encoding of Speech

Vector quantization enhances the quality of digitally transmitted speech.

The vector adaptive/predictive technique for the digital encoding of speech signals yields decoded speech of very good quality after transmission at a coding rate of 9.6 kb/s and of reasonably good quality at 4.8 kb/s. The vector adaptive/predictive technique requires 3 to 4 million multiplications and additions per second. It combines the advantages of adaptive/predictive coding, which performs very well but only at rates above 16 kb/s, and code-excited linear prediction, which yields speech of high quality but requires 600 million multiplications and additions per second at an encoding rate of 4.8 kb/s.

The basic idea of this technique is (1) to approximate each vector of speech samples for transmission by using each of the N code vectors stored in a vector quantization (VQ) "codebook" (actually an electronic memory that contains the code) and (2) to use the transmitted code vectors to excite a time-varying synthesis filter in the receiving decoder. In the encoder (see figure), the sampled speech waveform is first buffered and partitioned into frames, each of which contains several vectors of speech samples. Pitch-predictive analysis and linear-predictive-coding (LPC) analysis are then performed for each frame. The pitch period, the gain G, the pitch predictor, and the LPC predictor are determined in the analyses, and they are quantized and reset every frame. A perceptual-weighting filter based on the short-term spectral envelope of speech is used to help determine, the code vector that minimizes the perceptual distortion between the coded speech and the original speech. The perceptual-weighting filter is also reset every frame, but it is not quantized because the decoder does not need it.

At the beginning of each frame, N zero-state response vectors are computed and stored in a zero-state-response codebook. These N zero-state response vectors are obtained by setting the memory of the encoder LPC synthesis filter and the perceptual-weighting filter to zero and then exciting these cascaded filters by using one code vector at a time. In encoding each speech vector s_n within the frame, the zero-input response vector of the cascaded filter (the ringing from previous vectors) is first computed. Then, the pitch-predicted vector $\hat{s}_n$ is substracted from s_n, and the difference vector d_n is passed through the perceptual-weighting filter. The zero-input response vector is then subtracted from the filtered difference vector f_n, and the resulting vector v_n is compared with the N stored zero-state response vectors.

The index of the zero-state response

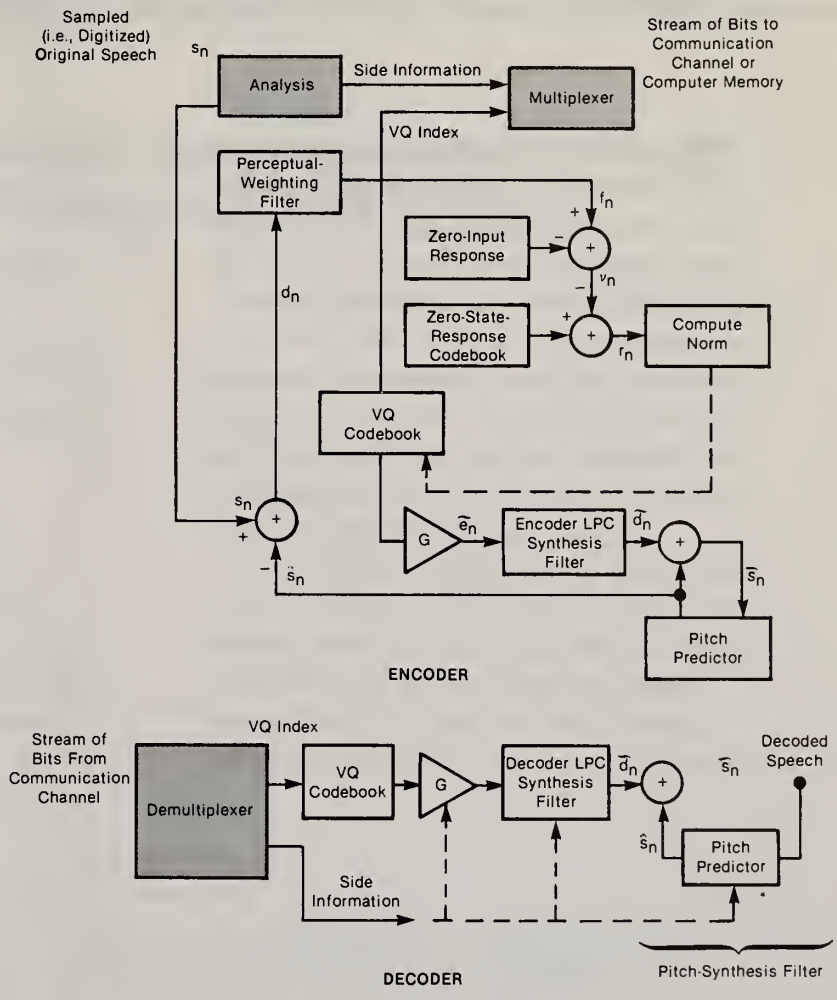

The Vector Adaptive/Predictive Coding Technique bridges the gaps in performance and complexity between adaptive/predictive coding and code-excited linear prediction.

vector that is closest to v_n identifies the best code vector in the VQ codebook. The best code vector is used to excite the LPC synthesis filter to generate $\tilde{d}_n$, which is used by the pitch predictor for following speech vectors. The index of the best code vector is combined with the side information (which specifies the pitch, the gain, and the two predictors) in the multiplexer. The resulting stream of bits is transmitted over a communication channel or stored in computer memory.

In the decoder, the stream of bits is first demultiplexed to separate the VQ index and side information. The VQ index is used to extract the corresponding code vector from the duplicated VQ codebook in the decoder, and the code vector is used to excite the decoder LPC synthesis filter and the pitch-synthesis filter. The output of the pitch-synthesis filter is the coded speech, which is perceptually close to the original speech.

This work was done by Juin-Hwey Chen and Allen Gersho of the University of California, Santa Barbara, for **NASA's Jet Propulsion Laboratory.**
NPO-17230/TN

FOR ADDITIONAL INFORMATION: *Contact: Director, Technology Transfer Division, P.O. Box 8757, BWI Airport, MD 21240; (301) 621-0100 Ext. 241*
REFER TO THE NUMBER LISTED AT THE END OF THIS ARTICLE

Department of Energy

Technology Application

Oak Ridge National Laboratories

Demodulation Circuit for AC Motor Current Signature Analysis

Motor current signature analysis (MCSA) diagnoses mechanical problems in equipment driven by electric motors by capturing, processing, and analyzing the electrical signals generated by the motor. This technology, developed at ORNL, is currently available for licensing from Energy Systems. In applying MCSA to ac-motor-driven equipment, one of the issues faced was how to deal with the 60-Hz line frequency and its harmonics.

Because of their magnitudes, the 60-Hz frequency and its harmonics dominate the frequency spectrum of any signal detected in the power line feeding the electric motor. In the original development of MCSA, this problem was solved by effectively demodulating the desired signal from the 60-Hz carrier by means of an rms-to-dc converter. However, because of the characteristics of this detection device, it also acted as a low-pass filter, partially suppressing the desired frequencies near and above 60 Hz.

An improvement to the existing demodulation technique, which provides a higher measurement resolution and sensitivity, has been developed for application to MCSA. This technique uses two well-known detection methods: amplitude and phase demodulation. The application of these methods to MCSA is shown in Fig. 1.

It has been found that periodic, load-induced variations in motor current signals simultaneously produce amplitude-modulation (AM) and phase-modulation (PM) effects. However, certain types of frequency sources tend to produce proportionately more of one type of modulation

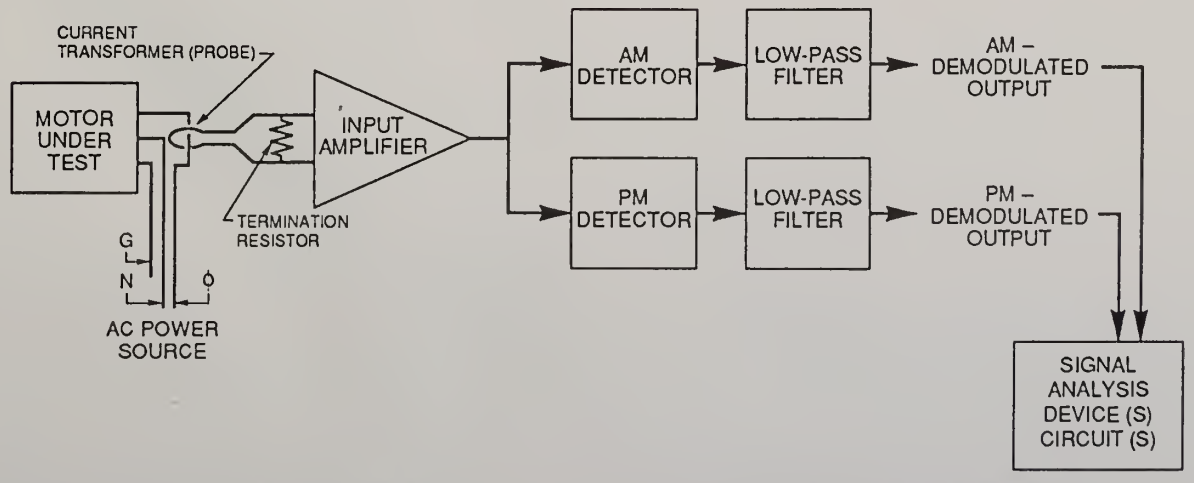

Fig. 1. Block diagram of the demodulation circuit for ac motor current signature analysis.

than the other. For that reason, both AM and PM detectors are provided in this design for analysis and comparison. The AM demodulator can be provided in the form of integrated electronic chips or discrete element circuits. It may be one of several types, but preferably it should be a synchronous or "product" detector. The PM demodulator can be a quadrature, discriminator, FM feedback, phase-locked loop, or pulse-counting/pulse-width type. In addition, the use of phase demodulation can provide an instantaneous power-factor measurement for the motor if the PM detector is referenced to the applied ac line voltage rather than to the current.

This demodulation system can be implemented with standard electronic components and added onto the other spectral analysis equipment needed to implement MCSA. Although the circuit and MCSA were developed initially for monitoring motor-operated valves and compressors in gaseous diffusion uranium-enrichment plants, the techniques may be applied as well in industry for monitoring, diagnostics, trend analysis, and preventive maintenance programs for a wide variety of electrically powered devices.

"Motor Current Signature Analysis Process," Bulletin No. 608, *Technology Applications Bulletins*, Oak Ridge National Laboratory (Winter 1988).

Additional information:

Office of Technology Applications
Oak Ridge National Laboratory
P.O. Box 2008
Oak Ridge, TN 37831-6257
(815) 574-4192

Energy

0143 Occupant Evaluation of Commercial Office Lighting

0144 Lightweight Nickel Composite Electrode

0145 Protecting Fuel Cells from Drowning—Water in the fuel is extracted before it reaches the cells.

Department of Energy

Technology Application

Oak Ridge National Laboratories

Occupant Evaluation of Commercial Office Lighting

Electric lighting accounts for an estimated one-third of the energy used in commercial buildings. Lighting energy standards and design guidelines are important determinants of energy use in buildings, but because of inadequate empirical data and analysis, these standards and guidelines have been based primarily upon professional judgment. Thus, there is little assurance that recommended lighting values requiring the lowest possible energy use provide optimal user satisfaction and comfort.

A research effort was undertaken to begin developing an archival data base to aid in better understanding the relationship between measures of lighting power density and the quality of the lighting environment. Initiated by the American Institute of Architects Foundation, this research has received extensive review by members of the professional, industrial, and research communities. The results are summarized in a three-volume report published by ORNL:

- Volume 1, a description of the research methodology and a bibliography;
- Volume 2, a preliminary analysis of the data; and
- Volume 3, a data archive and a data-base management system.

The research procedure included soliciting information from occupants via questionnaires and obtaining expert judgments (for the initial buildings) from a team of four experts who walked through the buildings and evaluated the sampled work stations. These subjective responses were complemented by a series of field measurements of photometric, acoustic, and thermal conditions. Conceptually, the process was to treat the subjective responses as the qualitative measures and to compare the unit-power-density and the photometric data against these measures.

This study is considered to be preliminary in nature; with further research, it may provide informed guidance for establishing lighting standards and other policy issues. Many tentative findings emerged from the analysis. For example, one surprising finding was that lighting satisfaction tends to decrease as lighting power density increases (Fig. 1). Occupants who described their work station spaces as "dim" also tended to be dissatisfied with the lighting at their

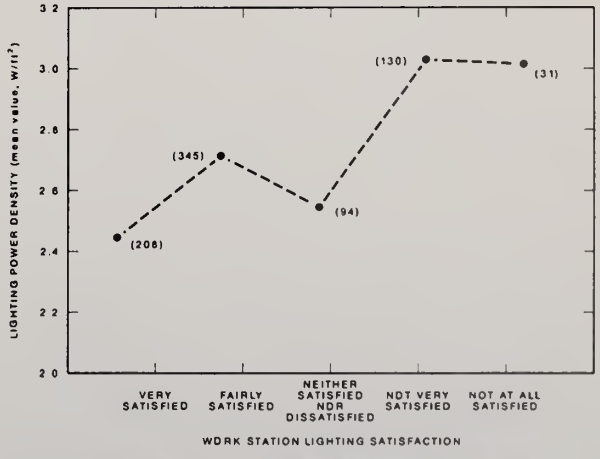

Fig. 1. Work station lighting satisfaction compared with lighting power density. (Numbers in parentheses refer to the numbers of work stations for which both lighting-power-density values and occupant responses have been recorded.)

work stations. Occupants who were most bothered by bright lights and glare were most likely to express dissatisfaction with the lighting at their work stations (Fig. 2). No relationship was found between work-related activities of employees and indicators of lighting quality.

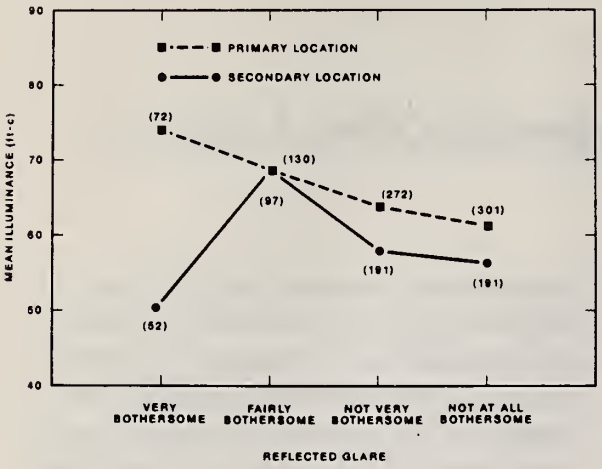

Fig. 2. Perceived discomfort from reflected glare compared with mean illuminance. (Numbers in parentheses refer to the numbers of work stations for which both lighting-power-density values and occupant responses have been recorded.)

G. Gillette and M. A. Brown (ed.), *Occupant Evaluation of Commercial Office Lighting, Volume 1: Methodology and Bibliography,* ORNL/TM-10264/V1, Oak Ridge National Laboratory (November 1986).

R. W. Marans and M. A. Brown (ed.), *Occupant Evaluation of Commercial Office Lighting, Volume II: Preliminary Data Analysis,* ORNL/TM-10264/V2, Oak Ridge National Laboratory (November 1987).

G. Gillette and M. A. Brown (ed.), *Occupant Evaluation of Commercial Office Lighting, Volume III: Data Archive and Database Management System,* ORNL/TM-10264/V3, Oak Ridge National Laboratory (August 1987).

Additional information:

National Technical Information Service
U.S. Department of Commerce
5285 Port Royal Road
Springfield, VA 22161

Telephone: (703) 487-4650; FTS 737-4650

NAVY
Domestic Technology Transfer Fact Sheet

Lightweight Nickel Composite Electrode

This product represents the results of several years of Naval Surface Warfare Center (NSWC) developmental research. A significant advance in energy storage capability of the nickel oxide electrode used in Nickel-Cadmium (Ni-Cd), Nickel-Iron (Ni-Fe), Nickel-Zinc (Ni-Zn), and Nickel-Hydrogen (Ni-H_2) cells has been achieved by the development of a porous sintered, nickel-plated graphite fiber plaque impregnated by the electrochemical process.

The electrode grid consists of a sintered mat or felt of graphite fibers, which are coated with a mixture of nickel and phosphorous. The electrode grid is strong, lightweight, and has good electrical performance.

The nickel composite electrode approach appears to offer promise for a new generation of economical, lightweight nickel alkaline battery systems.

For Additional Information:

Backup material on this effort is available from:

Navy Domestic Technology Fact Sheet Reader Reply Service
Code E211
Naval Surface Weapons Center
Dahlgren, VA 22448-5000
(703) 663-8921

Refer to 140604/TN

NASA Tech Brief
National Aeronautics and Space Administration
Lyndon B. Johnson Space Center, Houston, Texas

Protecting Fuel Cells From Drowning

Water in the fuel is extracted before it reaches the cells.

A water collector at the hydrogen inlet of a stack of fuel cells prevents moisture from "drowning" the cells; that is, condensing on them so that they can no longer function. The water collector includes an empty reservoir of the type normally used to hold electrolyte, a component that is used in considerable numbers in a fuel-cell powerplant.

The empty reservoir is placed next to a cooling plate (see figure). Water in the stream of hydrogen collects in the cooling plate. A wick carries the collected water to the reservoir. Because the reservoir is not part of any active cell, the water there does not degrade the performance of the stack.

The reservoir retains the water until it evaporates. The water does not pour out if the stack is tipped during handling.

This work was done by George T. Sulijak and Nunziato J. Maio of United Technologies Corp. for **Johnson Space Center.**
MSC-21477/TN

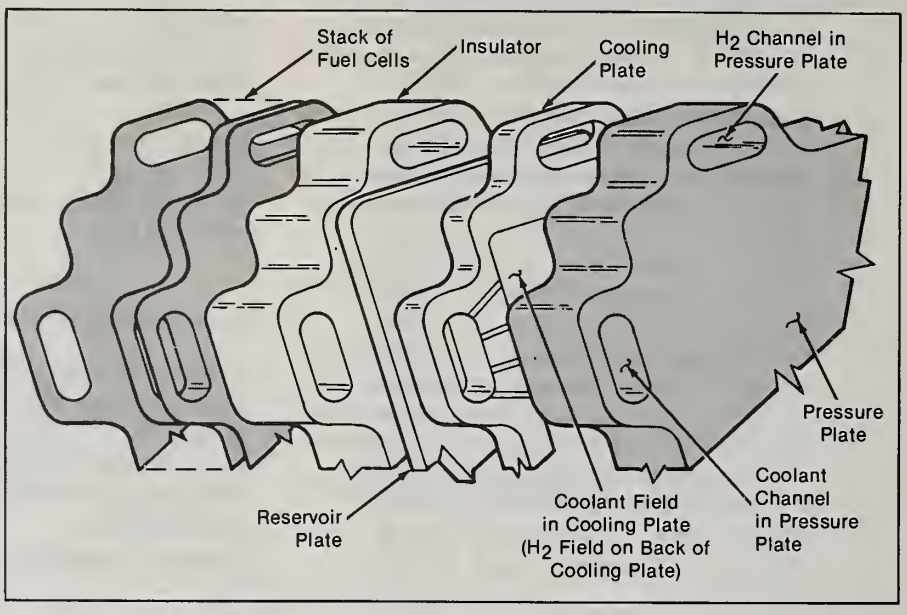
Stack of Fuel Cells
Insulator
Cooling Plate
H_2 Channel in Pressure Plate
Pressure Plate
Coolant Channel in Pressure Plate
Coolant Field in Cooling Plate (H_2 Field on Back of Cooling Plate)
Reservoir Plate

The **Stack of Fuel Cells** gets a supply of hydrogen from a manifold. The heat-exchanger plate and reservoir collect water from the flow of hydrogen. The water in the reservoir is evaporated with heat from the coolant heat-exchanger plate.

FOR ADDITIONAL INFORMATION: *Contact: Director, Technology Transfer Division, P.O. Box 8757, BWI Airport, MD 21240; (301) 621-0100 Ext. 241*
REFER TO THE NUMBER LISTED AT THE END OF THIS ARTICLE

Engineering

0146 Linear Harmonic Analysis of Free-Piston Stirling Engines

0147 Seven-Effect Absorption Chiller using Three Refrigeration Circuits (Licensing Opportunity)

0148 Reliability Studies for Compressed-Gas-Insulated Apparatus

0149 Sodium Sulfide/Ferrous Sulfate Treatment Process (Licensing Opportunity)

0150 'Standard Crack' Helps Detect Metal Fatigue in Aircraft

0151 Portland Cement Clinker Materials Available

0152 Triple-Effect Absorption Chiller using Two Refrigeration Circuits (Licensing Opportunity)

0153 Adaptive Control for Cooperative Dual Robot Arms (Licensing Opportunity)

0154 Analysis of Straight and Wavy Annular Seals (Licensing Opportunity)

0155 Adherent Thermal Barrier for Combustion Chamber

0156 Bearing-Bypass Loading on Bolted Composite Joints

0157 Mathematical Models of Turbulence in Transonic Flow—Predictions of several models are compared with well-documented flow.

0158 Mechanical Device Traces Parabolas

0159 Ozone/Ultraviolet-Photo-Oxidation Reactor

0160 Numerical Simulation of Turbine Rotor/Stator Interaction

0161 Rapidly-Indexing Incremental-Angle Encoder

0162 Silver Ink for Jet Printing—There are no silver particles to foul the printing head.

0163 Tamper-Resistant Secure Disposal Container

0164 Using NASTRAN to Analyze Vibrations of Rotor Blades

Software

0165 Computing Stress, Stability, and Vibration of Shells—Branched shells of revolution are analyzed by a finite-difference energy method.

Testing & Instrumentation

0166 Measuring Airflow with Digital Holographic Interferometry—Pressures on surfaces of airfoils are computed from interference fringes.

0167 Diode-Laser Doppler Velocimeter—Features include ruggedness and compactness (Licensing Opportunity)

0168 Multiple-Boundary-Condition Vibration Tests—Experiments build confidence in this emerging technique. (Licensing Opportunity)

Other Items of Interest

0171 New Calibration System Halves Gage Block Errors

0190 Predicting the Propagation of Cracks—Safe operating lives of components of structures can be estimated.

Technology Application

Oak Ridge National Laboratories

Linear Harmonic Analysis of Free-Piston Stirling Engines

Researchers in ORNL's Engineering Technology Division have developed the linear harmonic analysis (LHA) method, which provides insights into both the thermodynamics and dynamics of free-piston Stirling engines (FPSEs). Unlike a numerical approach, LHA provides a semiclosed-form solution that offers additional insights into the underlying physical processes of FPSEs and provides a solid basis for further theoretical development.

This research was based on the Sunpower RE-1000, a well-tested, well-documented commercial reference engine (Fig. 1). The RE-1000 engine contains a single power piston and a displacer sprung to the engine housing. For the current version of LHA, the working space of the engine is divided into three control volumes, and motion of the engine housing is neglected. However, LHA is not limited to such a simple representation; more control volumes or dynamic equations could be added if necessary.

Cylinder heat transfer, pressure drop, and seal leakage losses are all included in the current version of LHA. These variables are included simultaneously as part of the thermodynamic/dynamic calculations so that all of the interactions between the losses, thermal performance, and dynamic behavior are accounted for. Traditional solution methods have time-stepping integrations that can be plagued by numerical instabilities and can use large amounts of computer time. The LHA solution method accounts for the important thermodynamic losses that are coupled together in FPSEs, yet it is efficient enough for optimization studies.

Execution time for LHA is about 100 times less than the time required for an equivalent numerical integration method. Even with its

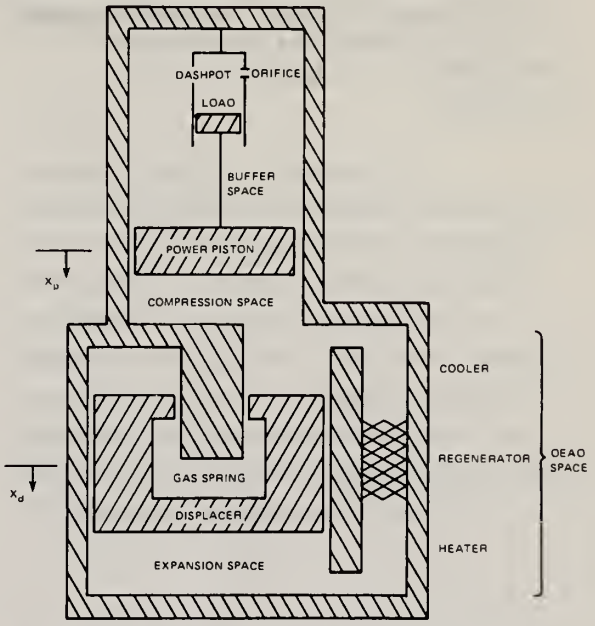

Fig. 1. Simplified schematic of a free-piston Stirling engine.

speed, LHA has sufficient mathematical accuracy for most practical Stirling engine applications. The mathematical accuracy of the LHA assumptions was verified by independently solving the same nonlinear equations using a numerical integration method and comparing the results. The differences between the LHA and numerical predictions were less than 5% for all important parameters, which is about equal to or less than the uncertainty associated with typical Stirling engine experimental measurements. This combination of computational speed and mathematical accuracy makes LHA ideal for FPSE optimization programs.

LHA also has advantages over other linear closed-form solution methods that have been developed for FPSE dynamic problems. All previously published closed-form solutions are second-order analyses in which the losses are

treated separately. LHA method is a third-order analysis where the losses, as well as their interactions, are included intrinsically in the FPSE dynamic solution.

N. C. J. Chen, F. P. Griffin, and C. D. West, *Linear Harmonic Analysis of Stirling Engine Thermodynamics*, ORNL/CON-155, Oak Ridge National Laboratory (August 1984).

N. C. J. Chen and F. P. Griffin, *Linear Harmonic Analysis of Free-Piston Stirling Engine Thermodynamics*, ORNL/CON-172, Oak Ridge National Laboratory (June 1986).

N. C. J. Chen, F. P. Griffin, and C. D. West, "Linear Harmonic Analysis for Stirling Machines and Second Law Analysis of Four Important Losses," pp. 1973-81 in *19th Intersociety Energy Conversion Engineering Conference*, Vol. 3, American Nuclear Society, San Francisco, Aug. 19-24, 1984.

Additional information:

Office of Technology Applications
Oak Ridge National Laboratory
P.O. Box 2008
Oak Ridge, TN 37831-6257
(815) 574-4192

Department of Energy

Technology Application

Oak Ridge National Laboratories

Seven-Effect Absorption Chiller using Three Refrigeration Circuits

The seven-effect absorption chiller is a concept currently being studied at ORNL. This new absorption chiller design, which uses three refrigerant circuits (Fig. 1), can be used as an absorption cycle for air-conditioning. Various configurations of this cycle are also possible that would provide heat during the winter.

Absorption refrigeration cycles are heat-operated cycles in which a primary fluid (refrigerant) in a gaseous state is absorbed by a secondary fluid (the absorbent). This absorbent/refrigerant combination is known as a solution pair. The unique feature of the seven-effect chiller is that three thermally coupled single-effect absorption cycles operate to effectively use heat input seven times, thereby increasing efficiency substantially. It is not possible to use the same solution pair for all three single-effect cycles; different solution pairs can be selected to maximize efficiency.

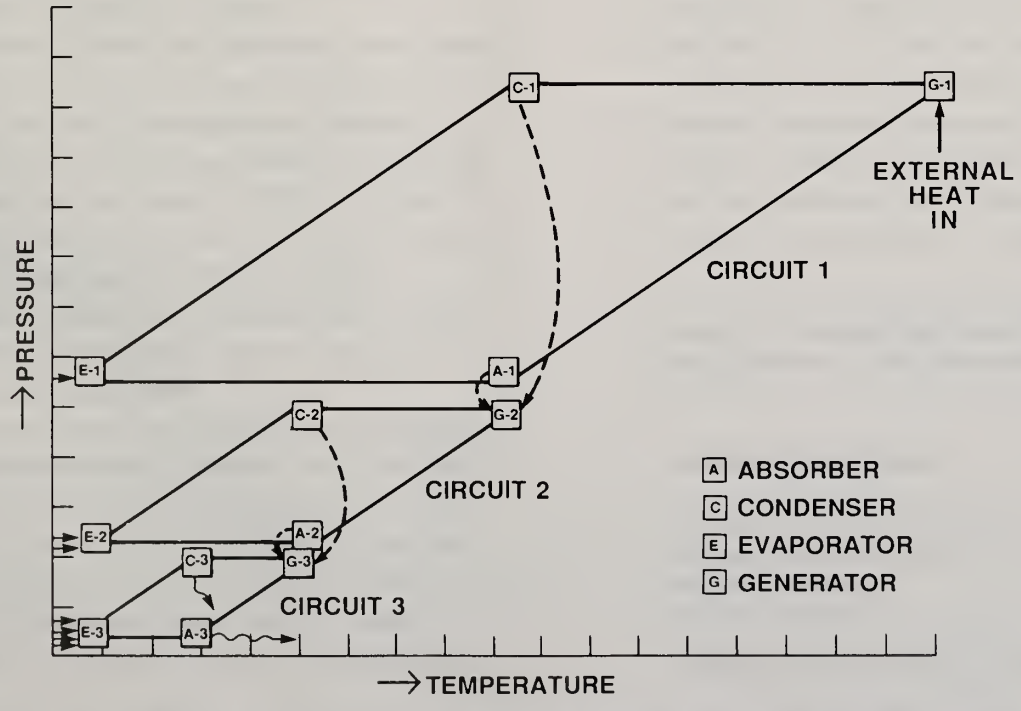

Fig. 1. The seven-effect absorption cycle. A heat exchanger transfers reject heat from the condenser and absorber from circuit 1 to circuit 2 and from circuit 2 to circuit 3. This concept produces 1 unit of refrigeration effect in the high-temperature evaporator (circuit 1), 2 units in the medium evaporator (circuit 2), and 4 units in the lower evaporator (circuit 3), yielding a total of 7 units of refrigeration effect for 1 unit of external thermal energy.

Because of its higher efficiency, the seven-effect system would use less than 50% of the primary energy needed to drive the best air-conditioning systems now available. This new concept offers the potential of an improved coefficient of performance (COP), the measure of efficiency given by the ratio of heat energy extracted for cooling (or heat added for heating) to the work needed to operate the cycle. The COP for the seven-effect absorption chiller is in the range 2.19 to 3.12. By comparison, the COP of a single-effect absorption cycle is typically 0.5 to 0.7. More-efficient double-effect and dual-loop cycles both have about the same COP (1.0 to 1.2).

No further documentation is available for this technology.

Additional information:

Office of Technology Applications
Oak Ridge National Laboratory
P.O. Box 2008
Oak Ridge, TN 37831-6257
(815) 574-4192

Oak Ridge National Laboratories

Reliability Studies for Compressed-Gas-Insulated Apparatus

Compressed sulfur hexafluoride gas (SF_6) is currently being used by the utilities industry as electrical insulation in high-voltage electrical apparatus. Compressed-gas insulated equipment is relatively new in electric-power technology. Consequently, long-term performance data and discriminating test procedures for these devices are somewhat lacking. Bases for comparison among manufacturers are sometimes difficult, and better information about the mechanisms, processes, and rates for low-voltage failures is needed. The uncertain reliability of compressed-gas-insulated apparatus has been cause for concern to the utilities industry.

Reliability studies and experiments were carried out for DOE's Office of Energy Storage and Distribution at the Massachusetts Institute of Technology's High-Voltage Research Laboratory, partially with the support of ORNL's Energy Division staff. This project had four broad goals: identify processes important to insulator reliability, model these processes, verify model concepts, and establish criteria for equipment design and specification.

These studies have provided basic information about low-probability insulation failures and have quantified the failures sufficiently to form the basis for improving insulator designs. They have also provided utilities with a means to better assess the expected performance of specific equipment. For example, factors important to reliability in compressed-gas-insulated apparatus can now be better modeled. Low-probability failures are better understood and more predictable as a result of this research, and recommendations have been made that can be used for improving and monitoring insulator reliability.

Results of the investigations are summarized in the ORNL report, *Research Factors That Affect the Reliability of Compressed Gas Insulated Apparatus*. This report contains a description of a reliability model, descriptions of the experimental apparatus, procedures and results for high-voltage tests of gas gaps and insulator surfaces, and the results of a full-scale application that combined the concepts developed during the gas-gap breakdown and surface flashover studies. In addition, a collection of journal articles that were generated by this research are reprinted as appendixes to this report.

C. M. Cooke et al., *Research on Factors That Affect the Reliability of Compressed Gas Insulated Apparatus,* ORNL/Sub/80-7979, Oak Ridge National Laboratory (July 1986).

Additional information:

National Technical Information Service
U.S. Department of Commerce
5285 Port Royal Road
Springfield, VA 22161

Telephone: (703) 487-4650; FTS 737-4650

Department of Energy

Technology Application

Idaho National Engineering Laboratory

Sodium Sulfide/Ferrous Sulfate Treatment Process

How to reduce the amount of waste and amount of money spent in disposing of the wastes in the electroplating industry? And, how to assist similar industries that produce an aqueous metal bearing waste stream, e.g., metal finishing, tanning, acid mine drainage, shipyards, and the automotive and aircraft industries?

The Sodium Sulfide/Ferrous Sulfate Treatment Process (SS/FS) invented by scientists at the Idaho National Engineering Laboratory (INEL) is one state-of-the-art answer to the problem.

In a full scale test at an electroplating industry waste treatment plant mentioned above, SS/FS reduced the yearly amount of sludge to 186 tons - a decrease of 94%. It also resulted in a 40% reduction in the amount of chemicals used; allowed reuse of treated water without the added cost of a softening cycle; met or exceeded all of EPA's latest requirements; and utilized most existing waste treatment system components. The previous chemical treatment and sludge disposal costs were $848,692. The SS/FS system cost $193,535, direct savings of $655,157. Paybacks of 6 months to 1 year are possible using the SS/FS treatment system.

The SS/FS system removes the hazardous metals, and recovers and recycles the waste water - thus reducing both disposal and feed water costs. In areas where water and land are at a premium, e.g., California and Hawaii, this represents a major breakthrough.

Typical metals removed by SS/FS include chrome, cadmium, zinc, lead, copper, and mercury. SS/FS can be used to clean up industrial waste sites such as settling ponds, dump sites, and other polluted areas far removed from the industrial site where the waste is being produced. Future applications can assist in cleaning up rivers and streams polluted with heavy metals as a result of mining and industrial processes. A "zero discharge" concept for all metals precipitation processes is being developed in conjunction with SS/FS.

The present SS/FS system is an in-line chemical treatment process that removes heavy metals from industrial waste water streams. It can be operated in either batch or continuous modes. SS/FS uses sodium sulfide, ferrous sulfate, a cationic polymer, and anionic polymers to precipitate out the heavy metals. An ultrasonic precipitation phase reduces the required chemicals and increases the efficiency of the treatment process while saving money. Many existing systems can be adapted to use SS/FS with substantial cost savings resulting from use of some components already in place.

FOR ADDITIONAL INFORMATION: Contact Jack G. Peterson, Idaho National Engineering Laboratory, P.O. Box 1625, Idaho Falls, Idaho 83415; (208)526-2893. Refer to DOE/INEL-049/TN.

NIST Technology Update

National Institute of Standards & Technology
(Formerly the National Bureau of Standards)
U.S. Department of Commerce, Gaithersburg, MD 20899

"Standard Crack" Helps Detect Metal Fatigue in Aircraft

A "standard crack" recently developed at the National Institute of Standards and Technology can help the airline industry do a better job of testing for metal fatigue in aircraft. The importance of testing aircraft for metal fatigue has been underscored by recent events, such as the Aloha Airlines fuselage that partially ripped open in flight last year. Eddy current testing is the method most often used to detect the cracks, normally invisible to the naked eye, that lead to this kind of failure. This type of testing uses an energized coil of wire to induce electrical currents in metals. These currents, which are affected by fatigue cracks, are monitored, and an interpretation is made as to the absence or presence of a defect and its extent.

A difficulty of the eddy current technique is the lack of samples of well-defined "flaws" that accurately simulate fatigue cracks. These are necessary to calibrate accurately eddy current instruments and to provide base data for interpreting test results.

Now engineers at the NIST Boulder, Colo., laboratories have invented a technique for producing artificial flaws of known sizes which can be used to calibrate test equipment.

The NIST Office of Standard Reference Materials in Gaithersburg, Md., will sell 3-inch by 2-inch blocks of metal containing these standard defects. The initial offerings will be research prototypes which should be available this summer.

"There is the potential for enormously wide application of these blocks," says Frederick R. Fickett, leader of the research group that designed the "standard crack." Virtually every segment of the transportation industry is concerned about fatigue cracking of metal; nuclear reactor operators also are interested.

Thomas E. Capobianco, a NIST engineer, developed the technique. In simplest terms, Capobianco softens a ¾-inch-thick piece of metal (in this case aluminum alloy 7075-T6) by heating it, notches it to a known length and depth with an indenting tool, and compresses the metal in the direction perpendicular to the notch until the notch "disappears" at the surface. " The beauty of this technique," says Capobianco, "is that by using an indenting tool to make the notch, we can make the geometry of the cracks anything we want. We can make them look like fatigue cracks of any configuration and still know their dimensions."

Capobianco will oversee production of the research materials and ensure their quality control. "We may not manufacture them entirely ourselves but we will measure their properties and customers will be getting a carefully characterized product," he says.

Purchase inquiries should be made to the Office of Standard Reference Materials, NIST, B311 Chemistry Building, Gaithersburg, MD 20899, or call 301/975-2012.

NIST Technology Update

National Institute of Standards & Technology
(Formerly the National Bureau of Standards)
U.S. Department of Commerce, Gaithersburg, MD 20899

Portland Cement Clinker Materials Available

Producers of Portland cement have three new cement clinker reference materials (RMs) for assessing the quality of materials during processing. Portland cements produced in the United States are evaluated by ASTM C150, "Standard Specification for Portland Cement" comprising chemical composition, fineness, and performance in physical tests. The materials selected for the RMs differ widely in phase abundance, crystal sizes, and distribution crystals. The phase abundances in weight percent, in RMs 8486, 8487, and 8488, respectively, are 58.47, 73.39, and 64.97 alite; 23.18, 7.75, and 18.51 belite; 1.15, 12.09, and 4.34 aluminate; and 13.68, 3.27, and 12.12 ferrite; along with concentrations of free calcium/oxide, periclase, and alkali sulfate. The phases were determined by point counting using reflected light microscopy. The other properties were determined by chemical analysis. Each RM consists of three hermetically sealed glass vials with approximately 10 grams of crushed clinker.

FOR ADDITIONAL INFORMATION: For information on RMs 8486, 8487, and 8488, available for $96 each, contact the Office of Standard Reference Materials, NIST, B311 Chemistry Bldg., Gaithersburg, Md. 20899; telephone: 301/975-OSRM(6776).

Department of Energy

Technology Application

Oak Ridge National Laboratories

Triple-Effect Absorption Chiller using Two Refrigeration Circuits

In the United States, most large buildings are air-conditioned using electrically driven chillers. Absorption chillers, which are driven by natural gas, provide an alternative to electric chillers. However, currently available absorption chillers that use conventional single-effect and double-effect cycles are relatively inefficient compared with good electric chillers. A new, triple-effect absorption circuit using two refrigeration circuits (Fig. 1), which greatly improves cooling efficiency of absorption systems, has been designed and demonstrated with computer simulations at ORNL.

Conventional absorption chillers are not economical in most parts of the United States, but because of high foreign fuel costs and scarce electricity, single-effect and double-effect chillers are widely used and are growing in use annually elsewhere in the world. In the late 1960s, U.S. manufacturers were virtually without foreign competition for the sales of absorption chillers worldwide. However, since the early 1970s, the Japanese have been steadily improving the conventional double-effect chillers. Japanese manufacturers now dominate world manufacturing and sales of absorption chillers.

The new triple-effect absorption chiller concept developed at ORNL is calculated to be 30 to 60% more efficient than the best equivalent double-effect chiller now manufactured by the

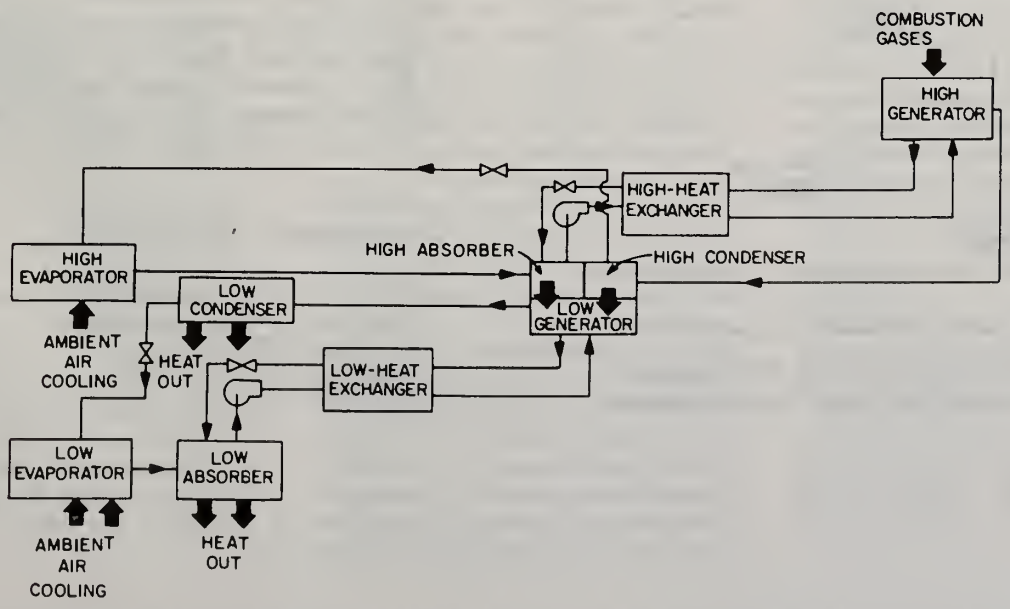

Fig. 1. Diagram of the new triple-effect absorption chiller using two refrigeration circuits.

Japanese. In addition, because the triple-effect cycle uses heat more efficiently than double-effect cycles, the total heat-exchange requirements for the triple-effect cycle are less than they are for double-effect cycles, making the triple-effect chiller potentially less expensive to build. Figure 2 shows the energy efficiencies of all existing technology compared with the triple-effect efficiency levels.

In an absorption refrigeration circuit, a primary fluid (refrigerant) in a gaseous state is absorbed by a secondary fluid (the absorbent). This absorbent/refrigerant combination is known as a solution pair. Heat absorbed by the refrigerant vapor is transferred to the absorbent and rejected by the absorbent to a heat sink. Heat from an external source is supplied to maintain the continuity of the cycle. Currently, absorption chiller designs include single-effect, double-effect, and dual-loop systems.

The cooling efficiency, or coefficient of performance (COP), of a cooling system is determined by the ratio of cooling effect to heat input. The COP of single-effect chillers is typically between 0.5 and 0.7. Performance can be improved to COPs between 0.7 and 1.25 by using the double-effect evaporation principle and a double-effect system, in which external fuel energy can be effectively used twice in the high- and low-temperature generators. The efficiency of dual-loop cycles is about the same as that for double-effect cycles in air-conditioning and refrigeration applications.

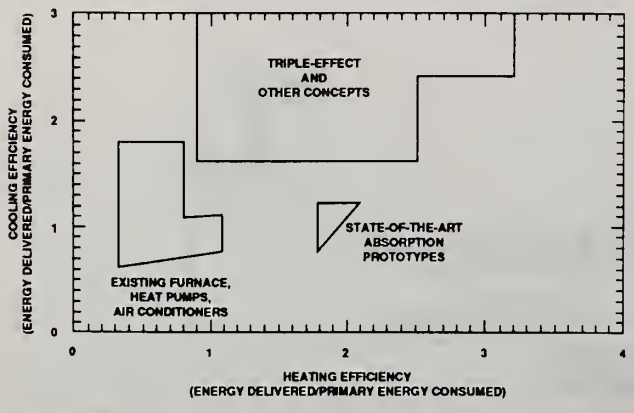

Fig. 2. Absorption cycles have been identified with performance potential well beyond current technology.

The new triple-effect absorption chiller design yields a cooling COP of about 1.7 to 1.9. Two distinct single-effect refrigeration circuits, operating at high and low temperatures, are combined to effectively use the external heat input three times. A modification to a typical refrigerant/absorbent solution pair allows the high-temperature circuit to operate at a higher temperature than can be obtained compared with conventional double-effect solutions. The reject heat of both the condenser and the the absorber of the high-temperature circuit is directed to the generator of the low-temperature circuit, thereby producing about 50% more refrigerant vapor than double-effect chillers can.

U.S. Patent Number 4,732,008 has been granted for the triple-effect absorption chiller.

R. C. DeVault, "Triple Effect Absorption Chiller Utilizing Two Refrigeration Circuits," U.S. Patent No. 4,732,008 (March 22, 1988).

R. C. DeVault, "DOE Absorption Program Overview," pp. 105-109 in *Proceedings of the 2nd DOE/ORNL Heat Pump Conference: Research and Development on Heat Pumps for Space Conditioning Applications, Crystal Gateway Marriott, Washington, D.C., April 17-20, 1988*, Oak Ridge National Laboratory, August 1988.

Additional information:

Office of Technology Applications
Oak Ridge National Laboratory
P.O. Box 2008
Oak Ridge, TN 37831-6257
(815) 574-4192

NASA Tech Brief
National Aeronautics and Space Administration
NASA's Jet Propulsion Laboratory, Pasadena, California

Licensing Opportunity

Adaptive Control for Cooperative Dual Robot Arms

Simple control strategies are derived from control strategies for single arms.

Three strategies have been proposed for the adaptive control of two cooperative robot arms. In comparison with other digital control systems that have been considered for multiple robot arms, controllers to implement these strategies would have simple structures and would be computationally fast enough for operation at high sampling rates. Dual-arm control strategies of the new type have yielded promising results in numerical simulations, and the general approach can be extended to greater numbers of arms.

The control architecture is based on the trilevel hierarchical control of two robot arms (see figure). The high level plans the task to be performed and decomposes the task into appropriate subtasks for the right and left arms. In the intermediate level, each subtask is transformed into a sequence of synchronous desired trajectories of end-effector motions and applied forces. The low level is concerned with the execution of the desired trajectories and employs feedback from the current status of the arms. In this hierarchy, the low level "achieves" the desired motion and operates in "millisecond" time scale, the intermediate level "determines" the motion desired for the subtask in "second" time scale, and the high level "plans" the subtask sequences in "minute" time scale.

Single-arm control strategies developed previously are applied at the low level of the hierarchy. In each dual-arm strategy, a suitable task-related coordinate frame of reference is chosen for both arms, and the desired motions and applied forces for each arm are expressed in this frame. Then each arm moves as though it were carrying out the commanded motion by itself in this frame. The adaptive controllers ensure that the controlled variables track the desired reference commands and reject the unwanted disturbances caused by interaction forces and torques exerted by each arm on the other arm through the load.

Jet Propulsion Lab.
NASA Resident Office
Technology Utilization Officer: Gordon S. Chapman
Mail Stop 180-801
4800 Oak Grove Drive
Pasadena, CA 91109
(818) 354-4849
Patent Counsel: Paul F. McCaul
Mail Code 180-801
4800 Oak Grove Drive
Pasadena, CA 91109
(818) 354-2734
Technology Utilization Mgr. for JPL: Norman L. Chalfin
Mail Stop 156-211
4800 Oak Grove Drive
Pasadena, CA 91109
(818) 354-2240

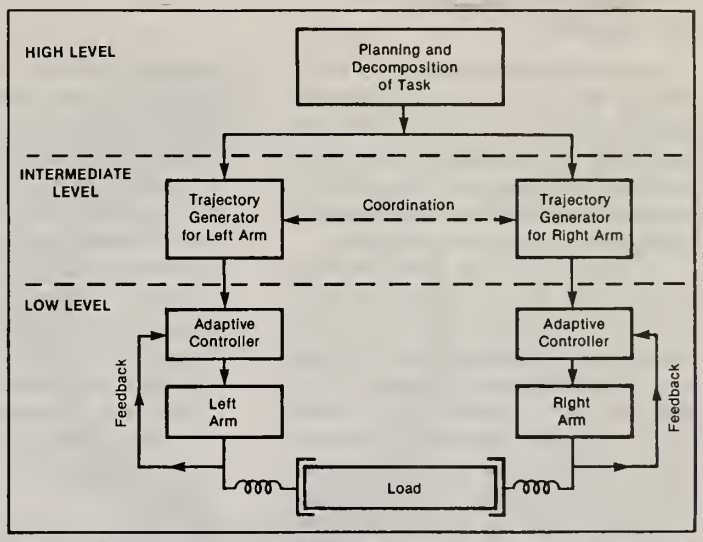

The **New Dual-Arm Control Strategies** are implemented at the low level of the control hierarchy. Each arm is operated independently under a single-arm control scheme that treats forces and torques transmitted through the load as though they were disturbances.

In the position/position control strategy, the adaptive controllers ensure that the end-effector positions of both arms track desired trajectories in Cartesian space despite unknown time-varying interaction forces exerted through the load. In the position/hybrid control strategy, the adaptive controller of one arm controls end-effector motions in the free directions and applied forces in the constraint directions, while the adaptive controller of the other arm ensures that the end effector tracks desired position trajectories. In the hybrid/hybrid control strategy, the adaptive controllers ensure that both end effectors track reference position trajectories while simultaneously exerting desired forces on the load.

In the generalization to N cooperative arms ($N > 2$), an important feature of this approach is that the overall control system is reduced to N decentralized independent single-arm controllers. Available techniques for single-arm control can be utilized directly in multiple-arm environments. The control schemes require no communication among individual controllers — an appealing feature in terms of both computation and reliability. The new control strategies do not require the knowledge of such load parameters as mass and stiffness or such dynamic parameters of the robot as the masses and inertias of links. Therefore, these strategies can cope with uncertainties or variations in the parameters. Furthermore, the complex dynamic models of the arms are not used in generating the control actions.

This work was done by Homayoun Seraji of Caltech for **NASA's Jet Propulsion Laboratory.**

Inquiries concerning rights for the commercial use of this invention should be addressed to the Patent Counsel, NASA Resident Office-JPL. Refer to NPO-17368/TN.

FOR ADDITIONAL INFORMATION: *Contact: Director, Technology Transfer Division, P.O. Box 8757, BWI Airport, MD 21240; (301) 621-0100 Ext. 241*
REFER TO THE NUMBER LISTED AT THE END OF THIS ARTICLE

NASA Tech Brief
National Aeronautics and Space Administration

Licensing Opportunity

Analysis of Straight and Wavy Annular Seals

Rotordynamic coefficients are derived.

A report presents an analysis of incompressible flow in an annular turbopump seal with a straight or radially/axially wavy (azimuthally symmetrical) surface facing the shaft. The purpose of the analysis is to quantify the effects of the waviness on the rotordynamic coefficients of the seal.

The basic equations of incompressible flow in the seal are derived by use of a control-volume model. The flow is assumed to be completely turbulent in the axial and circumferential directions with no separation and is modeled by Hirs' equations of turbulent lubrication. Linearized zeroth- and first-order perturbation equations are developed for small motion about a centered position by an expansion in the eccentricity ratio.

The zeroth-order continuity and momentum equations are solved exactly, yielding the axial and circumferential velocity components and the pressure distribution. The first-order equations are reduced to three ordinary complex differential equations in the axial coordinate. The equations are integrated to satisfy the boundary conditions and yield the perturbation pressure distribution. This resultant pressure distribution is integrated along and around the seal to yield the force developed by the seal and the corresponding dynamic coefficients.

A comparison of the rotordynamic coefficients for wavy smooth, wavy rough, straight smooth, and straight rough seals shows the following:

- A wavy seal produces less direct stiffness than does the corresponding straight seal.
- A wavy seal produces more direct damping than does the corresponding straight seal.
- A wavy seal produces more cross-coupled stiffness than does the corresponding straight seal.
- The whirl frequency is approximately the same in both of the smooth seal configurations. However, the whirl-frequency ratio of the wavy rough seal is considerably less than that of the straight rough seal.

This work was done by Joseph K. Scharrer of Rockwell International Corp. for **Marshall Space Flight Center.** *"The SSME HPFTP Wavy Interstage Seal: Part I — Seal Analysis."*

Inquiries concerning rights for the commercial use of this invention should be addressed to the Patent Counsel, Marshall Space Flight Center. Refer to MFS-29584/TN.

George C. Marshall Space Flight Center
Technology Utilization Officer: Ismail Akbay
Code AT01
Marshall Space Flight Center,
AL 35812
(205) 544-2223
Patent Counsel:
Leon D. Wofford, Jr.
Mail Code CC01
Marshall Space Flight Center,
AL 35812
(205) 544-0024

FOR ADDITIONAL INFORMATION: *Contact: Director, Technology Transfer Division, P.O. Box 8757, BWI Airport, MD 21240; (301) 621-0100 Ext. 241*
REFER TO THE NUMBER LISTED AT THE END OF THIS ARTICLE

NASA Tech Brief
National Aeronautics and Space Administration
Lewis Research Center, Cleveland, Ohio

Adherent Thermal Barrier for Combustion Chamber

An unusual fabrication process progresses from the inside outward.

A method of applying a heat-barrier coating to the interior wall of a rocket-engine combustion chamber produces a smooth coating with exceptional adherence. The essence of the method is to build the chamber wall around the barrier by electroforming, a reversal of the usual sequence of events.

In the previous method of applying a heat-barrier coating, a bond coat of nickel/chromium was applied to the interior of a chamber that was already fabricated, and a zirconia coat was plasma-sprayed on the bond coat. However, the substrate often oxidized during the application of the bond coat, and undesired compressive stress remained in the ceramic coat after the chamber returned to room temperature. In addition, the coating had a rough surface that increased the transfer of heat to the wall.

In the improved method, fabrication begins with the machining of an aluminum mandrel to the requisite cylindrical shape (see figure). The heat-barrier coating — yttria-stabilized zirconia — is plasma-sprayed on the mandrel to a thickness of 0.076 mm. A nickel/chromium layer about 0.025 mm thick is sprayed on the zirconia; this layer serves as an electrically conductive bond coat for electroplating. The assembly is then rotated continuously in a copper sulfate bath while copper is plated onto the bond coat.

Longitudinal grooves are machined into the copper layer. The grooves are filled with wax, and the assembly is returned to the plating bath, where a final layer of copper is plated overall, transforming the grooves into channels for the coolant. Finally, the wax is removed by melting, and the aluminum mandrel is etched away.

Heat-barrier coatings made by the new method were evaluated on a small rocket thrust chamber. The rocket engine was repeatedly started, run, and shut down with liquid oxygen and gaseous hydrogen as propellants and liquid hydrogen as the coolant. The testing was stopped after 1,450 cycles. The results of the tests were compared with those for an identical chamber without the heat-barrier coating.

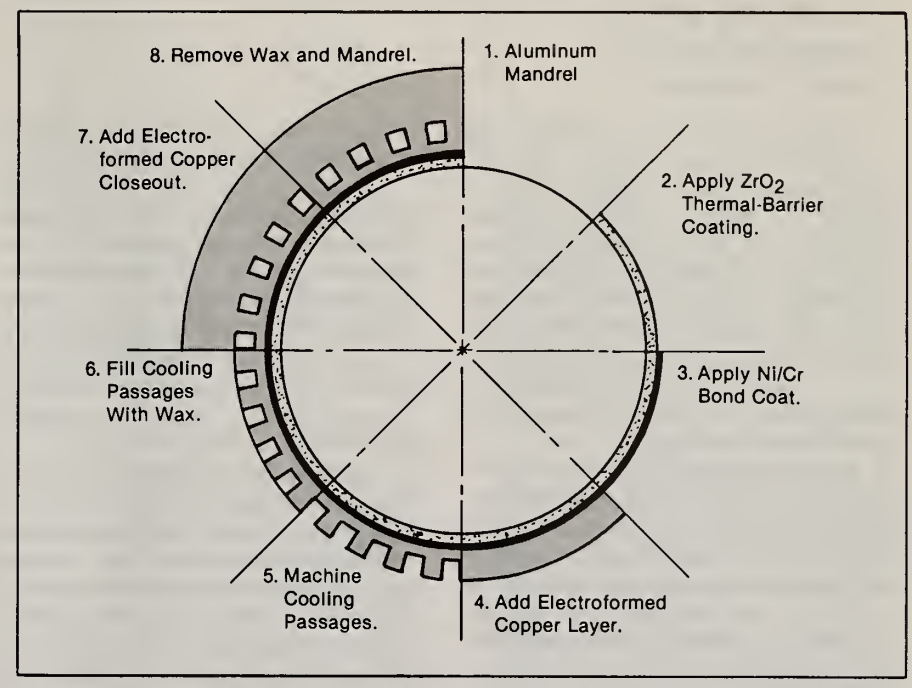
8. Remove Wax and Mandrel.
1. Aluminum Mandrel
7. Add Electro-formed Copper Closeout.
2. Apply ZrO_2 Thermal-Barrier Coating.
6. Fill Cooling Passages With Wax.
3. Apply Ni/Cr Bond Coat.
5. Machine Cooling Passages.
4. Add Electroformed Copper Layer.

Sectors of a Cross Section show how a cylindrical chamber is built. Starting with an aluminum mandrel, layers are added from the inside out.

The zirconia coat delaminated in some places in the region of low heat flux. However, the zirconia adhered well inasmuch as the delamination did not extend down to the bond coat. The coolant passages of the coated chamber retained their original sizes and shapes, and there was no apparent damage to the inner wall. In contrast, in the uncoated chamber, a crack developed in one of the coolant passages after 393 cycles, and the inner wall was deformed and thinned at the coolant passages.

The thin zirconia coating reduced the maximum operating temperature of the copper wall of the chamber from 844 to 334 K. At the lower temperature, the copper liner is stronger and undergoes less strain and thus has less tendency to distort and crack.

This work was done by Richard J. Quentmeyer of **Lewis Research Center**. *Further information may be found in NASA TM-100933 [N88-24690], Price Code: A03 "Thrust Chamber Thermal Barrier Coating Techniques."*

Copies may be purchased from the National Technical Information Service, Springfield, Virginia 22161, Telephone No. (703) 487-4650. Rush orders may be placed for an extra fee by calling (800) 336-4700.
LEW-14840/TN

FOR ADDITIONAL INFORMATION: *Contact: Director, Technology Transfer Division, P.O. Box 8757, BWI Airport, MD 21240; (301) 621-0100 Ext. 241*
REFER TO THE NUMBER LISTED AT THE END OF THIS ARTICLE

NASA Tech Brief
National Aeronautics and
Space Administration

Bearing-Bypass Loading on Bolted Composite Joints

An unexpected interaction between the effects of bypass and bearing loads is reported.

Joints of composite materials have often been designed by use of simple procedures developed for parts made of metals. In most such cases, the design strains in the affected structures have been limited by considerations of tolerance to damage, and at low levels of strain in the structures, the joints have been adequate. However, as tougher composites come into use, design strains will rise, and requirements on the joining of structures will become more stringent.

Analytical procedures for the design of joints should be based on a sound understanding of the responses of composite materials under loading conditions similar to those in multi-fastener joints. Within multi-fastener joints, fastener holes may be subjected to both bearing loads and loads that bypass the holes. The ratios of the bearing loads to the bypass loads depend on the stiffnesses and configurations of the joints.

As a joint is loaded, this bearing-bypass ratio at each fastener remains nearly constant until damage begins to develop. In general, different bearing-bypass ratios produce various failure modes and a different strength for each fastener hole. Accordingly, a combined experimental and analytical study described in a NASA technical memorandum was conducted to investigate the effects of simultaneous bearing and bypass loading on a graphite/epoxy laminate.

Tests were conducted with a test machine that enables the bearing-bypass load ratio to be controlled while a single-fastener coupon is loaded to failure in either tension or compression. Each test coupon consisted of 16-ply quasi-isotropic graphite/epoxy laminate with a centrally located 6.35-mm bolt that had a clearance fit. The center of the specimen was bolted between two bearing-reaction plates that were attached to the load frame via two load cells.

The ends of the specimen were then gripped and loaded independently by upper and lower servocontrol systems. Any difference between these two end loads produced a bearing load at the central bolt hole. This bearing load was measured by the load cells under the bearing-reaction plates. The end loads were synchronized by a common input signal. As a result, a constant bearing-bypass ratio was maintained throughout each test.

Damage-onset and ultimate strengths were determined for each test case. The computed local stresses were used with appropriate failure criteria to analyze the observed failure modes and strengths. An unexpected interaction of the effects of the bypass and bearing loads was found for the onset of compression-reacted bearing damage. This interaction was caused by a decrease in the bolt-hole contact arc and a corresponding increase in the severity of the bearing loads. The amount of bolt-hole contact had a significant effect on local stresses and thus on the calculated damage-onset strengths.

An offset-compression mode of failure of the laminate was identified under compression bearing-bypass loading. This mode of failure appears to be unique to compression bearing-bypass loading and, therefore, cannot be predicted from simple tests. Therefore, there may be a need to combine predictions of laminate bearing-bypass strengths with selected bearing-bypass testing to account for the offset-compression failure mode.

These results are important in the emerging technology of composites for use in a wide range of applications. These include applications in aircraft, boats, and automobiles, in which bolted connections to composites will be increasingly important.

This work was done by John H. Crews of **Langley Research Center** *and Rajiv-Vikas A. Naik of PRC/Kentron. Further information may be found in NASA TM-89153 [N87-25437], Price Code: A03 "Bearing-Bypass Loading on Bolted Composite Joints."*

Copies may be purchased from the National Technical Information Service, Springfield, Virginia 22161, Telephone No. (703) 487-4650. Rush orders may be placed for an extra fee by calling (800) 336-4700.
LAR-14106/TN

FOR ADDITIONAL INFORMATION: *Contact: Director, Technology Transfer Division, P.O. Box 8757, BWI Airport, MD 21240; (301) 621-0100 Ext. 241*
REFER TO THE NUMBER LISTED AT THE END OF THIS ARTICLE

NASA Tech Brief
National Aeronautics and Space Administration

Mathematical Models of Turbulence In Transonic Flow

Predictions of several models are compared with measurements of a well-documented flow.

A report reviews the performances of a variety of mathematical models of turbulence in transonic flow. The predictions of these models are compared with measurements of the flow in a wind tunnel along the outside of a cylinder that has an axisymmetric bump of circular-arc cross section in a meridional plane. This review is part of a continuing effort to calibrate and verify computer codes for the prediction of transonic flows about airfoils.

The bumpy-cylinder experiment was chosen as the standard of comparison for two reasons: (1) the aerodynamic effect of the bump is similar to that of the upper surface of an airfoil, and (2) the experiment is well documented and free of both uncertainties in the angle of attack and interference from the walls of the wind tunnel. The measurements included surface pressures, mean velocities, and Reynolds stresses.

The flow about the cylinder was computed by a series of computer codes that accommodate the various turbulence models under test. The codes used an explicit second-order, predictor/corrector finite-difference algorithm modified by an efficient implicit algorithm. The computational mesh had variable spacing in the radial and axial directions. The upstream boundary conditions were uniform free-stream conditions, with the total pressure and temperature held constant and the static properties found from relationships based on the method of characteristics. Downstream, the boundary conditions were the setting of all axial gradients to zero. In all cases, the surface boundary conditions were zero velocity and nearly adiabatic wall temperature. Uniform free-stream conditions were applied at the far radial boundary.

The models tested are summarized as follows:

- The Cebeci-and-Smith turbulence model divides the boundary layer into inner and outer sublayers. In the inner sublayer, the eddy viscosity is expressed algebraically with a length scale that is the distance from the surface and with a velocity scale that is the shear velocity. In the outer sublayer, these scales are the displacement thickness and the velocity at the edge of the boundary layer.
- The model of Johnson and King also divides the boundary layer into two sublayers wherein the eddy viscosities are expressed algebraically. In the inner sublayer, the velocity scale in this model depends on the maximum shear stress within the boundary layer. This stress is found from the solution of an ordinary differential equation that represents the rate of the development of the maximum shear stress with distance along the surface. Compared to the Cebeci-and-Smith model, the Johnson-and-King model contains two additional coefficients.
- The model of Jones and Launder is an example of models that employ two additional partial differential field equations to evaluate the velocity and length scales of the turbulence, thereby allowing for the rate processes in the development in the local state of the scales of turbulence. In this model, the dependent variable in the first equation is the kinetic energy of turbulence, whereas that in the second equation is the rate of dissipation of the kinetic energy of turbulence.
- The model of Wilcox and Rubesin is similar to that of Jones and Launder in that two turbulence field equations also are employed to yield turbulence scale quantities on which to base the eddy viscosity. In this model, the variable used to develop the length scale is the rate of dissipation divided by the kinetic energy.
- Two models developed by Coakley are modified versions of the Jones-and-Launder and Wilcox-and-Rubesin models, designed to ease numerical difficulties encountered with them.

The Johnson-and-King model proved superior in predicting the transonic flow over the bumpy cylinder. However, as the authors are careful to indicate, it is generally accepted that there is no unique way of mathematically modeling turbulence in transonic flow fields, and some field-equation models with wall-function boundary conditions can be competitive with the Johnson-and-King model.

This work was done by Morris W. Rubesin and John R. Viegas of **Ames Research Center.** *"Turbulence and Modeling in Transonic Flow."*
ARC-12292/TN

FOR ADDITIONAL INFORMATION: *Contact: Director, Technology Transfer Division, P.O. Box 8757, BWI Airport, MD 21240; (301) 621-0100 Ext. 241*
REFER TO THE NUMBER LISTED AT THE END OF THIS ARTICLE

NASA Tech Brief
National Aeronautics and Space Administration
Lyndon B. Johnson Space Center, Houston, Texas

Mechanical Device Traces Parabolas

Continuous curves are generated and points located with ease.

A mechanical device simplifies the generation of parabolas of various focal lengths. The device is simple in design and easy to use because it is based on the fundamental geometric construction of the parabola. Likely applications of the device include the design of paraboloidal antennas, approximating catenaries on drawings of powerlines or long-wire antennas, and general tracing of parabolas on drawings.

The device (see figure) includes a radius track (dimension *r*) and a perpendicular focal-point track that lies along the axis (dimension *z*) of the parabola. A depth track, also aligned along the *z* direction, is joined to the radius track by a pair of back-to-back linear bearings. These bearings allow the depth track to slide along its own length or to move along the radius track, while constraining the depth and radius tracks perpendicular to each other.

A nonrotating pulley is clamped at the desired position along the focal-point track. The center of this pulley defines the focal point. A cable clamped to this pulley extends to and around a movable pulley of equal diameter on the $-z$ end of the depth track and terminates at a cable clamp on the back-to-back linear bearings on the *r* axis. The vertex of the parabola is chosen to lie at the desired focal distance, *f*, along the *z* axis below the focal point. (Alternatively, the vertex could be chosen first and the focal point located at a distance *f* along the *z* axis above the vertex.)

After the focal point and vertex are chosen, the depth track is moved near the focal-point axis and adjusted until the center of the movable pulley lies at the vertex. While the depth track remains in this position, the cable is unclamped at one end, tightened to remove slack, and then reclamped.

Thereafter, pulling downward and rightward on the depth track while keeping the cable in tension causes the center of the pulley at its end to move along the locus of points for each of which the sum of the distance to the focal point and the distance to the radius track is the total length of the clamped cable less the length of cable wrapped on the two pulleys. By definition, this locus is the parabola

$$z = (r^2/4f) - a$$

where *a* is the distance from the *r* axis to the vertex. It is not necessary to correct for the wrap of the cable on the pulleys because the total length of wrap about both pulleys remains constant as the curve is traced.

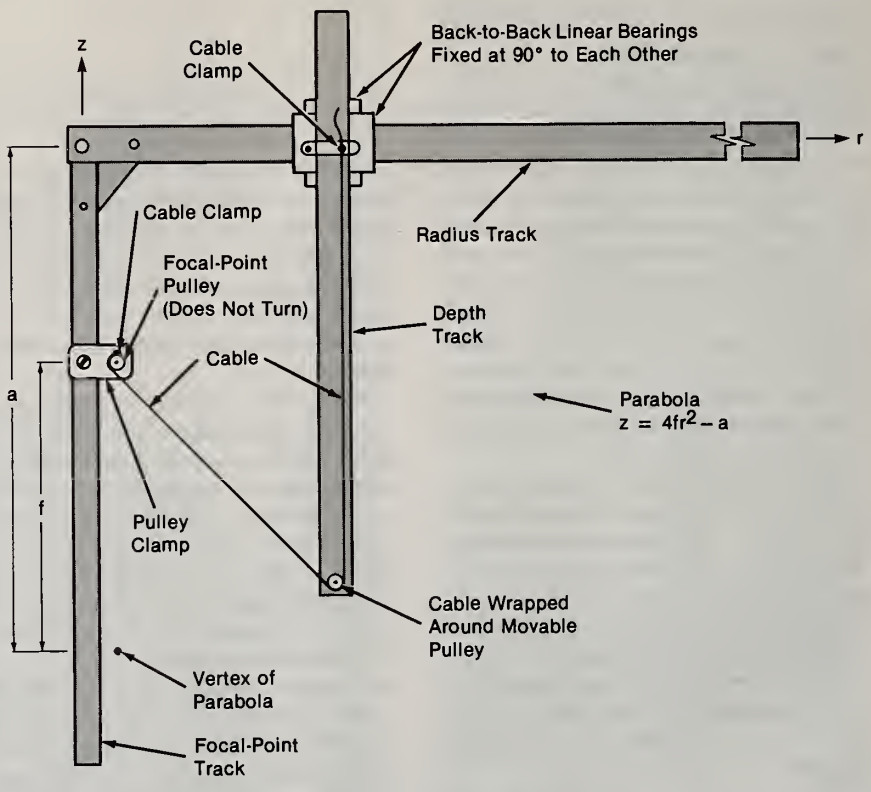

The **Parabola-Tracing Device** is based on the fundamental geometrical construction of the parabola. The constancy of the critical total distance is enforced by maintaining the cable in tension.

This work was done by Terry A. Soper of Lockheed Engineering and Management Services Co. for **Johnson Space Center.**
MSC-21421/TN

FOR ADDITIONAL INFORMATION: *Contact: Director, Technology Transfer Division, P.O. Box 8757, BWI Airport, MD 21240; (301) 621-0100 Ext. 241*
REFER TO THE NUMBER LISTED AT THE END OF THIS ARTICLE

NASA Tech Brief
National Aeronautics and Space Administration
Lyndon B. Johnson Space Center, Houston, Texas

Ozone/Ultraviolet-Photo-oxidation Reactor

Hydrazines are processed more thoroughly into harmless substances.

An experimental chemical-processing system destroys waste hydrazine in water by use of ozone in an ultraviolet-photo-oxidation reactor. The conventional process for the disposal of hydrazines is chlorination and oxidation by stirring with calcium hypochlorite in open tanks. This process emits partially oxidized compounds and chlorinated and cyclic hydrocarbons, some of which are more dangerous than the hydrazines. In contrast, the new process reduces the concentrations of hydra-

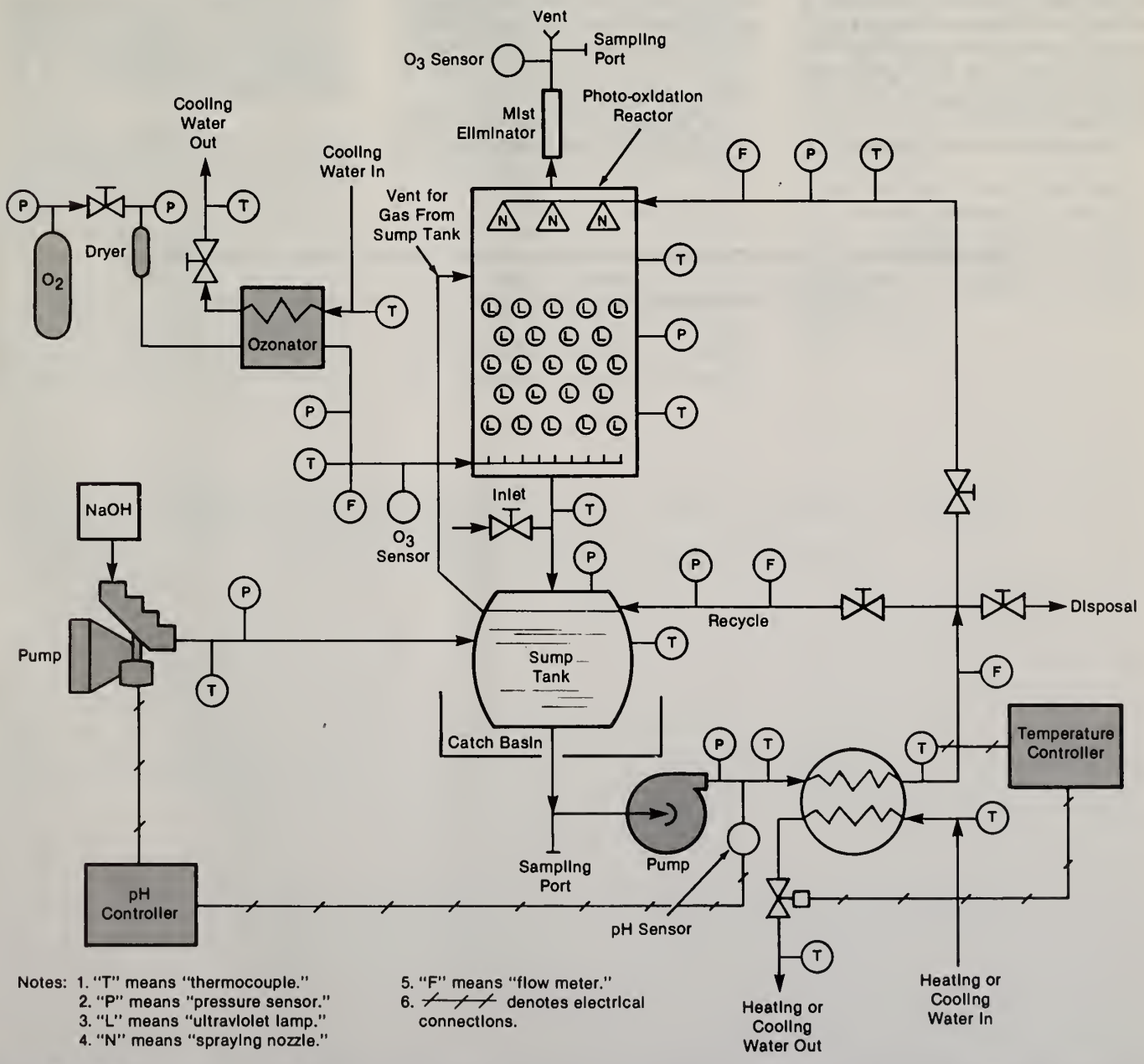

Notes:
1. "T" means "thermocouple."
2. "P" means "pressure sensor."
3. "L" means "ultraviolet lamp."
4. "N" means "spraying nozzle."
5. "F" means "flow meter."
6. ⟋⟋⟋ denotes electrical connections.

Liquid Is Sprayed in a reaction chamber past ultraviolet lamps, against a flow of oxygen and ozone. Hydrazines and intermediate decomposition products thereof are oxidized to harmless substances.

zines and intermediate decomposition products in the effluent liquid and gas to below the limit of detectability.

The batch of water containing hydrazines is circulated between a sump tank and the photo-oxidation reactor (see figure). The liquid is sprayed downward from 6 nozzles at the top of the reactor, past a bank of 23 mercury-vapor germicidal lamps that generate the ultraviolet light. A flow of oxygen containing ozone is introduced through sparging tubes at the bottom of the reactor, directed upward against the spray. The ultraviolet light excites the ozone molecules to a more reactive state. The top of the reactor is vented to the atmosphere through a stainless-steel-wire-mesh mist eliminator. The reactor chamber and many of the other components of the system are also made of stainless steel.

To generate the stream of oxygen containing ozone, oxygen from a tank is passed through a drier to eliminate contamination by moisture, then fed to a high-voltage discharge in a commercially available ozonator. The ozonator is cooled to a temperature of about 287 K (14 °C, slightly below room temperature) to increase the concentration of ozone from the manufacturer's stated figure of 2 weight percent to about 2.75 weight percent.

The effectiveness and speed of the process depend on the maintenance of the circulating liquid at the correct pH, which appears to determine the lower limit of oxidation by ozone. A pH sensor and controller maintain the pH of the basic hydrazine solution within ± 0.5 of the optimum value, which lies between 9 (for low concentrations of chlorine-oxidizable species) and 11 (for high concentrations).

The temperature of the circulating liquid is sensed and controlled because it strongly affects the process in two competing ways: higher temperature increases the rate of reaction but also hastens the dissolution and decomposition of the ozone. Which of these effects predominates depends on the concentration of the solution to be processed. The results of some experiments suggest that a higher temperature (~314 K) should be used initially because the net effect is to speed the reaction at a high concentration of chlorine-oxidizable species. Once the concentration is reduced to 2.5 ppm, a lower temperature (~286 K) favors faster and more-complete chemical reactions.

This work was done by Ari Ben Swartz and Richard E. Agthe of Lockheed Engineering & Management Services Co. for **Johnson Space Center.**
MSC-21488/TN

FOR ADDITIONAL INFORMATION: *Contact: Director, Technology Transfer Division, P.O. Box 8757, BWI Airport, MD 21240; (301) 621-0100 Ext. 241*
REFER TO THE NUMBER LISTED AT THE END OF THIS ARTICLE

NASA Tech Brief
National Aeronautics and Space Administration

Numerical Simulation of Turbine Rotor/ Stator Interaction

Unsteady effects in flows are studied.

A report describes the numerical simulation of time-varying flows around multiple rotor and stator airfoils in a turbine. Studies like this one can be helpful in improving the performance obtainable from various turbine designs and in studying unsteady effects — for example, unsteady loads on the airfoils.

The study is conducted with the help of a new computer program that can simulate the flow in a turbine stage configured with unequal numbers of rotor and stator airfoils. The program is based on the thin-layer Navier-Stokes equations of unsteady, two-dimensional flow. The region of interest is discretized with patched and overlaid grids that move relative to each other to simulate the motion of the rotor airfoils with respect to the stator airfoils. The program integrates the Navier-Stokes equations via an upwind finite-difference scheme that is spatially accurate to third order, temporally accurate to second order, and set in an iterative implicit framework.

The computer code was used to simulate subsonic flow past a turbine stage for which considerable experimental data have been collected. Numerical results are obtained for a one-rotor/one-stator configuration and for a four-rotor/three-stator configuration. The four-rotor/three-stator case had a pitch ratio much closer to that of the experimental case.

Numerical results presented include time-averaged pressures on the surfaces of the airfoils, the amplitudes and phases of the fluctuations in those pressures, and instantaneous pressure contours. The time-averaged surface pressures for the two configurations are almost identical and agree well with the experimental data. The surface-pressure amplitudes and phases calculated for the four-rotor/three-stator configuration are found to agree much better with the experimental data than do the data calculated for the one-rotor/one-stator configuration.

This work was done by Man Mohan Rai of **Ames Research Center** *and Nateri K. Madavan of Sterling Federal Systems. "Multi-Airfoil Navier-Stokes Simulations of Turbine Rotor-Stator Interaction.*
ARC-12293/TN

FOR ADDITIONAL INFORMATION: *Contact: Director, Technology Transfer Division, P.O. Box 8757, BWI Airport, MD 21240; (301) 621-0100 Ext. 241*
REFER TO THE NUMBER LISTED AT THE END OF THIS ARTICLE

NASA Tech Brief
National Aeronautics and Space Administration
Goddard Space Flight Center, Greenbelt, Maryland

Rapidly-Indexing Incremental-Angle Encoder

The absolute position can be determined after rotation through a small angle.

An optoelectronic system that measures the relative angular position of a shaft or other device to be turned can also measure the absolute angular position after the device has turned through a small angle. In contrast, a conventional optoelectronic incremental-shaft-angle encoder has to be "indexed" (that is, calibrated with respect to the absolute angle) by turning it until the index or starting angle is found; in some cases, this can require nearly a complete revolution. Thus, the new angle encoder helps to save energy and reduce wear in the bearings. Its principle of operation is also applicable to incremental-linear-position encoders.

As in a conventional encoder, the relative angular position is measured with fine resolution by optoelectronically counting finely- and uniformly-spaced light and dark areas on the encoder disk as the disk turns past the position-sensing device (see figure). However, the disk also includes a track containing coarsely- and nonuniformly-spaced light and dark areas, the angular widths of which vary in proportion to the absolute angular position. This second track provides a gating and indexing signal.

The output signals from the position sensor — one for each track — are fed to the counting circuit. The circuit counts the number of fine-increment pulses that occur during each coarse-increment pulse. This count gives a measure of the absolute angle because each coarse interval can be identified by its unique number of fine increments. Thereafter, the angle is determined to a finer resolution by counting the number of fine increments after the start of the gating signal.

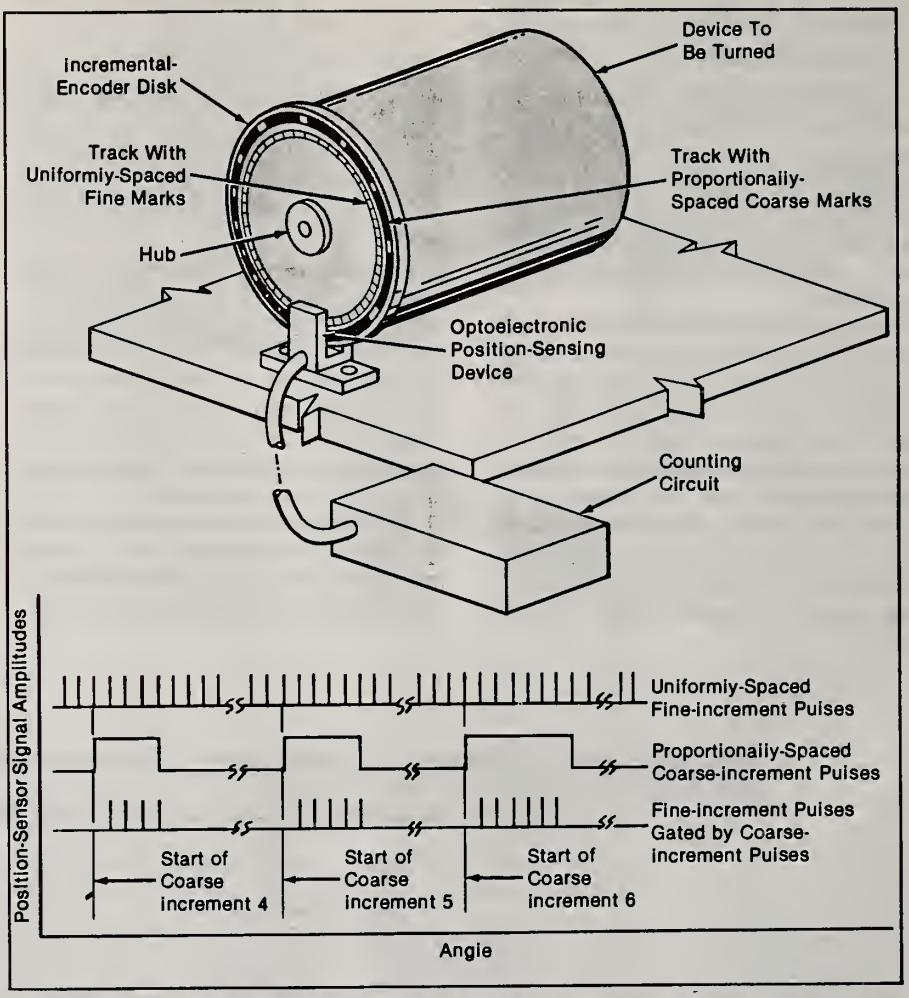

The **Number of Fine Increments in Each Coarse Increment** of angle can be counted to determine the absolute angle of the device.

This work was done by Philip R. Christon and Wallace W. Meyer of Ball Corp. for **Goddard Space Flight Center**. *No further documentation is available.*
GSC-13154/TN

FOR ADDITIONAL INFORMATION: *Contact: Director, Technology Transfer Division, P.O. Box 8757, BWI Airport, MD 21240; (301) 621-0100 Ext. 241*
REFER TO THE NUMBER LISTED AT THE END OF THIS ARTICLE

NASA Tech Brief
National Aeronautics and Space Administration
NASA's Jet Propulsion Laboratory, Pasadena, California

Silver Ink for Jet Printing

There are no silver particles to foul the printing head.

A metallo-organic ink containing silver (with some bismuth as an adhesion agent) is applied to printed-circuit boards and pyrolized in air to form electrically conductive patterns. The ink contains no particles of silver, does not have to be mixed during use to maintain homogeneity, and can be applied to the boards by ink-jet printing heads.

The ink consists of silver neodecanoate and bismuth 2-ethylhexanoate dissolved in xylene and/or toluene. In an experimental synthesis, ammonium neodecanoate soap was prepared by reacting neodecanoic acid with ammonium hydroxide; this soap was then reacted with silver nitrate, producing impure silver neodecanoate and ammonium nitrate (see figure). The silver neodecanoate was washed and dried, forming a white, powdery solid that was stored in dark bottles.

Similarly, ammonium 2-ethylhexanoate soap was prepared from 2-ethylhexanoic acid and ammonium hydroxide. The soap was reacted with a clear solution of bismuth nitrate in nitric acid. The resulting white oil of bismuth 2-ethylhexanoate was extracted in toluene or xylene and dried over molecular sieves.

To prepare the ink, the silver neodecanoate was dissolved in xylene or toluene, and the solution was assayed by thermogravimetric analysis to determine the fractional weight of silver. The bismuth 2-ethylhexanoate was analyzed similarly to determine the fractional weight of bismuth oxide produced on thermal decomposition. The two solutions were then mixed to obtain an ink that, upon thermal decomposition in air, would leave a residue of 99 weight percent silver and 1 weight percent bismuth oxide. Three drops of neodecanoic acid per 100 mL of ink were added as a stabilizer.

The viscosity of the ink was measured and adjusted to bring it into the range of 3 to 10 mPa•s. The viscosity was decreased by adding toluene or xylene, then increased by bubbling dry nitrogen through the ink to evaporate the toluene or xylene. The ink was stored in a tightly-covered amber bottle until needed.

This work was done by R. W. Vest and Saraswathi Singaram of Purdue University for **NASA's Jet Propulsion Laboratory.** *NPO-17153/TN*

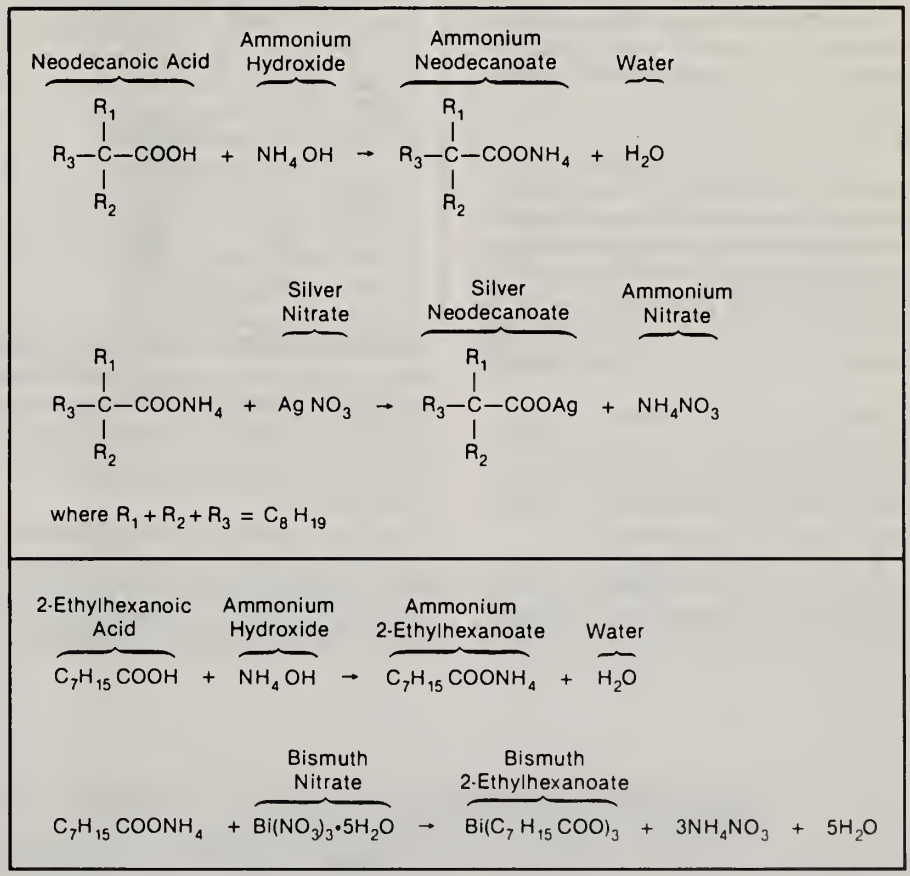

These **Two Sequences of Reactions** are used to prepare the main ingredients of the ink.

FOR ADDITIONAL INFORMATION: *Contact: Director, Technology Transfer Division, P.O. Box 8757, BWI Airport, MD 21240; (301) 621-0100 Ext. 241*
REFER TO THE NUMBER LISTED AT THE END OF THIS ARTICLE

NASA Tech Brief
National Aeronautics and Space Administration
NASA's Jet Propulsion Laboratory, Pasadena, California

Tamper-Resistant Secure Disposal Container

A closure device shuts the container when it is tipped on its front, back, or sides.

A closure device for secure waste containers prevents classified papers and other proprietary articles from being withdrawn when the container is turned on its side. In an earlier version of this device, a secure container has interdigitating combs hanging at its opening. If the container is turned upside down in an attempt to shake out its contents, the combs flop downward and mesh over the opening, preventing the contents from falling out. However, if this type of container is laid sideways, it could be vulnerable to tampering by a pair of tongs.

The new closure has a pendulum that swings a comb into its closed position when the container is turned on its side. The pendulum is suspended with its axis of rotation perpendicular to the axes of the combs (see figure). The pendulum extends through a D-shaped cam ring, that is attached to the upper comb with standoff struts.

When the container is tilted sideways, the pendulum swings along the arc side of the D-shaped ring. In so doing, it forces the cam ring aside, thereby moving the upper comb toward the closed position.

If the container is tilted forward or backward so that the combs close, the pendulum does not interfere with the comb movement. The width of the D ring accommodates the closing motion of the upper comb without engaging the pendulum on the flat side.

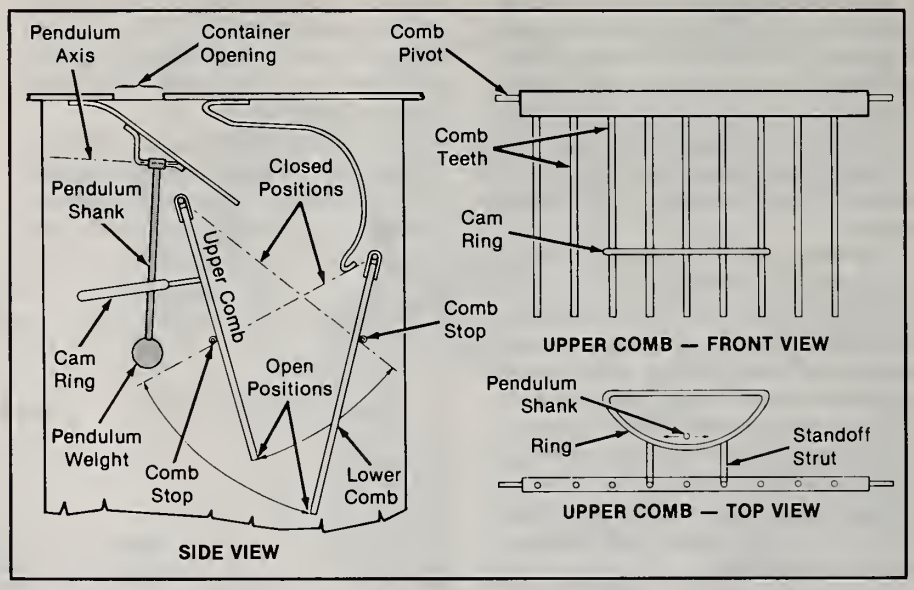

The **Sideward Movement of the Container** swings the pendulum, which drives the upper comb toward the container opening. Forward or backward movement of the container actuates both the upper and lower combs in the conventional manner but does not involve the pendulum.

Like the combs, the pendulum shank and the cam ring can be made of inexpensive, heavy-gauge wire. The pendulum should be quite heavy so that it can overcome pivot friction and other restraining forces. Spring catches can be added to the combs so that if they are actuated and close the container opening, they lock in place to prevent further tampering.

This work was done by Earl R. Collins, Jr., of Caltech for **NASA's Jet Propulsion Laboratory.**
NPO-16639/TN

FOR ADDITIONAL INFORMATION: *Contact: Director, Technology Transfer Division, P.O. Box 8757, BWI Airport, MD 21240; (301) 621-0100 Ext. 241*
REFER TO THE NUMBER LISTED AT THE END OF THIS ARTICLE

NASA Tech Brief
National Aeronautics and Space Administration

Using NASTRAN To Analyze Vibrations of Rotor Blades

Nonlinear and linear analyses are combined.

A report gives information on the use of the NASTRAN computer program in the finite-element analysis of rotating flexible blades like those in compressors and on turboprop engines. The program predicts steady-state components of deflections and stresses under centrifugal forces, generates data for plots of natural frequency versus rotational speed, and provides vibration-mode data for calculations of flutter. NASTRAN is well suited to such analyses because it can compute steady-state displacements by geometrically nonlinear analysis and can use the results for normal-modes analysis.

The report describes the use of NASTRAN solution sequence 64 for geometrical nonlinear analysis and solution sequence 63 for the determination of the frequencies and vibrational-mode shapes. It includes a sample problem with NASTRAN input data. It emphasizes key factors in the analysis of rotating blades, such as the setting angle and centrifugal softening effects.

Solution sequence 64 performs a large-displacement analysis on a rotating blade, computes the displacements and stresses caused by rotation, and stores the final stiffness and mass matrices of the blade in a data base. The large-displacement analysis is necessary because the blades are flexible and deflect considerably.

Solution sequence 63 computes the modal parameters from the final mass and stiffness matrices. The matrices corresponding to the deformed blade must be used so that centrifugal stiffening and other effects of rotation are included in the modal analysis.

The combined analyses of solution sequences 64 and 63 reduce computer time and the number of output listings, in comparison with those of separate analyses. In general, central-processing-unit time can be cut in half.

This work was done by Charles Lawrence, Robert A. Aiello, and Michael A. Ernst of **Lewis Research Center** *and Oliver G. McGee of Ohio State University. Further information may be found in NASA TM-89861 [N87-21375], Price Code: A02 "A NASTRAN Primer for the Analysis of Rotating Flexible Blades."*

Copies may be purchased from the National Technical Information Service, Springfield, Virginia 22161, Telephone No. (703) 487-4650. Rush orders may be placed for an extra fee by calling (800) 336-4700.
LEW-14799/TN

FOR ADDITIONAL INFORMATION: *Contact: Director, Technology Transfer Division, P.O. Box 8757, BWI Airport, MD 21240; (301) 621-0100 Ext. 241*
REFER TO THE NUMBER LISTED AT THE END OF THIS ARTICLE

Computing Stress, Stability, and Vibration of Shells

Complicated, branched shells of revolution are analyzed by a finite-difference energy method.

The BOSOR4 computer program was developed as a comprehensive program for the analysis of stress, stability, and vibration of complex, branched shells of revolution made of elastic materials. It can be used to analyze prismatic shells and panels. BOSOR4 performs large-deflection axisymmetric stress analysis, small-deflection nonsymmetric stress analysis, modal vibration analysis with axisymmetric nonlinear prestress included, and buckling analysis with axisymmetric or nonsymmetric prestress. One of the main advantages of the BOSOR4 code is the provision for such realistic engineering details as eccentric load paths, internal supports, arbitrary branching conditions, and a "library" of wall constructions.

The program is based on the finite-difference energy method and offers very rapid convergence with increasing numbers of mesh points. The BOSOR4 analyses are based on minimization of energy with constraint conditions. The total energy of the system is taken to include the strain energy of the segments of the shell, the strain energy of the discrete rings, the potential energy of applied line loads and pressures, the kinetic energy of the shell segments, and the kinetic energy of the discrete rings.

The constraint conditions arise from displacement conditions imposed anywhere in the composite shell and from conditions of compatibility between segments and branches of the composite shell. These components of energy and the constraint conditions are expressed in differential form in terms of the components of displacement of the reference surface of the shell at the finite-difference mesh points and in terms of the Lagrange multipliers. The integration is performed numerically by means of the trapezoidal rule. Now in algebraic form, the energy is minimized with respect to the discrete dependent variables.

The BOSOR4 program is written in FORTRAN 77 for interactive execution. It was developed on a DEC VAX 11/780 computer under VMS 4.0. It has a central-memory requirement of approximately 984K. With use of the DI-3000 plot library (available from Precision Visuals), the program plots the shape of the prebuckling state, buckling, or vibration mode. The BOSOR4 program was developed in 1986.

This program was written by David Bushnell of Lockheed Palo Alto Research Laboratory for **Langley Research Center.**
LAR-13940/TN

FOR ADDITIONAL INFORMATION

CONTACT:
COSMIC®
112 Barrow Hall
University of Georgia
Athens, GA 30602
(404) 542-3265

NASA Tech Brief
National Aeronautics and Space Administration
Ames Research Center, Moffett Field, California

Measuring Airflow With Digital Holographic Interferometry

Pressures on surfaces of airfoils are computed from interference fringes.

A digital image-processing system assists in the analysis of holographic interferometric images of flow about an airfoil. Operating semiautomatically, the system identifies, counts, and labels interference fringes, then processes the distances between fringes into the distribution of pressure on the surface of the airfoil. The system yields data on pressure faster than do manual image-analyses techniques, and these data compare favorably with those obtained by manual analysis and by probe measurements of pressure.

The equipment is illustrated by the block diagram of Figure 1. A video camera views the interferometric hologram. The video image has a resolution of 512 × 512 picture elements, the intensity of each of which is digitized to 8 bits. The digitized image is stored in two memory planes. Another memory plane stores a graphical and alphanumerical overlay digitized to 4 bits.

The system includes an arithmetic logic unit (ALU), which performs addition, subtraction, or comparison of the data in one or more memory planes in real time. The contents of each memory plane can be routed through lookup tables before entry into the ALU and can be shown on a color display. A joystick control device is used for interactive input. It controls two cursors, which can be used in a number of operating modes. A color printing system augments the color monitor.

The system uses computer programs that evaluate the interferograms along straight or curved lines represented by polygon segments. The user is prompted for such inputs as reference points and fringe numbers. After starting the program, a fringe pattern is digitized and frame-averaged to improve the signal-to-noise ratio. The user enters the location of two reference points to map the image-processor coordinates to the user's coordinate system by directing a cursor to the appropriate locations and entering the corresponding positions in the user's system. The selected reference points are usually the leading and trailing edges of the airfoil.

During numbering, the cursor can be moved along the segmented polygon line, positioning itself along the white segments.

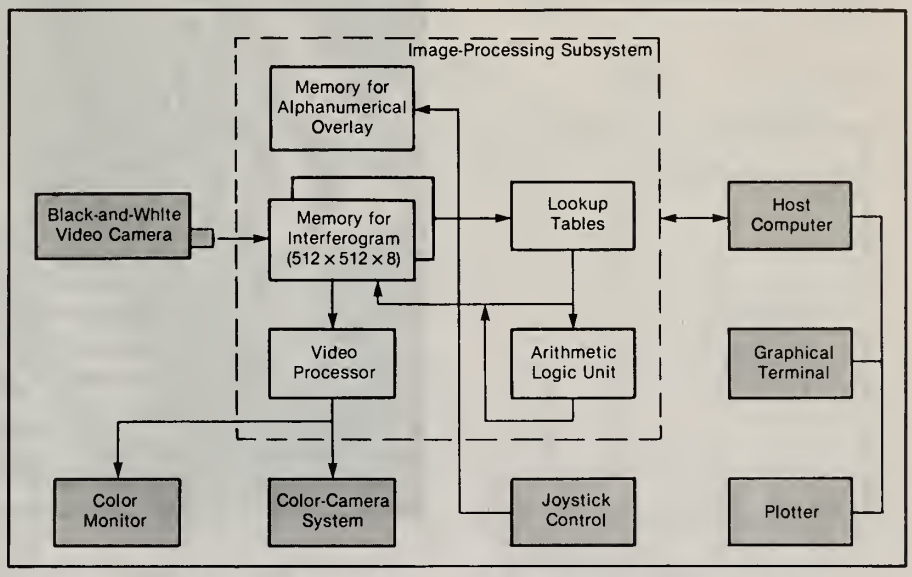

Figure 1. The **Image-Processing System** digitizes holographic interferograms of flow and processes them into data of pressure or other properties of the flow.

A reference fringe, the density along which is known, is selected and assigned the value 0. Subsequent fringes are numbered relative to the reference fringe in increments of 1. The user determines the correct numbers to be assigned to each fringe by observing the entire flow pattern of the interferogram. If the surface pressure is known to increase to a certain point and then decrease, the user correspondingly assigns fringe numbers that indicate this increase and decrease. Depending on the polygon line being used, some fringes have the same number as the fringe pattern bends in the opposite direction. Two different numbering modules can be used to set the fringe numbers. Only one number and the direction in which the fringe numbers increase have to be entered by the user to number the entire line. During the numbering process, the black segments are overwritten by colors to show the difference in the fringe order of two adjacent fringes. The color coding is an ergonomic feature that facilitates the detection of errors in numbering.

To be able to handle a wide range of fringe frequencies or increase the accuracy of the detection of fringes, the image processor can handle digitizations of several sections of one interferogram taken with different resolutions. Alternate lenses on the video camera are used to focus on appropriate sections. Each section is digitized separately until the entire polygon line has been evaluated. The data from different portions of the interferogram are then merged into one set of data. The output consists of the fringe numbers and location (fringe-order function) along the polygon line being evaluated. The fringe-order function is automatically fed to a file from which it can be converted to the distribution of pressure coefficients by a post-processing program (see Figure 2).

This work was done by Francisco J. Torres of **Ames Research Center**. *Further information may be found in NASA TM-88358 [N87-24681], Price Code: A02 "Application of Digital Holographic Interferometry to Pressure Measurements of Symmetric, Supercritical, and Circulation-Control Airfoils in Transonic Flow Fields."*

Copies may be purchased from the National Technical Information Service, Springfield, Virginia 22161, Telephone No. (703) 487-4650. Rush orders may be placed for an extra fee by calling (800) 336-4700.

ARC-12131/TN

Figure 2. **Analysis of the Interferogram** by the image-processing system produces results in close agreement with those obtained by manual analysis and by direct probe measurements of pressure. In regions along the airfoil where the fringe pattern is clear, the probe measurements and the output of the image-processing system agree within 1 percent.

Interferogram of 64A010 Airfoil at Mach 0.8 and Angle of Attack of 6.5°

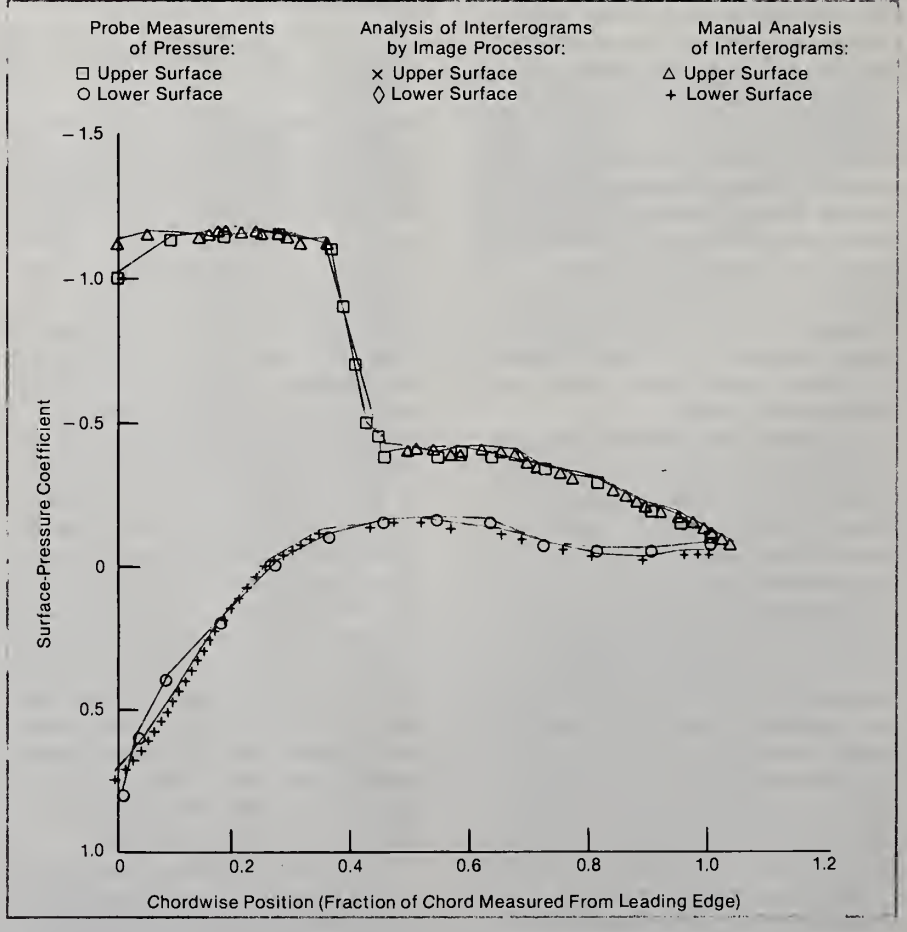

FOR ADDITIONAL INFORMATION: *Contact: Director, Technology Transfer Division, P.O. Box 8757, BWI Airport, MD 21240; (301) 621-0100 Ext. 241*

REFER TO THE NUMBER LISTED AT THE END OF THIS ARTICLE

NASA Tech Brief
National Aeronautics and Space Administration
Marshall Space Flight Center, Alabama

Licensing Opportunity

Diode-Laser Doppler Velocimeter

Features include ruggedness and compactness.

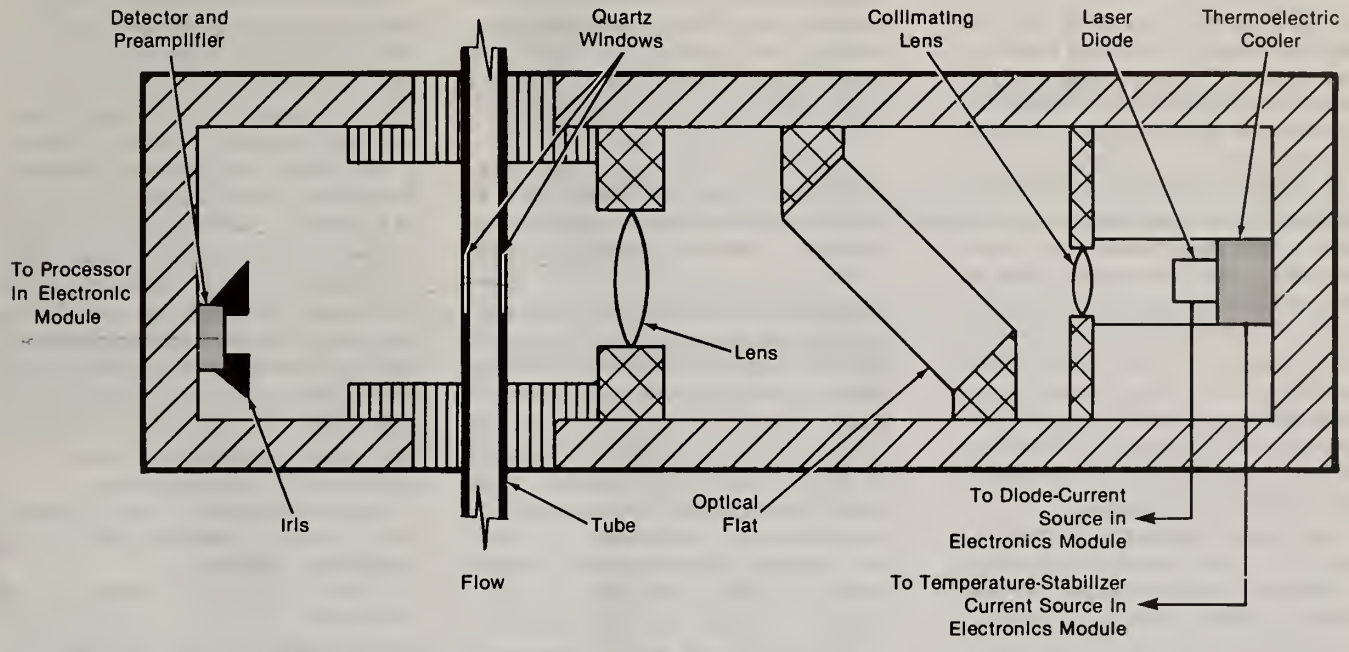

The Diode-Laser Doppler Velocimeter includes a compact, rugged three-section optical head that is mounted on the tube containing the flow. In a slightly different version, a beam splitter and mirror would be used to split the laser beam into two beams.

A diode-laser Doppler velocimeter measures nonintrusively the flow of an incompressible fluid in a narrow tube. In comparison with other flowmeters suitable for this purpose, the new velocimeter is rugged, compact, and competitive in cost.

The velocimeter includes a three-section optical head (see figure) and a separate electronics module. The right section houses a laser diode that operates at a wavelength of ~780 nm. A thermoelectric cooler controls the temperature of the laser diode to keep the wavelength stable. An optical flat splits the output beam from the laser into two beams, which are then focused by a lens.

The middle section of the optical head contains the tube, which is equipped with quartz windows for optical access to the flow. The focused beams intersect at the measuring position in the flow. The left section of the optical head contains the heterodyne receiver, which consists of a positive/intrinsic/negative photodiode with an iris aperture and preamplifier.

The electronics module contains current sources that drive the diode and the thermoelectric cooler. It also contains circuits to process the output of the receiver. The output of the processing electronics is fed to display electronics, which are also included in this module.

This work was done by Gregory J. Getzer of OPHIR Corp. for **Marshall Space Flight Center**. *No further documentation is available.*

Inquiries concerning rights for the commercial use of this invention should be addressed to the Patent Counsel, Marshall Space Flight Center. Refer to MFS-26104/TN.

George C. Marshall Space Flight Center
Technology Utilization Officer: Ismail Akbay
Code AT01
Marshall Space Flight Center,
AL 35812
(205) 544-2223
Patent Counsel:
Leon D. Wofford, Jr.
Mail Code CC01
Marshall Space Flight Center,
AL 35812
(205) 544-0024

FOR ADDITIONAL INFORMATION: *Contact: Director, Technology Transfer Division, P.O. Box 8757, BWI Airport, MD 21240; (301) 621-0100 Ext. 241*
REFER TO THE NUMBER LISTED AT THE END OF THIS ARTICLE

NASA Tech Brief
National Aeronautics and Space Administration
NASA's Jet Propulsion Laboratory, Pasadena, California

Licensing Opportunity

Multiple-Boundary-Condition Vibration Tests

Experiments build confidence in this emerging technique.

The multiple-boundary-condition testing method is gaining acceptance as a technique to improve the analysis of vibrations in large structures. The method was conceived for the vibrational testing, in a terrestrial environment, of large, complicated three-dimensional structures intended for use in outer space. The objective of such testing is to identify the parameters (e.g., nodal masses, stiffnesses of elements, and other quantities related to the shapes, sizes, and frequencies of vibrational modes) of mathematical models used to predict the vibrations of such structures in the absence of gravitation and air. The technique has potential terrestrial uses in the testing and evaluation of the dynamics of towers and offshore structures and of the safety of large buildings in Earthquakes.

The multiple-boundary-condition test method can help in overcoming the distorting effects of the atmosphere and mechanical supports, which can overwhelm the effects that one seeks to measure. In this method, the structure is supported and/or restrained at several positions; the structure is excited at the desired vibrational frequencies, and the vibrations are measured to determine the characteristics of the vibrational modes. The supports and/or restraints are then moved to different positions and the tests conducted anew to measure the resulting new vibrational modes. This procedure may be repeated several times under different support/restraint (boundary) conditions.

No single test of this type yields data on all the parameters of the structure, and, in particular, a test yields no data on the parameters of the parts located at the restraints. However, each test under different boundary conditions excites different portions of the structure and can be related to a small subset of the total mathematical formulation; this facilitates the modification or verification of the affected parts of the mathematical model, and recent theoretical developments make it possible to determine quantitatively the sensitivities of the parameters to the results of a given test. In addition, many different combinations and positions of the mechanical constraints can be used to obtain many different estimates of any desired parameter. Statistical theory suggests that the data from many different boundary conditions can increase the accuracy of the mathematical model.

Experiments were performed on an aluminum beam of uniform cross section, an aluminum beam of two different cross sections alternating along the length, and a 12-bay truss structure. These structures were simply supported at their ends and at various intermediate positions (see figure). Each beam was tested in four and the truss in two different configurations of supports. In each case, the vibrational data were used to update a mathematical model of the affected structure containing deliberately and grossly erroneous parameters of the beams and cross-sectional areas of the truss members (areal moments of inertia of which the true values were known), to test the corrective power of the multiple-boundary-condition approach. In all cases, the test data led to updated parameters within a few percent of the true values.

This work was done by Chin-Po Kuo and Ben K. Wada of Caltech for **NASA's Jet Propulsion Laboratory**.

Inquiries concerning rights for the commercial use of this invention should be addressed to the Patent Counsel, NASA's Jet Propulsion Laboratory. Refer to NPO-17351/TN.

Jet Propulsion Lab.
NASA Resident Office
Technology Utilization Officer: Gordon S. Chapman
Mail Stop 180-801
4800 Oak Grove Drive
Pasadena, CA 91109
(818) 354-4849
Patent Counsel: Paul F. McCaul
Mail Code 180-801
4800 Oak Grove Drive
Pasadena, CA 91109
(818) 354-2734
Technology Utilization Mgr. for JPL: Norman L. Chalfin
Mail Stop 156-211
4800 Oak Grove Drive
Pasadena, CA 91109
(818) 354-2240

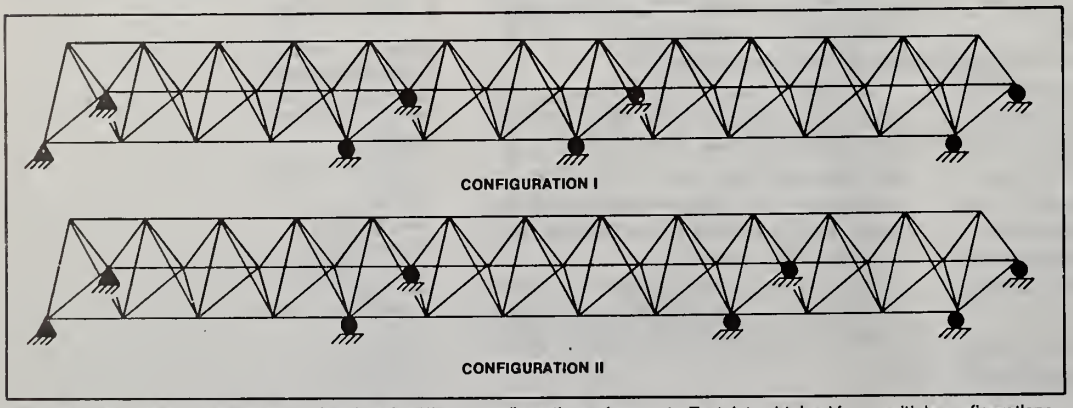

This Truss Was Tested by measuring its vibrations in different configurations of supports. Test data obtained from multiple configurations are more useful than are data from one configuration, in which the supports could mask important effects.

FOR ADDITIONAL INFORMATION: *Contact: Director, Technology Transfer Division, P.O. Box 8757, BWI Airport, MD 21240; (301) 621-0100 Ext. 241*
REFER TO THE NUMBER LISTED AT THE END OF THIS ARTICLE

Environmental Science & Technology

0169 High Energy Lithium Battery

Other Items of Interest

0149 Sodium Sulfide/Ferrous Sulfate Treatment Process (Licensing Opportunity)

0153 Adaptive Control for Cooperative Dual Robot Arms—Simple control strategies are derived from control strategies for single arms. (Licensing Opportunity)

0154 Analysis of Straight and Wavy Annular Seals—Rotordynamic coefficients are derived. (Licensing Opportunity)

NAVY
Domestic Technology Transfer Fact Sheet

High Energy Lithium Battery

Since the early sixties, scientists have conducted a great deal of research and development work, seeking the "ideal lithium battery." The effort has centered on achieving high energy and power density. Two oxysulfur cathode systems, Li/SO_2 and $Li/SOCl_2$, assumed importance during the seventies. They have proven to be very successful in yielding high energy density with excellent discharge characteristics. However, safety problems persisted with these systems. Under some conditions, they are prone to fires and explosions with the venting of toxic gases. The objective of the Naval Surface Warfare Center 's (NSWC) task was to investigate various alternatives to current lithium systems that are of equal energy density but would be much safer and less toxic.

The resulting product of the NSWC investigation provides for a new nonaqueous, high energy lithium battery. The properties of this lithium battery design are safe storage, does not ignite or explode, does not vent toxic gases, and has a high output voltage and a high storage capacity.

For Additional Information:

Backup material on this effort is available from:

Navy Domestic Technology Fact Sheet Reader Reply Service
Code E211
Naval Surface Weapons Center
Dahlgren, VA 22448-5000
(703) 663-8921

Refer to 140601/TN

Manufacturing, Machinery & Tools

0170 Optical Spectral Radiometric/Laser Reflectance System for Weld Pool Surface Temperature Measurement

0171 New Calibration System Halves Gage Block Errors

0172 Arc-Light Reflector for Television Weld Monitoring—Light is spread more evenly over the image area. (Licensing Opportunity)

0173 Expansion Valve with Temperature-Sensitive Flow Regulation—A variable-area orifice adjusts the flow of cryogenic vapor.

0174 Improving a Remote Manipulator—The latest parameters, tools, adaptations, and software are documented.

0175 Intelligent Welding Controller—A control system would adapt to changing design requirements and operating conditions.

0176 Making Internal Molds of Long, Curved Tubes—Mold material is carried to an internal weld joint and removed after an impression is taken.

0177 Making Jointless Dual-Diameter Tubes—Welds between sections that have different diameters are eliminated.

0178 Making Large Composite Vessels Without Autoclaves—Differential thermal expansion provides the requisite pressure.

0179 Robotic Tool for Tightening and Cutting—The tool can be used in the assembly of truss structures.

0180 Roller Bearings Survive Loss of Oil Supply—A ring holds a small emergency supply of oil.

0181 Spray Deflector for Water-Jet Machining—A cheap disk shields expensive parts from erosion. (Licensing Opportunity)

Technology Application

Idaho National Engineering Laboratory

Optical Spectral Radiometric/Laser Reflectance System for Weld Pool Surface Temperature Measurement

This system is the first to allow high resolution measurements of weld pool surface absolute temperature. Such measurements are taken for a variety of welding conditions in order to compile a data base. The data are then used for refinement/verification of a theoretical thermal computer model which would then have broad applicability for the process under consideration. There is a continuing strong movement in the welding industry to develop systems to interactively control the welding process to obtain optimum weld bead size, penetration and micro/macro structural characteristics. A key part of this process is the ability to sense or model the weld in real time so that automatic or robotic control of the welding process can be implemented. OSRLRS based models will be used in this environment to interactively model the weld, based on workpiece material properties and real time input of welding process parameters.

Why is this better than existing technology? No other system provides for high resolution absolute temperature maps of weld pool surfaces at an instant in time; no other related system operates in the visible light spectrum or uses a laser beam as an integral part of the system. The system has use by any industry in which steels are used and welded; e.g., transportation, construction, ship/submarine, utilities, communications.

FOR ADDITIONAL INFORMATION: Contact Jack G. Peterson, Idaho National Engineering Laboratory, P.O. Box 1625, Idaho Falls, Idaho 83415; (208)526-2893. Refer to DOE/INEL-052TN.

NIST Technology Update

National Institute of Standards & Technology
(Formerly the National Bureau of Standards)
U.S. Department of Commerce, Gaithersburg, MD 20899

New Calibration System Halves Gage Block Errors

A new system developed by the NIST Center for Manufacturing Engineering has made possible substantial improvements in the uncertainty for gage block calibrations. Under the new system, typical estimates for the uncertainty of calibrations by mechanical intercomparison have been reduced from between 2 to 4 microinches (0.05 to 0.10 micrometer) to between 1 to 2 microinches (0.02 to 0.05 micrometer). Gage blocks remain an important calibration tool for instrument and standards makers and in high-precision industries such as aerospace or defense. The new system includes a database and analysis software to record and monitor the measurement history of each customer's gage blocks, thereby reducing risks of reporting inaccurate measurements and improving overall measurement confidence. NIST has more than 300 regular customers for gage block calibrations, which typically cost about $3000 a set.

FOR ADDITIONAL INFORMATION: To discuss these efforts further, contact Mr. Jay Zimmerman, Metrlogy Building, Room A107, National Institute of Standards & Technology, Gaithersburg, MD 20899; (301)975-3480.

NASA Tech Brief
National Aeronautics and Space Administration
Marshall Space Flight Center, Alabama

Licensing Opportunity

Arc-Light Reflector for Television Weld Monitoring

Light is spread more evenly over the image area.

A conical, stainless-steel mirror attached to the end of a welding torch improves the distribution of light on the workpiece as its welding is monitored through the torch by television. An auxiliary light source is therefore not needed. Television monitoring not only protects the operators from the intense arc light but also facilitates automated welding.

In earlier versions of television weld monitoring, the extremely bright light of the welding arc closed down the camera aperture enough to lose the detail of the relatively dark surrounding region, particularly on overlays. The solution of this problem was to use auxiliary light sources to illuminate the area surrounding the arc. These sources were large, expensive, bright, quartz/halogen lights that did not work well.

The new conical mirror (see figure) on the other hand, reflects the already-available arc light onto the darker surrounding areas, providing the monitor with a clearer, more detailed image of the welding operation. Simple, small, and easy to install and remove, the mirror is relatively nonintrusive. For example, it does not interfere with the addition of filler wire.

This work was done by Stephen S. Gordon of Rockwell International Corp. for **Marshall Space Flight Center**. *No further documentation is available.*

This invention has been patented by NASA (U.S. Patent No. 4,633,060). Inquiries concerning nonexclusive or exclusive license for its commercial development should be addressed to the Patent Counsel, Marshall Space Flight Center Refer to MFS-29134/TN.

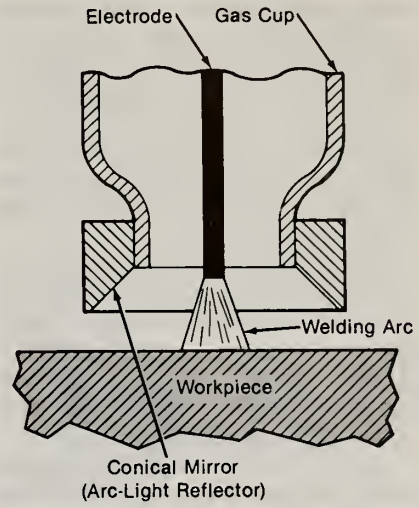

An **Arc-Light Reflector** directs light from the welding arc back onto the workpiece, enabling television monitoring of the welding operation and protecting the operator from the arc light.

George C. Marshall Space Flight Center
Technology Utilization Officer: Ismail Akbay
Code AT01
Marshall Space Flight Center,
AL 35812
(205) 544-2223
Patent Counsel:
Leon D. Wofford, Jr.
Mail Code CC01
Marshall Space Flight Center,
AL 35812
(205) 544-0024

FOR ADDITIONAL INFORMATION: *Contact: Director, Technology Transfer Division, P.O. Box 8757, BWI Airport, MD 21240; (301) 621-0100 Ext. 241*
REFER TO THE NUMBER LISTED AT THE END OF THIS ARTICLE

NASA Tech Brief
National Aeronautics and
Space Administration
John F. Kennedy Space Center, Florida

Expansion Valve With Temperature-Sensitive Flow Regulation

A variable-area orifice adjusts the flow of cryogenic vapor.

A Joule-Thomson expansion valve is designed so that particles or condensed contaminants in the vapor flowing through it are unlikely to clog its orifice. In addition, the new valve automatically adjusts the flow of the vapor; it allows a high initial flow for rapid cooling, but gradually reduces the flow as the operating temperature is reached. The flow can also be adjusted manually when necessary.

The valve was developed for the expansion of high-pressure vapors to condense them into low-pressure cryogenic liquids. The valve could be used, for example, to conserve helium coolant in a superconducting system by condensing the vapor boiling from a liquid-helium bath.

In a conventional small Joule-Thomson nozzle, the apertures are so fine that they soon become blocked by condensed contaminants in the expanding medium. In the new valve, however, expansion takes place in an annulus rather than in a single circular hole (see figure). The annulus provides a relatively-large peripheral surface for a small cross-sectional flow area, so that complete clogging by particles is less likely than in the case of fine apertures. In addition, grooves in the annulus region serve as reservoirs for particles, further reducing the possibility of clogging.

The automatic flow adjustment of the new valve results from the carefully chosen coefficients of thermal expansion of the valve components. The core of the valve is made of glass-reinforced epoxy resin, which combines a low coefficient of expansion with a low thermal conductivity. Covering the core is a sheath of aluminum, which combines a high coefficient of expansion with a high thermal conductivity. The sheath tapers at the grooved tip of the core, forming the annulus. At startup, the cross-sectional area of the annulus is at a maximum, and the mass flow of the fluid is high. As the sheath and core are cooled by the medium, which flows around them through a coiled tube, the sheath contracts more than the core does, becoming both shorter and smaller in diameter. It thus reduces the cross-sectional area of the annulus and reduces the flow.

The valve is equipped with a locking micrometer with which the operator can manually vary the initial flow or make fine adjustments in the steady-state flow. This feature allows the same nozzle to be used over a range of flow rates and in a variety of applications.

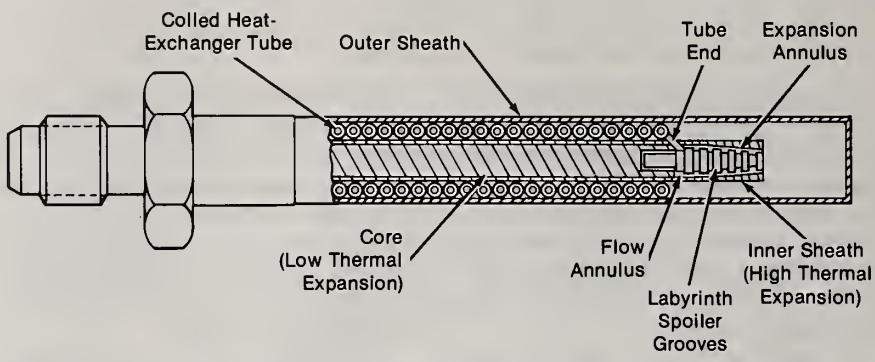

Cryogenic Vapor Flows Through a Coiled Tube and into an annulus, where it expands and condenses. In flowing through the tube, the vapor cools the supporting core and its sheath. Because the sheath contracts thermally more than the core does, the flow area of the annulus is gradually reduced.

This work was done by Graham Walker and Kelly Hedegard of General Pneumatics Corp. for **Kennedy Space Center**.

In accordance with Public Law 96-517, the contractor has elected to retain title to this invention. Inquiries concerning rights for the commercial use of this invention should be addressed to

General Pneumatics Corporation
7662 E. Gray Road, Suite 107
Scottsdale, AZ 85260

Refer to KSC-11372/TN.

FOR ADDITIONAL INFORMATION: *Contact: Director, Technology Transfer Division, P.O. Box 8757, BWI Airport, MD 21240; (301) 621-0100 Ext. 241*

REFER TO THE NUMBER LISTED AT THE END OF THIS ARTICLE

NASA Tech Brief
National Aeronautics and
Space Administration

Improving a Remote Manipulator

The latest parameters, tools, adaptations, and software are documented.

A set of three reports describes work on the Protoflight Manipulator Assembly (PFMA), a 2.4-meter remote manipulator with six degrees of freedom, counterbalanced for operation in Earth gravity. "Performance Characteristics of the Protoflight Manipulator Assembly" presents the parameters of the PFMA after a refurbishment of operating components. The document is intended to help simulation engineers understand the electromechanical responses of the manipulator arm. Data are furnished on dimensions, maximum joint travel, joint torques, mechanical backlash, voltages for releasing and resetting joint brakes, end-effector closure force, frequency response of each joint, rate scale factor for the control input to each joint, the position scale factor for the joint-angle-measuring sensors, and transient responses of the joints.

"End Effector and Task Board Development for the Protoflight Manipulator Assembly" describes special tools and adaptations that allow the PFMA to be used for servicing equipment. The tools include end-effector jaws for grasping and manipulating the equipment, an all-purpose end-effector mount that can accept special tools, and a device to connect and disconnect fluid couplings. A task board was modified by the addition of a rotating antenna, half of a fluid coupling, and a removable modular box and door. These additions enable the development of operation and simulation techniques.

"Modular Software Development for the Protoflight Manipulator Assembly" documents the interface and control software for the PFMA. It includes hierarchy charts, data-flow diagrams, a data dictionary, and logic flows, as well as a listing of the software. A section of the report details the operator choices and input requirements. It explains the prompts given to the operator by the program and the data needed to respond to the prompts. It also explains the layout of the data-base and automatic-sequence files.

This work was done by John W. Haslam, Jr., Nicholas Shields, Jr., Mary F. Fagg, and Ricardo C. Rodriguez of Essex Corp. for **Marshall Sapce Flight Center.**
MFS-27067/TN

FOR ADDITIONAL INFORMATION: *Contact: Director, Technology Transfer Division, P.O. Box 8757, BWI Airport, MD 21240; (301) 621-0100 Ext. 241*
REFER TO THE NUMBER LISTED AT THE END OF THIS ARTICLE

NASA Tech Brief
National Aeronautics and Space Administration
Marshall Space Flight Center, Alabama

Intelligent Welding Controller

A control system would adapt to changing design requirements and operating conditions.

A proposed control system for gas/tungsten arc welding would require only that an operator specify such direct parameters of welds as widths and depths of penetration. From this information, the controller would drive a welding robot to produce welds that meet specifications. In contrast, the operator of a typical conventional welding controller must provide values of such indirect parameters as currents, voltages, and speeds and hope that they would yield welds that have the required geometries. The proposed control system would calculate the indirect parameters from the direct parameters.

The equipment and computer programs of the system would be divided into a controller domain and a supervisor domain (see figure). The controller domain would contain mainly components tightly bound to the welding process; for example, sensors and mathematical models. While welding is in progress, sensors would measure some of the direct parameters of the weld, while mathematical models would estimate the values of parameters that could not be measured. Comparators would produce error signals in the form of differences between the measured and estimated values of the direct parameters and the corresponding design values of parameters supplied by the user.

A multivariable controller would use the error signals to produce control signals, which would tend to reduce the errors. The number of input variables to the controller should exceed or equal the number of the output variables, which are control signals for the indirect parameters of the weld. These control signals would be fed simultaneously to the welding equipment and to a mathematical model that would simulate the dynamics of the weld puddle.

The portion of the system in the supervisor domain would adaptively tune the mathematical models, control algorithms, and other components in the controller domain, and would restructure the system when appropriate. In addition, it would maintain and update information on the welding process for later use, communicate with users, and perform other general tasks.

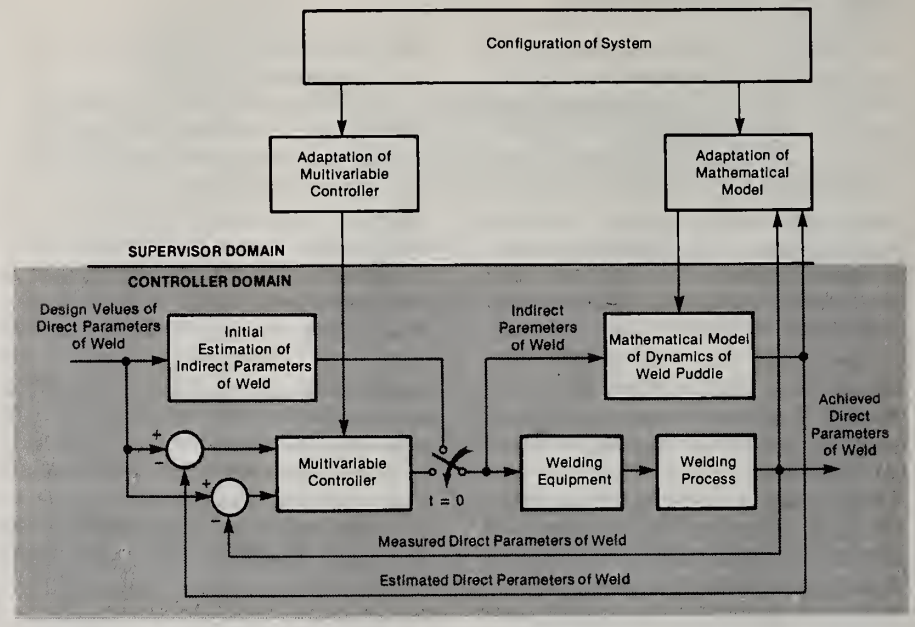
Configuration of System
Adaptation of Multivariable Controller
Adaptation of Mathematical Model
SUPERVISOR DOMAIN
CONTROLLER DOMAIN
Design Values of Direct Parameters of Weld
Initial Estimation of Indirect Parameters of Weld
Indirect Parameters of Weld
Mathematical Model of Dynamics of Weld Puddle
Achieved Direct Parameters of Weld
Multivariable Controller
t = 0
Welding Equipment
Welding Process
Measured Direct Parameters of Weld
Estimated Direct Parameters of Weld

In the Control System for a Robotic Welder, components and functions intimately connected with the welding process would be assigned to the controller domain. More general functions would be assigned to the supervisor domain. The initial estimate of indirect parameters of the welding process would be applied to the system only at the beginning of a weld ($t = 0$); after the start of welding, outputs from the multivariable controller would take the place of the estimate.

Tuning (which would be done before welding operation) would be an iterative process in which the measured direct parameters would be compared to corresponding values of those parameters calculated by models, and the internal parameters of the models would be adjusted until the calculated and measured values would coincide. Because tuning would have to be carried out in a context of environmental conditions and other factors known only at a high level in the system, adaptation of the multivariable controller would be assigned to the supervisor domain.

The supervisor might choose to restructure the control system when welding conditions changed in such a way that another available model became more accurate than the one in use. Such restructuring would be done quickly so that welding could continue without interruption.

This work was done by George E. Cook, Ramaswamy Kumar, and Tanuja Prasad of Vanderbilt University and Kristinn Andersen and Robert J. Barnett of Mid-South Engineering, Inc., for **Marshall Space Flight Center.**

MFS-27195/TN

FOR ADDITIONAL INFORMATION: *Contact: Director, Technology Transfer Division, P.O. Box 8757, BWI Airport, MD 21240; (301) 621-0100 Ext. 241*

REFER TO THE NUMBER LISTED AT THE END OF THIS ARTICLE

NASA Tech Brief
National Aeronautics and Space Administration
Marshall Space Flight Center, Alabama

Making Internal Molds of Long, Curved Tubes

Mold material is carried to an internal weld joint and removed after an impression is taken.

A remotely operated device makes an impression mold of the interior surface of a tube at a weld joint. The mold provides an indication of the extent of the mismatch between the members at the joint. The device can be maneuvered to the weld to be inspected through a curved tube 3 in. (7.6 cm) in diameter by 50 in. (127 cm) long. It can readily be adapted to making molds to measure the depth of corrosion in boiler tubes or other pipes.

The device includes a V-notched head on the end of a set of hoses (see figure). The operator inserts the device in the tube and manipulates color-coded lines to guide it through the curves in the tube until the V-notch in the head engages a splitter rod at the weld joint. The operator inflates an airbag on the head to lock it in place. The operator then applies air pressure to an air cylinder that pushes a platen outward, forcing the molding material against the inner wall of the tube.

The operator releases the pressure in the cylinder and bag after the impression has been made. A retractor spring in the head draws the platen and molding material inward so that the device can be withdrawn. A steel cable acts as a redundant tether to ensure that all parts are extracted.

The V-notch can be indexed in 15° increments about the axis of the tube. This feature enables the taking of a series of impressions that cover all or a portion of the inner circumference of the tube.

This work was done by Richard K. Burley of Rockwell International Corp. for **Marshall Space Flight Center.**
MFS-29435/TN

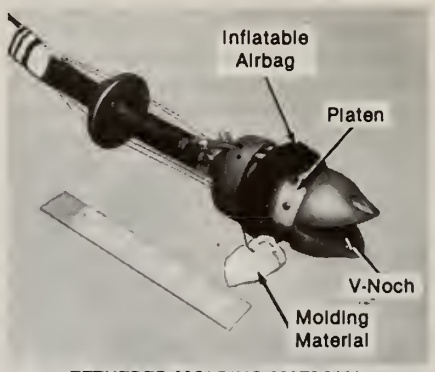

TETHERED MOLDING MATERIAL SEPARATED FROM HEAD TO SHOW PLATEN

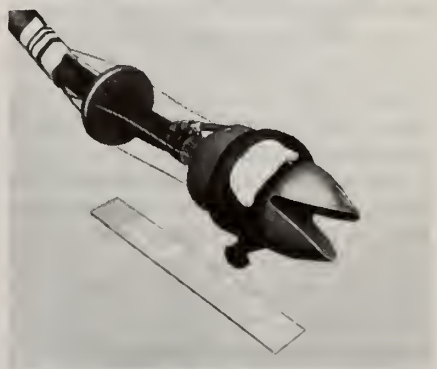

MOLDING MATERIAL MOUNTED ON PLATEN

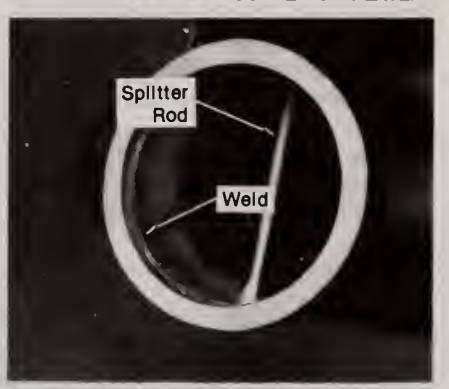

CUTAWAY VIEW OF TUBE SHOWING SPLITTER ROD AND WELD

When Pressurized, an Air Cylinder in the Head of the mold-making device forces the platen and mold material against the inner wall of the tube. The splitter rod, revealed in the cutaway tube, aids in the positioning of the V-notched head.

FOR ADDITIONAL INFORMATION: *Contact: Director, Technology Transfer Division, P.O. Box 8757, BWI Airport, MD 21240; (301) 621-0100 Ext. 241*
REFER TO THE NUMBER LISTED AT THE END OF THIS ARTICLE

NASA Tech Brief
National Aeronautics and Space Administration
Marshall Space Flight Center, Alabama

Making Jointless Dual-Diameter Tubes

Welds between sections that have different diameters are eliminated.

A single tube can be made with an integral tapered transition section between straight sections of different diameters and wall thicknesses. The tube is made from a single piece; it contains no joints, welded or otherwise. It therefore is not prone to such weld defects as voids and need not be inspected for them.

The tube can be fabricated by either of two methods: drawing or reduction. In the drawing method, a straight tube is first drawn over a tapered mandrel to produce the tapered reduction in the thickness of the wall. The tube is then drawn through a series of segmented dies to reduce the diameter. The segments of a die (see figure) move together radially, under the action of a cam, as the tube passes through. The shape of the cam determines the shape of the taper in the diameter.

The inner surfaces of the die segments do not constitute a perfect cylinder until they are contracted together at the minimum diameter. To minimize out-of-roundness, the tube is rotated about its axis during drawing, and reduction in diameter by a single die is typically limited to 0.05 in. (1.3 mm). Because the tube can be annealed after any pass, it can be reduced to an extremely small diameter by several passes. The tapered section can be made as long as the dimensions of the drawbench will allow.

In the reduction method, the wall thickness and diameter are reduced in a single step by rolling the straight tube between grooved dies as it passes over a tapered mandrel. When a sufficient length of the narrower section has been produced at one end of the wider tube, the piece is removed from the rolling mill. The shape of the taper between the wide and narrow sections is determined on the inside by the shape of the mandrel and on the outside by the shape of the groove in the roller.

Because intermediate annealing is not possible in the single-step reduction method, the maximum reduction is determined by the working characteristics of the material. Usually, the smaller outside diameter cannot be less than 0.25 in. (6.4 mm). The length of the tapered section is limited by the diameter of the die rollers.

Both methods have been used to fabricate tubes of 316L corrosion-resistant stainless steel for use as a heat-exchanger coil. The wide end of the tube had an outside diameter of 0.5 in. (12.7 mm) with a wall, 0.032 in. (0.81 mm) thick, tapering to an outside diameter of 0.262 in. (6.7 mm) and a wall thickness of 0.026 in. (0.66 mm) over a transition section 10 in. (25.4 cm) long. A wide variety of wide and narrow tube sizes and taper lengths is possible, depending on the tube material and on the tapering method.

This work was done by Kathleen E. Kirkham of Rockwell International Corp. for **Marshall Space Flight Center.**
MFS-29004/TN

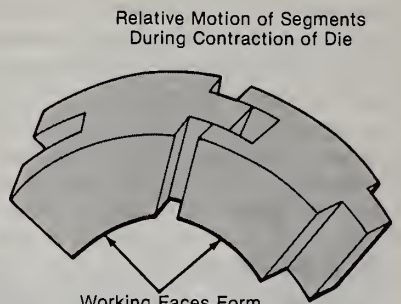

TWO ADJACENT SEGMENTS OF AN EIGHT-SEGMENT DRAWING DIE

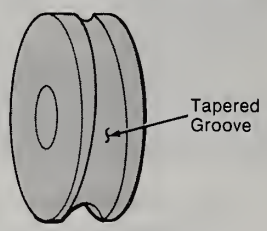

DIE ROLLER FOR REDUCTION METHOD

Alternative Methods of creating a taper between wider, thicker-walled and narrower, thinner-walled sections of tube employ contracting die segments, two of which are shown at left, or a tapered-groove roller (right). In either case, the tube is rotated around a tapered mandrel inside the tube to reduce the thickness of the wall.

FOR ADDITIONAL INFORMATION: *Contact: Director, Technology Transfer Division, P.O. Box 8757, BWI Airport, MD 21240; (301) 621-0100 Ext. 241*
REFER TO THE NUMBER LISTED AT THE END OF THIS ARTICLE

NASA Tech Brief
National Aeronautics and Space Administration
Marshall Space Flight Center, Alabama

Making Large Composite Vessels Without Autoclaves

Differential thermal expansion provides the requisite pressure.

A method for making a fiber-reinforced composite structure relies on heating and differential thermal expansion to provide the temperature and pressure necessary to develop full strength, without having to place the structure in a large, expensive autoclave. The method is suitable for such cylindrical structures as pressure vessels and tanks. It can be used for both resin-matrix (such as graphite-reinforced epoxy) and metal-matrix (such as graphite-reinforced aluminum) composites.

A layer of thermally expansive material such as aluminum surrounds a release layer on a mandrel (see figure). The uncured composite is wrapped tightly around the aluminum layer, separated from it by a thin layer of polytetrafluoroethylene or other nonsticking material so that the composite can later be easily released from the mandrel. A tight wrapping of graphite filaments surrounds the composite, separated from it by another layer of polytetrafluoroethylene.

As the assembly is heated, the aluminum expands about 22 times as much as the graphite-filament wrap does. Thus, the composite is squeezed between the aluminum and the graphite wrapping. For example, heating layers of aluminum, graphite/epoxy composite, and graphite wrap — each 0.25 in. (0.6 cm) thick on a mandrel 19 in. (48 cm) in diameter — through a temperature rise of 350 °F (194 °C) would create a pressure of about 790 lb/in.^{2} (5.5 MPa) in the composite layer. The pressure can be increased or decreased by increasing or decreasing the thickness of the expansion layer.

The assembly could be heated in an oven. Alternatively, if the structure is very large, electromagnetic induction from conductive coils around the assembly could heat the graphite-filament wrapping. Supplemental heating can be furnished by resistance elements within the mandrel.

This work was done by W.A. Sigur of Martin Marietta Corp., for **Marshall Space Flight Center.**

Inquiries concerning rights for the commercial use of this invention should be addressed to the Patent Counsel, Marshall Space Flight Center. Refer to MFS-28390/TN.

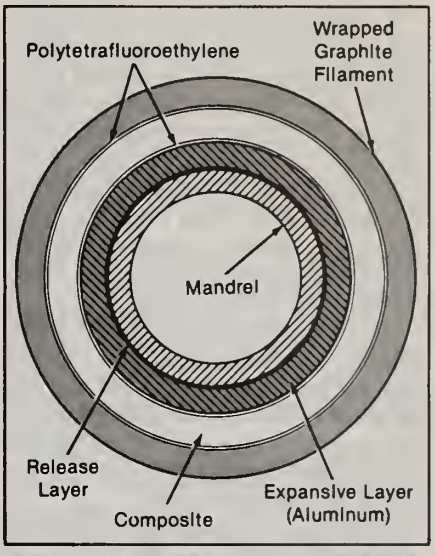

Layers of Differentially Expanding Material squeeze a fiber-reinforced composite between them when heated.

FOR ADDITIONAL INFORMATION: *Contact: Director, Technology Transfer Division, P.O. Box 8757, BWI Airport, MD 21240; (301) 621-0100 Ext. 241*
REFER TO THE NUMBER LISTED AT THE END OF THIS ARTICLE

NASA Tech Brief
National Aeronautics and Space Administration

Lyndon B. Johnson Space Center, Houston, Texas

Robotic Tool for Tightening and Cutting

The tool can be used in the assembly of truss structures.

A robot end effector is designed for tightening tube couplers and for cutting tubes. Intended for use in building structures in space, the end effector can also be used as a hand tool for assembling truss structures for terrestrial buildings, tents, and oil rigs. It can also be used in place of a pipe wrench in plumbing work. The tool is operable by simple movements and thus can be manipulated by a technician wearing heavy protective clothing.

The tool reaches around an object, grasps it, locks in place around the object, and rotates the object (see figure). The tool can tighten or loosen a nut or collar in the middle of a tube, for example. The tool can also be fitted with a blade so that, when the tool rotates, it cuts into the tube.

The tool can be used even if electrical power fails. In that case, the operator releases one of two head-attaching pins. A worm gear on the tool then acts as a pawl on a ratchet wheel, and the tool can be operated manually just like a ratchet wrench.

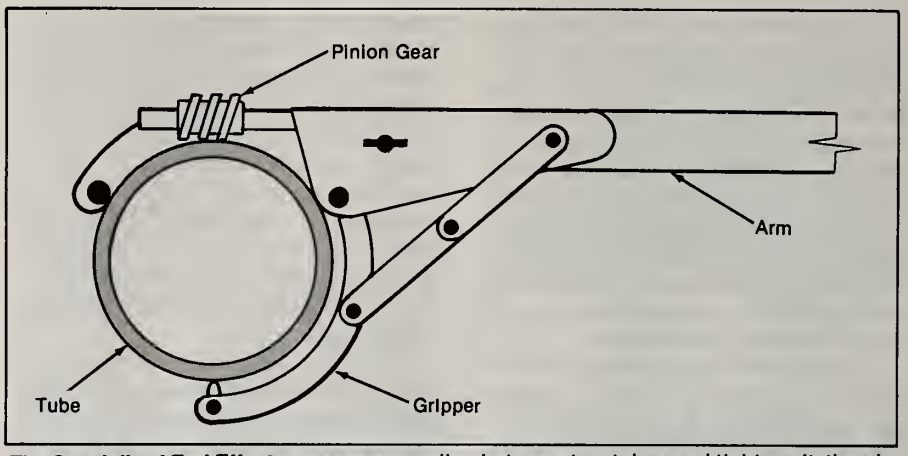

The **Specialized End Effector** grasps a coupling between two tubes and tightens it, thereby joining the tubes securely. The tool operates on the principle of a worm and pinion gear.

This work was done by Earl T. Cooney of McDonnell Douglas Corp. for **Johnson Space Center.**
MSC-21538

FOR ADDITIONAL INFORMATION: *Contact: Director, Technology Transfer Division, P.O. Box 8757, BWI Airport, MD 21240; (301) 621-0100 Ext. 241*
REFER TO THE NUMBER LISTED AT THE END OF THIS ARTICLE

NASA Tech Brief
National Aeronautics and Space Administration
Lewis Research Center, Cleveland, Ohio

Roller Bearings Survive Loss of Oil Supply

A ring holds a small emergency supply of oil.

A tapered roller bearing can operate for at least 30 min at speeds up to 11,000 r/min after its oil supply stops. The bearing was developed to enable such high-speed machinery as a helicopter transmission to continue to operate safely when its oil pump fails.

The bearing cup includes a porous rib ring (see figure) that contains a residual oil supply to lubricate the rollers when the external oil supply is lost. The ring is made by sintering powdered metal, the pores of which hold the emergency oil. The residual oil impregnated into the ring bleeds out to the ends of the rollers by capillary action. The bleeding is initiated as the temperature of the bearing rises after the failure of the primary oil supply. The heating also squeezes oil out of the ring because the coefficient of thermal expansion of the oil exceeds that of the ring.

The critical aspects of the fabrication of the ring include the preparation of the metal powder and the final treatment of the surface. These operations determine the internal and surface porosity and, therefore, the amount of oil that can be stored and the rate at which it can be dispensed. After the ring has been compacted, sintered, and heat-treated, it is impregnated with oil. It is then ground to final shape, using a coolant to prevent retempering. To ensure that pores open into the interior of the bearing, the grinding smear that blocks the surface pores is removed by electroetching in an aqueous solution that contains perchloric acid.

Experimental bearings were evaluated at six speeds from 0.26 million to 2.4 million DN with a 65-mm-diameter tapered bearing. (DN is the product of the bearing diameter in millimeters and the angular speed in revolutions per minute.) The best results were obtained with porous rings made of CBS1000M steel at 75 percent of maximum density, which operated for the requisite half hour at speeds up to 0.72 million DN (11,000 r/min). At higher speeds, the bearings failed after decreasing intervals ranging from many minutes to a few seconds.

This work was done by G. E. Kreider and P. W. Lee of The Timken Co. for **Lewis Research Center**. *Further information may be found in NASA CR-180804 [N85-11135], Price Code: A05 "Improved Oil-Off Survivability of Tapered Roller Bearings."*

Copies may be purchased from the National Technical Information Service, Springfield, Virginia 22161, Telephone No. (703) 487-4650. Rush orders may be placed for an extra fee by calling (800) 336-4700.
LEW-14749/TN

This Bearing Was Still Operating after 22 min without externally supplied oil at 12,000 r/min. The rib ring is made of porous high-speed steel.

FOR ADDITIONAL INFORMATION: *Contact: Director, Technology Transfer Division, P.O. Box 8757, BWI Airport, MD 21240; (301) 621-0100 Ext. 241*
REFER TO THE NUMBER LISTED AT THE END OF THIS ARTICLE

NASA Tech Brief
National Aeronautics and Space Administration
Lewis Research Center, Cleveland, Ohio

Licensing Opportunity

Spray Deflector for Water-Jet Machining

A cheap disk shields expensive parts from erosion.

A disk on a water-jet-machining nozzle protects the nozzle and parts behind it from erosion by deflected spray. The disk is part of the water-jet-machining unit. The water jet strikes the surface of the workpiece and rebounds toward the nozzle, impinging on the nozzle nut. The energetic water spray can wear away the nut and then attack the collet that holds the nozzle.

The disk consists of a stainless-steel backing with a neoprene facing that deflects the spray so that it does not reach the nut or other vital parts of the water-jet apparatus (see figure). Instead, the spray erodes the neoprene-rubber face of the disk. The disk is rotated to a new position from time to time to prolong its life by spreading the wear across its surface.

This work was done by Michael A. Cawthon of **Lewis Research Center**. *No further documentation is available.*

Inquiries concerning rights for the commercial use of this invention should be addressed to the Patent Counsel, Lewis Research Center. Refer to LEW-14863/TN.

Lewis Research Center
Technology Utilization Officer: Daniel G. Soltis
Mail Stop 7-3
21000 Brookpark Road
Cleveland, OH 44135
(216) 433-5567
Patent Counsel: Gene E. Shook
Mail Code 301-6
21000 Brookpark Road
Cleveland, OH 44135
(216) 433-5753

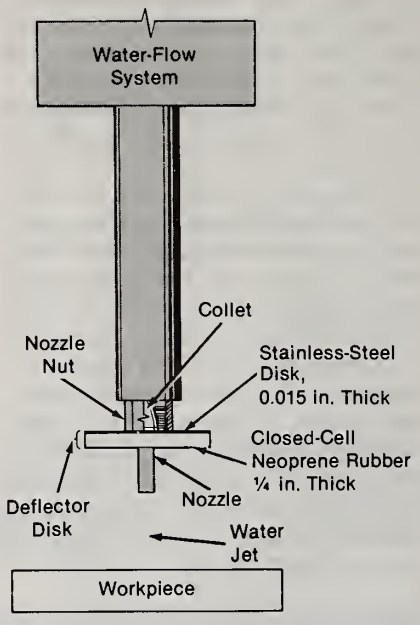

The **Deflector Disk** is a barrier between the erosive bounced jet and the nozzle nut.

FOR ADDITIONAL INFORMATION: *Contact: Director, Technology Transfer Division, P.O. Box 8757, BWI Airport, MD 21240; (301) 621-0100 Ext. 241*
REFER TO THE NUMBER LISTED AT THE END OF THIS ARTICLE

Materials

0182 Examination of the Shot Peening Process

0183 'Next-Generation' Scintillation Material Discovered

0184 Non-Chromate Surface Preparation of Aluminum

0185 Superplastic Forming of Al-Li Alloys

0186 Dynamic Delamination Buckling in Composite Laminates—A finite-element computer program performs a linear buckling analysis at each time step.

0187 Bonding Gauges to Carbon/Carbon Composites—Thermal-expansion properties are modified to prevent bonds from failing. (Licensing Opportunity)

0188 Making Polymeric Microspheres—A combination of advanced techniques yields uniform particles for biomedical applications. (Licensing Opportunity)

0189 Screen-Printed $YBa_2Cu_3O_{7-x}$ Films on Alumina—Superconducting films are made in a relatively simple process.

0190 Predicting the Propagation of Cracks—Safe operating lives of components of structures can be estimated.

Other Items of Interest

0134 Healing Voids in Interconnections in Integrated Circuits—A seemingly harsh treatment fills voids (cracks) in aluminum conductors. (Licensing Opportunity)

0156 Bearing-Bypass Loading on Bolted Composite Joints—An unexpected interaction between the effects of bypass and bearing loads is reported.

0195 Non-Toxic Acids are the Basis for a New Class of Cements

0205 Fluid Properties of Lennard-Jones Mixtures

0209 HRXRP-5 High-Resolution X-Ray Microprobe

U.S. Air Force Fact Sheet

Examination of the Shot Peening Process

The results of an extensive study of the shot peening process conducted by investigators at Advanced Material Process Corporation for the Air Force under the Small Business Innovative Research Program are described in a technical report issued recently.(1) The objective of these studies was to develop a data base from which a mathematical model could be developed relating fatigue life to shot peening variables.

Tension-tension fatigue specimens (R = 0.1) were prepared from eleven different titanium alloys, aluminum alloys, or steels and given various types of controlled shot peening treatments. Fatigue properties of these specimens were then determined and correlated with shot peening variables. Most of the materials behaved similarly in that shot peening first increased, then decreased fatigue life as peening intensity increased. An exception was unalloyed titanium which showed a progressive decrease in fatigue life with increased shot peening. The existence of an optimum intensity shot peening range for most of the materials was related to whether fatigue initiated at the surface or internally. At low intensities, fatigue tended to initiate at the surface. As shot peening intensity entered the optimum range, initiation occurred internally with significant increases in fatigue life. At still higher intensities, surface initiation was again observed, originating from surface defects designated as "peened surface extrusion folds" and fatigue life was reduced to values below that of unpeened material.

Several observations were made in this report that will be of interest to those involved with shot peening processes. For example, it was shown that shot peening intensity as defined by the standard Almen test has varying effects on the fatigue properties of peened specimens. This was attributed to the effect on peening saturation of the difference between the hardness of the Almen test specimen (e.g., a 1020 steel) and the hardness of the material being peened. The relationship between Almen saturation and material saturation as a function of material hardness is shown in Figure 1. It was also shown that there was little effect of the type of shot or the shot size on the fatigue properties of shot peened materials when peening was conducted within the optimum intensity range. Surface finish prior to shot peening had a significant effect on the optimum intensity range, the poorer the initial surface condition, the higher the optimum intensity range. Surface finish did not affect fatigue life however, assuming that the parts were peened within the optimum intensity range. Factors that tended to reduce fatigue life included fragmentation of shot and decreased impact angle.

Although the investigation has not yet resulted in the development of a model relating shot peening parameters to fatigue performance of peened parts, the authors include considerable discussion in this report of the significance of their findings and how the results may be used to achieve improved benefits from shot peening.

FOR ADDITIONAL INFORMATION: A copy of the report is available from NTIS, Springfield, VA 22161 (407)487-4600.

NTIS order number: AD-A204759NAC

Price code: A09

Lawrence Berkeley Laboratory

'Next-Generation' Scintillation Material Discovered

Researchers at the Lawrence Berkeley Laboratory are enlisting the aid of American industry in producing a radiation-detecting substance that could revolutionize a wide variety of scientific and medical instruments.

The LBL scientists have discovered that lead carbonate, a clear, crystalline material found in association with lead deposits all over the world, has scintillation properties that make it ideal for use in a large class of scientific detectors.

Scintillation materials are those that produce light when bombarded with ionizing radiation. The phenomenon is a rare one (fewer than 20 scientifically-useful scintillation materials have been discovered), since most materials simply dissipate ionizing energy in the form of heat.

Scintillation crystals are crucial components of life-saving medical imaging instruments like radioisotope cameras and positron emission tomography (PET) systems, and also of detectors for nuclear and high-energy physics.

The LBL team discovered that crystalline lead carbonate - compared to other scintillation materials in common use - has a superior combination of high stopping power (the ability to record energetic forms of radiation), fast time response, and short "dead time" (i.e., time between responses). It also does not absorb moisture from the air, which means that it need not be sealed in metal and glass, like many other commonly used scintillators. This combination of features could lead to major advances in PET and high-energy physics detectors, and could also make such instruments available at a reasonable price for the first time.

The catch is that the naturally occurring form of crystalline lead carbonate (known as cerussite) is usually found in small crystals only several millimeters in size, while scientific applications call for single crystals up to a centimeter or larger. Moreover, natural cerussite is usually full of impurities and imperfections that diminish its performance.

A far better approach, the researchers believe, would be to produce the crystal synthetically from its chemical components. However, no process yet exists for growing synthetic crystals of lead carbonate on a commercial scale. That's where American industry comes in, according to biophysicist Steve Derenzo of the LBL team.

The LBL effort involved a two-step approach, beginning with a broad survey of potential materials. Scintillation is a property of crystals, but under certain conditions likely scintillators can be spotted in the more readily available form of powder samples. The team obtained powder samples of more than 200 different substances and bombarded them with brief, intense bursts of x-rays in the National Synchrotron Light Source at Brookhaven National Laboratory, New York.

FOR ADDITIONAL INFORMATION: Public Information Department, Lawrence Berkeley Laboratory, Berkeley, CA 94720; Telephone (415) 486-5771.

U.S. Air Force Fact Sheet

Non-Chromate Surface Preparation of Aluminum

Many physical and chemical treatments have been used to prepare aluminum surfaces for improved adhesive bonding. The objectives of these treatments are (1) to remove contaminants such as dirt and grease, (2) to increase the macroscopic surface roughness through mechanical abrasion or to increase the microscopic surface roughness through chemical etching, and (3) to improve the resistance of the bonds formed on these surfaces to environmental degradation. The surface preparation procedure, originally developed by Forest Products Laboratories (FPL) and described in ASTM D2651, Method G, involves the etching of aluminum in an aqueous solution of sodium dichromate and sulfuric acid. The FPL procedure has been used for many years to prepare aluminum surfaces for adhesive bonding. The environmental durability of aluminum bonded joints has been improved by supplementing the FPL etch with an aqueous phosphoric acid anodizing (PAA) treatment (ASTM D3933). However, the chromate compounds in the FPL etch solution present disposal problems, which have lead to a desire for more environmentally acceptable alternative methods of surface preparation. Accordingly, a program to evaluate bonded aluminum specimens that were processed with several surface preparation methods which did not include chromate compounds was carried out by the University of Dayton Research Institute for the Air Force Wright Aeronautical Laboratories/Materials Laboratory.

The bonded specimens were evaluated using the Wedged Crack Extension Test (ASTM D3762), Floating Roller Peel Test (ASTM D3167), and the Double Lap Sheer Test (ASTM D3528). The Wedged Crack Extension Test was used as a screening test to determine whether a candidate surface treatment method looked promising or not. If the method looked promising, the test was repeated to ensure reproducibility and then the method was used to prepare bonded specimens for the peel and lap-sheer tests. If the method was not promising, it was dropped from the study.

Using the results of the peel and lap-sheer tests, four candidate treatment methods based on modified versions of the PAA procedure (ASTM D3933) were identified and found to be very promising replacement treatments for the chromate surface preparation of aluminum for adhesive bonding. The four modified PAA treatment methods are as follows:

1. Phosphoric acid used as deoxidizing solution, followed by PAA
2. Dilute sulfuric acid deoxidizing, followed by PAA
3. Scuffing the surface with Scotchbrite® pad, followed by methyl-ethyl ketone (MEK) solvent wipe and the PAA
4. Just the PAA treatment (no deoxidizing step).

From these results, it appears that phosphoric acid anodizing (PAA) is very tolerant and forgiving of preceding treatment steps. The PAA seems to produce a durable adhesive bond with a wide variety of deoxidizing techniques. The first three of these modified procedures listed above appeared equivalent to the standard FPL/PAA process for the treatment of aluminum surfaces for adhesive bonding. The three best involved the substitution of a phosphoric acid etch, a sulfuric acid etch, or a mechanical surface abrasion for the normal sulfuric acid/sodium dichromate deoxidation treatment of FPL. The fourth approach, simply omitted the deoxidation step completely. For detailed information and data on the FPL, PAA, and other surface treatment procedures for aluminum, together with detailed peel and lap-sheer test results, the reader is referred to the original report.

FOR ADDITIONAL INFORMATION: A copy of the report is available from NTIS, Springfield, VA 22161; (703)487-4600.

NTIS order number: AD-A200527

Price code: A03

U.S. Air Force Fact Sheet

Superplastic Forming of Al-Li Alloys

A study is under way at Rockwell International, with input from several subcontracts including Lockheed, Alcoa, Washington State University, and Edison Welding Institute, to fabricate and evaluate aluminum-lithium alloy aircraft structural components utilizing superplastic forming. The results obtained in the first year of this planned two year investigation are described in an interim report issued in October 1988.

The interim report describes studies directed toward the selection of an aircraft component suitable for use in the program. Components were examined to determine such factors as potential for weight or cost reduction, complexity and size of the component, and type of loading to which the component would be subjected.

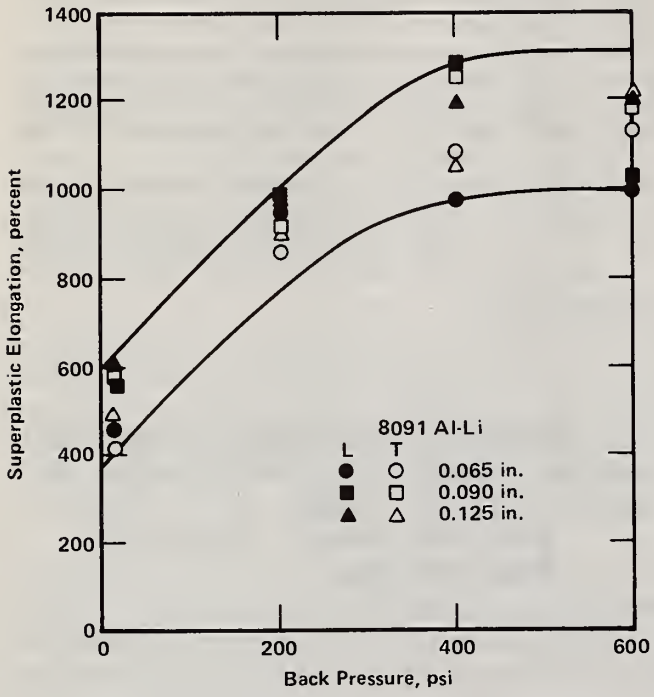

Figure 2. Superplastic Elongation in 8091 Al-Li Alloy as a Function of Back Pressure

A number of components are presently undergoing detailed design evaluation, but thus far a final selection has not been made.

Selection of an alloy for use in this study appears to be complete. One criterion used in selecting an appropriate aluminum-lithium alloy was that it had to be a production alloy, one that could be obtained in the near future in quantities of at least 500 pounds. Other factors considered included superplastic behavior and properties observed in the superplastically formed part after post-fabrication heat treatment. Alcan alloy 8091-SP was selected as the most promising for further study based on preliminary examination of a number of candidate materials. The results of detailed studies of superplastic behavior of that alloy are presented in the October 1988 report. Elongation achieved in the 8091 alloy as a function of back pressure in tests of sheet of three thicknesses is shown in Figure 2. These data were obtained using a forming temperature of 986 F and a two stage strain rate process, 2×10^{-3} per second to 0.72 strain followed by 2×10^{-4} per second. Back pressure was quite effective in reducing porosity resulting from cavitation. Several simple shapes have been formed from this alloy and evaluated to determine ability to control part thickness and cavitation. The response of the alloy to post-fabrication heat treatment has also been examined.

Future studies will consist of the design and fabrication of tooling to produce the component finally selected for detailed study followed by the fabrication of constituent parts, assembly of the component, and evaluation of the properties of the completed component. Based on the schedule presented in this report, this work should have been completed in mid-1989. Presumably, a report describing the results of this work will be issued later this year.

FOR ADDITIONAL INFORMATION: A copy of the report is available from NTIS, Springfield, VA 22161; (407)487-4600.

NTIS order number: AD-A200245NAC

Price code: A07

NASA Tech Brief
National Aeronautics and Space Administration
Lewis Research Center, Cleveland, Ohio

Dynamic Delamination Buckling in Composite Laminates

A finite-element computer program performs a linear buckling analysis at each time step.

Under impact loading, composite laminates are subject to dynamic local delamination and buckling, with consequent loss of both stiffness and strength. A procedure for the mathematical modeling of dynamic delamination buckling and propagation of delamination, with plate bending elements and multipoint constraints, has been developed and incorporated into a finite-element computer program. The program predicts

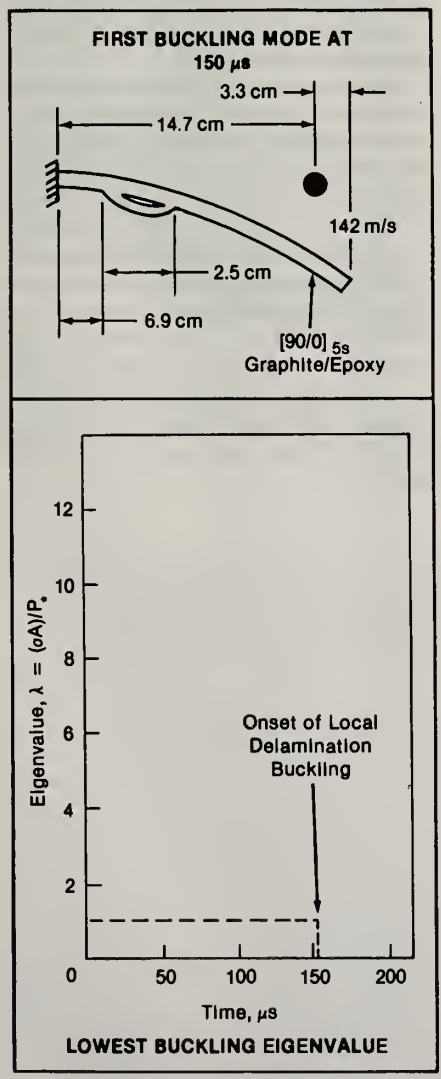

Figure 2. In a **Cantilevered Laminate Specimen** with an initial delamination, the lowest eigenvalue reached unity at 150 μs, indicating the onset of buckling.

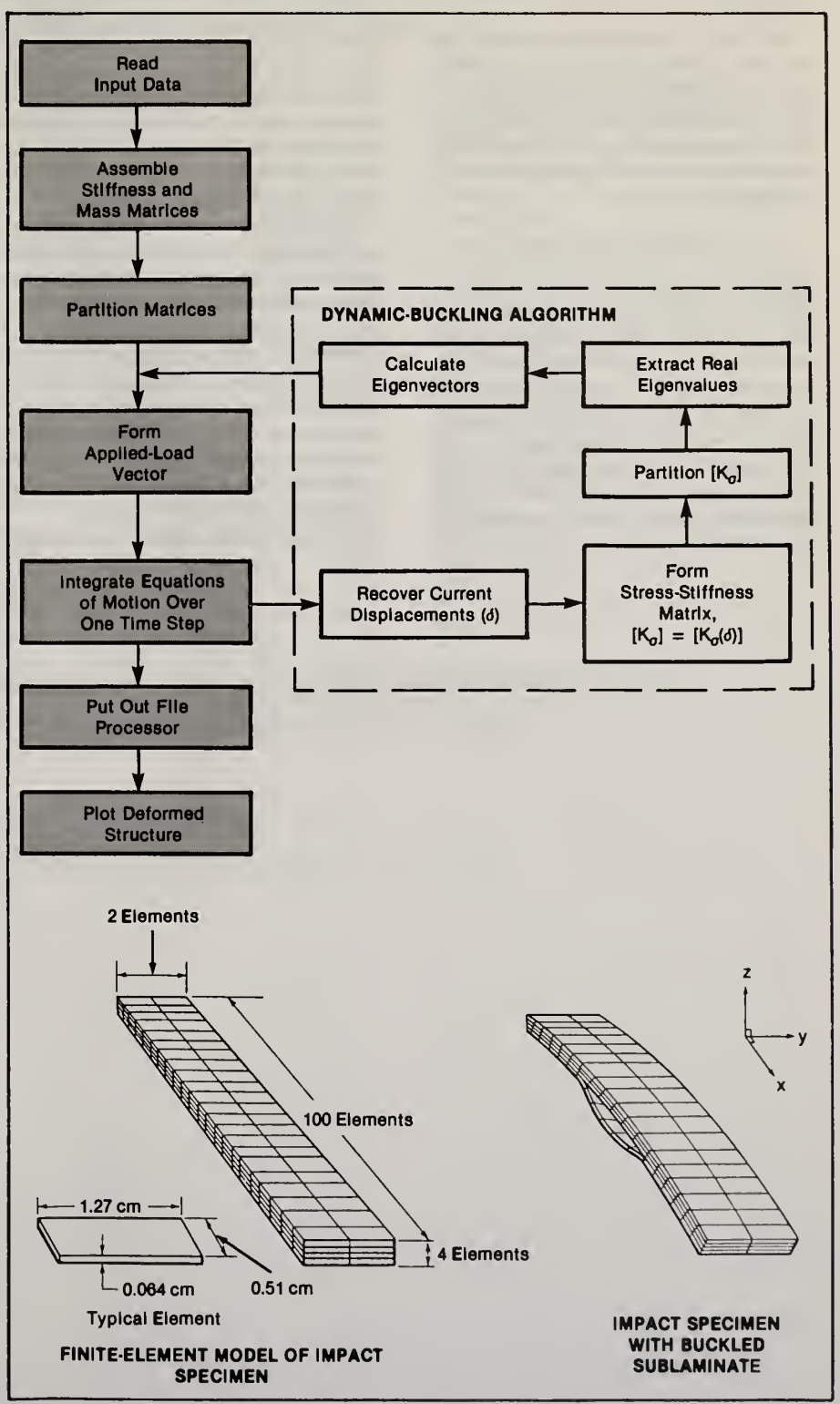

Figure 1. A **Dynamic-Buckling Algorithm** is added to a finite-element-analysis program to model dynamic local delamination and buckling in composite laminates subjected to impact loads.

the time at which delamination buckling occurs, the shape of the dynamic-buckling mode, and the strain-energy-release rate due to the extension of the delamination crack. The method could be extended to handle such other defects as transply and edge cracks.

The direct time-integration solution sequence in the finite-element program MSC/NASTRAN, Version 65A, is altered so that a linear buckling analysis is performed at each time step (see Figure 1). The buckling analysis requires the solution of the eigenvalue equation

$$[K] + \lambda[K_\sigma] \quad \{\phi\} = 0$$

where $[K]$ is the structural-stiffness matrix and $[K_\sigma]$ is the stress-stiffness matrix. Each scalar eigenvalue that satisfies this equation represents the dimensionless ratio $\lambda = (\sigma A)/P_*$, where σ is the time-dependent compressive longitudinal stress in the delaminated sublaminate, A is the cross-sectional area of the sublaminate, and P_* is the critical compressive load that will make the sublaminate buckle. When such an eigenvalue falls to unity, buckling occurs in the mode, the shape of which is described by the corresponding eigenvector $\{\phi\}$.

The propagation of the initial delamination is modeled by removing, at the appropriate nodal points, the constraints that prevent the elements of neighboring plies from penetrating or separating from each other. This procedure increases slightly the total number of degrees of freedom while keeping the number of elements and the element mesh in the finite-element analysis constant as the delamination crack extends, but it greatly simplifies the simulation of the extension of the crack.

Numerical simulations of transverse impact loading of a unidirectional-laminate beam rigidly supported at both ends show that delaminations near the outer surface are susceptible to dynamic buckling and buckling-induced propagation. In the absence of reflections of flexural waves from the ends and/or the supports, transverse impact at a point near a delamination causes the delamination to propagate toward the point of impact, with little or no extension in the opposite direction.

The validity of the method has been tested experimentally by using it to predict buckling in a cantilevered specimen for which experimental data were available (see Figure 2). The calculated onset of delamination at approximately 150 μs after the beginning of impact is in reasonable agreement with data from high-speed photography, which showed that the buckling of the delamination and the initial extension of the crack started between two frames taken 125 and 187.5 μs after the beginning of the impact.

This work was done by Joseph E. Grady, Christos C. Chamis, and Robert A. Aiello of **Lewis Research Center**. *Further information may be found in NASA TM-100192 [N87-28611], Price Code: A03 "Dynamic Delamination Buckling in Composite Laminates Under Impact Loading: Computational Simulation."*

Copies may be purchased from the National Technical Information Service, Springfield, Virginia 22161, Telephone No. (703) 487-4650. Rush orders may be placed for an extra fee by calling (800) 336-4700. The report is also available on microfiche at no charge. To obtain a microfiche copy, Cricle 102 on the TSP Request Card.
LEW-14745/TN

FOR ADDITIONAL INFORMATION: *Contact: Director, Technology Transfer Division, P.O. Box 8757, BWI Airport, MD 21240; (301) 621-0100 Ext. 241*
REFER TO THE NUMBER LISTED AT THE END OF THIS ARTICLE

NASA Tech Brief
National Aeronautics and Space Administration
Marshall Space Flight Center, Alabama

Licensing Opportunity

Bonding Gauges to Carbon/Carbon Composites

Thermal-expansion properties are modified to prevent bonds from failing.

A proposed transition layer would be deposited between a substrate and a strain or temperature gauge to be bonded to the substrate. The layer is intended particularly for gauges that must operate at temperatures above 600 °F (320 °C) and substrates like fiber-reinforced carbon/carbon composites, which are difficult to bond. The transition layer would reduce the stress caused by the difference between the thermal expansions of the gauge and substrate materials. Without the transition layer, the stress often weakens or breaks the bond.

The following process was proposed to deposit a transition layer on a carbon/carbon material that consists of graphitized rayon-fiber cloth in a glassy carbon matrix processed to 1,500 °C: The material is first cleaned in methanol and baked at 100 °C for 1 h to drive out hydrocarbons and unpyrolized phenolic resin. The surface on which the strain gauge is to be placed is cleaned by radio-frequency sputtering in argon. The sputtering removes a layer 50 Å thick and removes such contaminants as water vapor, oxide layers, and any residual hydrocarbons.

A film of 80 percent nickel, 20 percent chromium 1,000 Å thick is deposited on the surface by radio-frequency sputtering in argon. Then a beam of argon ions is directed onto the surface at a kinetic energy of 90 keV to mix the nickel/chromium film and drive it into the substrate. The dose is 10^{17} ions/(cm)^2.

The surface is once again sputter-cleaned to a depth of 50 Å, and a nickel/chromium layer 5 μm thick is sputtered onto the surface as a protective layer for subsequent steps. The surface is masked so that only the gauge area is exposed, and the area is plasma-arc-sprayed with 80 percent nickel and 20 percent chromium to a thickness of 0.003 in. (0.076 mm). Next, a transition layer of half nickel/chromium, half aluminum oxide is plasma-arc-sprayed onto the surface. Finally, an insulating layer of aluminum oxide is rod-flame-sprayed onto the transition surface. The next step would be the attachment of the gauge.

This work was done by M. M. Lemcoe, for **Marshall Space Flight Center**, *A. H. Deutchman of Beam Alloy Corp., R. G. Brasfield of Morton Thiokol Corp., and D. E. Crawmer of Bettelle Columbus Laboratories.*

Inquiries concerning rights for the commercial use of this invention should be addressed to the Patent Counsel, Marshall Space Flight Center. Refer to MFS-28315/TN.

George C. Marshall Space Flight Center
Technology Utilization Officer: Ismail Akbay
Code AT01
Marshall Space Flight Center,
AL 35812
(205) 544-2223
Patent Counsel:
Leon D. Wofford, Jr.
Mail Code CC01
Marshall Space Flight Center,
AL 35812
(205) 544-0024

FOR ADDITIONAL INFORMATION: *Contact: Director, Technology Transfer Division, P.O. Box 8757, BWI Airport, MD 21240; (301) 621-0100 Ext. 241*
REFER TO THE NUMBER LISTED AT THE END OF THIS ARTICLE

NASA Tech Brief
National Aeronautics and Space Administration

NASA's Jet Propulsion Laboratory, Pasadena, California

Licensing Opportunity

Making Polymeric Microspheres

A combination of advanced techniques yields uniform particles for biomedical applications.

A process combines ink-jet and irradiation/freeze-polymerization techniques to make polymeric microspheres of uniform size in diameters from 100 to 400 μm. The microspheres can be used in chromatography, cell sorting, cell labeling, and the manufacture of pharmaceutical materials.

The liquid droplets are formed by a liquid-injection technique similar to that used in ink-jet printers. Liquid monomer flows through a nozzle vibrated by a piezoelectric transducer. The vibrations break the stream into droplets. The nozzle size, the flow rate, and the vibration frequency determine the droplet size and the size distribution, which can be kept within a narrow range.

The drops of liquid monomer are sprayed directly onto the surface of liquid nitrogen. The droplets freeze into an amorphous glassy phase, maintaining their spherical shape as they do so.

The frozen monomer particles, suspended in liquid nitrogen, are exposed to gamma radiation from cobalt-60. No significant polymerization occurs at the low temperature, but the particles store the free radicals created by the ionizing radiation. While the particles thaw slowly, polymerization by the radicals proceeds, and the particles solidify as spheres. The polymer molecules are only lightly cross-linked; they can be further cross-linked by more gamma radiation, this time suspended in an aqueous solution at room temperature.

In a demonstration of the process, 2-hydroxyethylacrylate (HEMA) monomer was sprayed downward through an 80-μm-diameter orifice at a rate of 2.5 mL/min. A piezoelectric crystal vibrated the nozzle at 10 kHz. The resulting droplets had a diameter about twice that of the orifice. Their uniform size and formation rate was observed under stroboscopic light. The falling droplets passed through an electrode ring at 1.5 kV just below the nozzle. The ring charged the droplets so that they repelled each other as they fell instead of joining in larger globules.

The monomer HEMA droplets fell on the surface of liquid nitrogen in a bowl. The warm droplets boiled the liquid nitrogen as they impinged on it, creating a cushion of gas that supported the drops on the surface. Still charged, the floating droplets continued to repel each other and spread to the edge of the bowl where a corona discharge neutralized the droplet charge. The frozen droplets sank into the liquid-nitrogen pool.

The droplets were gently brushed into a smaller container of liquid nitrogen and exposed to gamma radiation at a rate of 0.1 Mrad/h for about 5 h. They were allowed to heat slowly at 0.2 °C/min to a temperature at which polymerization began. The resulting polyHEMA microspheres (see figure) had an average diameter of 180 μm. In some experiments, more than 95 percent of the monomer was converted to polymer.

Production rates of 10,000 spheres per second from a single nozzle are feasible. The process can be adapted to making hollow microspheres filled with gas or with biological and pharmaceutical materials.

This work was done by Won-Kyu Rhim, Michael T. Hyson, Sang-Kun Chung, Michael S. Colvin, and Manchium Chang of Caltech for **NASA's Jet Propulsion Laboratory.**

In accordance with Public Law 96-517, the contractor has elected to retain title to this invention. Inquiries concerning rights for its commercial use should be addressed to

Edward Ansell
Director of Patents and Licensing
Mail Stop 301-6
California Institute of Technology
1201 East California Boulevard
Pasadena, CA 91125

Refer to NPO-17023/TN.

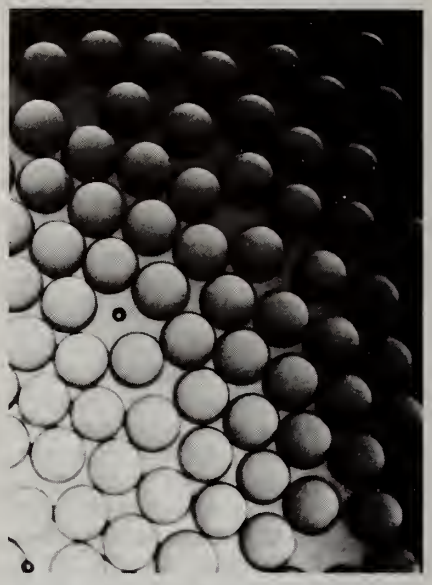

Microspheres of Polymeric Material have uniform size and shape after freezing, gamma irradiation, and slow thawing. The particles, shown here greatly magnified, are suspended in a solution of water and ethanol.

Jet Propulsion Lab.
NASA Resident Office
Technology Utilization Officer: Gordon S. Chapman
Mail Stop 180-801
4800 Oak Grove Drive
Pasadena, CA 91109
(818) 354-4849
Patent Counsel: Paul F. McCaul
Mail Code 180-801
4800 Oak Grove Drive
Pasadena, CA 91109
(818) 354-2734
Technology Utilization Mgr. for JPL: Norman L. Chalfin
Mail Stop 156-211
4800 Oak Grove Drive
Pasadena, CA 91109
(818) 354-2240

FOR ADDITIONAL INFORMATION: *Contact: Director, Technology Transfer Division, P.O. Box 8757, BWI Airport, MD 21240; (301) 621-0100 Ext. 241*
REFER TO THE NUMBER LISTED AT THE END OF THIS ARTICLE

NASA Tech Brief
National Aeronautics and Space Administration
Lewis Research Center, Cleveland, Ohio

Screen-Printed $YBa_2Cu_3O_{7-x}$ Films on Alumina

Superconducting films are made in a relatively simple process.

Thick films of $YBa_2Cu_3O_{7-x}$ superconductor have been deposited on highly-polished alumina substrates by screen printing. In addition to simplicity, the screen-printing technique offers the advantage that patterns for electronic and microwave circuits and devices can be printed directly, without additional etching steps.

The experiments on the screen-printing technique began with the preparation of the $YBa_2Cu_3O_{7-x}$ powder by solid-state reaction between Y_2O_3, $BaCO_3$ and CuO powders. The $YBa_2Cu_3O_{7-x}$ powder was then passed through a 500-mesh screen and mixed thoroughly with an organic vehicle to form a paste. The paste was then printed directly on the highly-pure alumina substrates through 325-mesh screens, some of which were stainless steel and some of which were silk.

The substrate-and-paste specimens were heated at 5 °C/min to various sintering temperatures from 900 to 1,000 °C, where they were held for various intervals from 5 min. to 4 h. The specimens were cooled at 3 °C/min to 450 °C, where they were annealed for 3 h. Finally, the specimens were cooled slowly to room temperature. The entire sintering-and-annealing process was carried out in flowing oxygen.

The thickness of the processed films ranged from ~30 to 50 μm. Those sintered at or above 980 °C were hard and adhered well to the substrates. The films were examined by x-ray diffraction to determine which solid-state phases were present. Microstructures were observed by optical and scanning electron microscopy. Electrical resistivities were measured in the standard four-probe configuration over a range of temperatures down to that of liquid helium (see figure).

The examinations and measurements showed that the properties of the films depend strongly on the sintering-and-annealing treatment. In terms of the adherence and superconducting-transition temperature of the films, the optimum annealing temperature and time were found to be 1,000 °C and 15 min, respectively. Films with higher superconducting-transition temperatures but poorer adhesion were formed at 945 °C. Thus, there appears to be a need to increase adhesion at lower sintering temperatures.

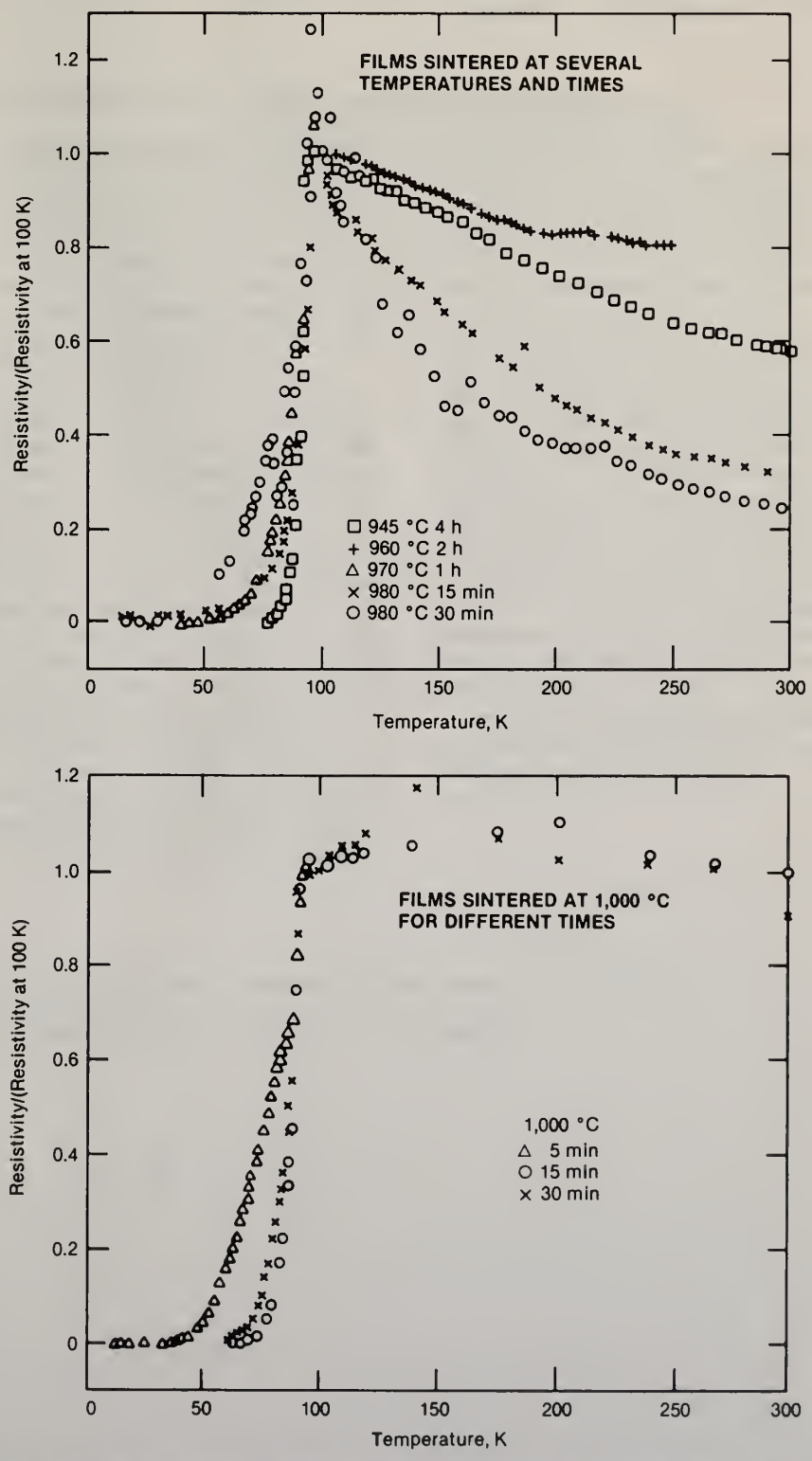
FILMS SINTERED AT SEVERAL TEMPERATURES AND TIMES
Resistivity/(Resistivity at 100 K)
Temperature, K
□ 945 °C 4 h
+ 960 °C 2 h
△ 970 °C 1 h
× 980 °C 15 min
○ 980 °C 30 min
FILMS SINTERED AT 1,000 °C FOR DIFFERENT TIMES
1,000 °C
△ 5 min
○ 15 min
× 30 min

Plots of Normalized Resistivity Versus Temperature show the effects of annealing temperatures and times.

This work was done by Narottam P. Bansal and Rainee N. Simons of **Lewis Research Center** *and D. E. Farrell of Case Western Reserve University. Further information may be found in NASA TM-100860 [N88-22805], Price Code: A03 "Synthesis and Characterization of High T_c Screen-Printed Y-Ba-Cu-O Films on Alumina."*

Copies may be purchased from the National Technical Information Service, Springfield, Virginia 22161, Telephone No. (703) 487-4650. Rush orders may be placed for an extra fee by calling (800) 336-4700.
LEW-14829/TN

FOR ADDITIONAL INFORMATION: *Contact: Director, Technology Transfer Division, P.O. Box 8757, BWI Airport, MD 21240; (301) 621-0100 Ext. 241*
REFER TO THE NUMBER LISTED AT THE END OF THIS ARTICLE

NASA Tech Brief
National Aeronautics and Space Administration

Predicting the Propagation of Cracks

Safe operating lives of components of structures can be estimated.

Flaws and cracks in a structure can grow under fatigue-inducing loads and, upon reaching a critical size, cause the structure to fail. The growth of these flaws and cracks may occur at load levels well below the ultimate load-bearing capabilities of the structure. The Advanced Crack Propagation Predictive Analysis Program, FLAGRO4, was developed as an aid in predicting the growth of preexisting flaws and cracks in structural components. FLAGRO4 provides the fracture-mechanics analyst with a computerized method of evaluation of the "safe crack-growth life" capabilities of structural components. FLAGRO4 could also be used to evaluate the tolerance-to-damage aspects of a given structural design.

The propagation of an existing crack is governed by the stress field in the vicinity of the tip of the crack. The stress-intensity factor is defined in terms of the relationship between the magnitude of the stress field and the size of the crack. The propagation of the crack becomes catastrophic when the local stress-intensity factor reaches the fracture toughness of the material.

FLAGRO4 predicts the growth of a crack by use of a two-dimensional model that independently predicts the growth of the flaw in two directions based on the calculation of stress-intensity factors. The analyst can specify that the rate of growth be controlled by Collipriest's equation, Forman's equation, Paries' equation, or tabulated data supplied by the user.

FLAGRO4 can model partly-through, through, and corner cracks located on panels, on edges of panels, at open holes, at holes or lugs loaded with pins, and on tub or bar surfaces. The mathematical modeling of the growth of a crack can be continued until propagation becomes catastrophic. FLAGRO4 can accommodate transitions from partly-through to through cracks, gradients of stress across the width and thickness, residual stresses at cold-worked holes, variations in the properties of materials due to changes in the environment, and Willenberg retardation.

The input to FLAGRO4 consists of the initial definition of a crack (which can be defined automatically), type of rate solution, type and geometry of flaw, properties of the material (if they are not in the built-in material table), data on the load spectrum, load-stress functions, and design-limit stress levels. The output from FLAGRO4 includes an echo of the input with any error or warning messages and a history of propagation of the crack.

FLAGRO4 is written in FORTRAN IV for batch execution and is available in CDC, IBM, and DEC machine versions. The CDC version has been implemented on a CDC 6000-series machine with a central-memory requirement of approximately 150K (octal) of 60-bit words. The IBM version has been implemented on an IBM 360-series machine with a central-memory requirement of approximately 260K (octal) of 8-bit bytes. The DEC version has been implemented on a DEC VAX 11/780 computer operating under VMS. The FLAGRO4 program was developed in 1979.

This program was written by Hu Tianlai of Rockvwell International Corp. for **Goddard Space Flight Center.**
GSC-13084/TN

FOR ADDITIONAL INFORMATION: *Contact: Director, Technology Transfer Division, P.O. Box 8757, BWI Airport, MD 21240; (301) 621-0100 Ext. 241*
REFER TO THE NUMBER LISTED AT THE END OF THIS ARTICLE

Medicine & Biology

0191 Animal Disease Diagnostic and Investigative Laboratory

0192 Animal Resources Diagnostic and Investigative Laboratory

0193 Dexter—A Finger-Spelling Hand

0194 Animal Resource Support for Biomedical Research

0195 Non-Toxic Acids are the Basis for a New Class of Cements

0196 Biomedical Telectrodes—Compact transmitters would eliminate the need for wires to monitors.

0197 Cleaning Animal's Cages with Little Water—Freezing and thawing may save energy and time.

Testing & Instrumentation

0198 Radiolabeling Technique for Early Cancer Detection (Licensing Opportunity)

Other Items of Interest

0120 New Material Will Help Gauge Cholesterol in Eggs

0131 Eye-Safe Lidar—Experimental solid-state systems may find use in meteorology.

NIH
Research & Technology
U.S. Department of Health and Human Services Public Health Service National Institutes of Health

Animal Disease Diagnostic and Investigative Laboratory

Principal Investigator:
Patrick J. Manning, D.V.M.
Research Animal Resources
Box 351, UMHC
420 Delaware Avenue, S.E.
University of Minnesota
Minneapolis, Minnesota 55455
(612) 376-5097

Resources Provided

- *Diagnostic Services:* This laboratory is staffed to provide general competence in gross and microscopic pathology, microbiology, parasitology, clinical chemistry, hematology, and selected serology. Diagnostic resources are designed primarily to serve the grantee and affiliated institutions. However, when approved by the principal investigator, they are available for collaboration in investigating laboratory animal disease problems.
- *Contact Person:* Patrick J. Manning, D.V.M., (612) 376-5097.

Research Emphasis or Application

- *Current Research:* Pathobiology of chronic bacterial infections. Pasteurellosis of rabbits with emphasis on the roles of bacterial cell wall lipopolysaccharides as diagnostic antigen and immunogen.

Animal Resources Diagnostic and Investigative Laboratory

Principal Investigator:
Steven P. Pakes, D.V.M., Ph.D.
Southwestern Medical Center at Dallas
University of Texas
5323 Harry Hines Boulevard
Dallas, Texas 75235
(214) 688-3340

Resources Provided

- *Diagnostic Services:* This laboratory is staffed to provide general competence in gross, microscopic, and ultrastructural pathology, microbiology, parasitology, clinical chemistry, and hematology. Diagnostic resources are designed primarily to serve the grantee and affiliated institutions. With approval by the principal investigator, however, they are available for collaboration in investigating laboratory animal disease problems.
- *Contact Person:* Steven P. Pakes, D.V.M., Ph.D., (214) 688-3340.

Research Emphasis or Application

- *Basic Objectives:* To maintain the quality of research animals through control and diagnosis of diseases within research animal facilities at the University of Texas. To recognize and define abnormal physiologic conditions and comparative diseases that may be of interest to biomedical researchers. To support teaching/training in laboratory animal medicine and pathology.
- *Current Research:* Pathogenesis, control, and prevention of murine mycoplasmosis; pathogenesis, control, and prevention of rabbit pasteurellosis; genetic susceptibility and resistance to infectious agents; genetic and environmental influences on hypertension and atherosclerosis.

Dexter—A Finger-Spelling Hand

Dexter is a mechanical hand that enables an individual who is deaf-blind to receive tactile messages during person-to-person communication—substituting for a human interpreter—and to gain access to computer-based information.

Dexter's finger movements correspond to the one-hand fingerspelling alphabet which is already in wide use by deaf people. During communication, the deaf-blind user touches the mechanical hand as it moves and translates the finger positions into the letters of the message. In this way, the problems with and dependence on human interpreters are eliminated.

Messages can originate from a variety of sources: an able-bodied person typing on a keyboard, a computer, a TDD (Telecommunications Device for the Deaf) user, or a modified closed-captioned device for the deaf. Thus, users of Dexter can receive information from people who aren't familiar with fingerspelling, from computer systems, from deaf telephone users, and from the television. The telephone application of Dexter might be supported by the telephone company in states that collect fees for the purchase of specialized telecommunications devices for disabled people.

DEXTER forming the letter "V".

For the 20,000 deaf-blind individuals in the United States, Dexter promises to open communication with people and with electronic systems currently inaccessible with traditional manual fingerspelling techniques.

A second generation Dexter prototype is now undergoing clinical evaluation. It was initially tested by a deaf-blind woman who is extremely proficient at receiving tactile fingerspelling. Her many suggestions have been incorporated into Dexter's design to improve the intelligibility of its letter shape configurations. Subsequently, the device was introduced to twelve deaf-blind people during their annual retreat. Their ability to initially understand Dexter's particular fingerspelling 'dialect' varied considerably, and long–term evaluations are now planned.

The device uses low-cost servo motors, available at hobby stores for radio-controlled (RC) models to flex its Delrin fingers. The motors rotate pulleys connected to wire cables

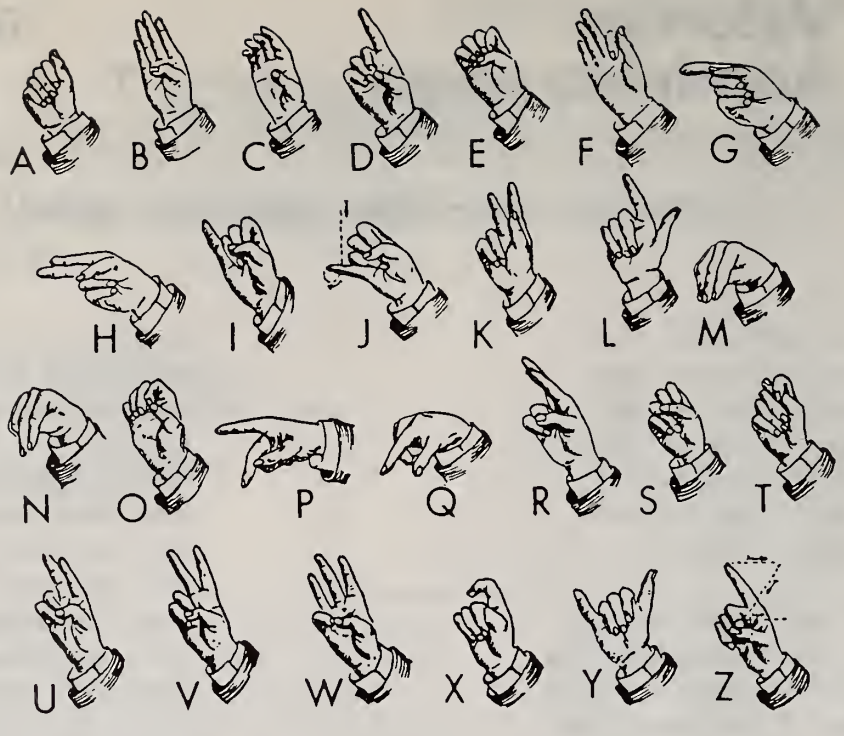

One Hand Manual Alphabet

which are the fingers' tendons. An inexpensive microprocessor system translates incoming messages into control signals that operate the motors in a coordinated fashion. It is anticipated that commercial versions of Dexter would be portable and could cost less than $500 if built in quantity.

Dexter is intended to serve deaf-blind users as a complete receptive communication system, useful beyond face-to-face situations. It can also be used with a TDD to provide deaf-blind people with telephone communication and be connected to computers to provide employment opportunities.

Mechanical drawings, software listings, and technical assistance are available for further development of Dexter. Please contact me at the Center if you have additional questions about this project or are interested in pursuing commercialization of Dexter.

FOR ADDITIONAL INFORMATION: Mail to: Al Sacks, Rehabilitation R&D Center, VA Medical Center/153, 3801 Miranda Avenue, Palo Alto, California 94304. Refer to I-I-No. 1.

NIH
Research & Technology
Federal Laboratory Resource
U.S. Department of Health and Human Services Public Health Service National Institutes of Health

Animal Resource Support for Biomedical Research

Principal Investigator:
John D. Strandberg, D.V.M., Ph.D.
Johns Hopkins University
720 Rutland Avenue
Baltimore, Maryland 21205
(301) 955-3273

Resources Provided

- *Diagnostic Services:* This laboratory is staffed to provide general competence in gross and microscopic pathology, microbiology, parasitology, clinical chemistry, and hematology in support of animal research and related clinical problems. Diagnostic resources are designed primarily to serve the grantee and affiliated institutions. However, with approval by the principal investigator, they are available for collaboration in investigating laboratory animal disease problems.
- *Contact Persons:* John D. Strandberg, D.V.M., Ph.D., or Robert J. Adams, D.V.M., (301) 955-3273.

Research Emphasis or Application

- *Basic Objectives:* To recognize, define, and investigate abnormal conditions and diseases of animals that may interfere with biomedical research; to identify and explore animal models of human disease; to facilitate development of improved humane techniques for animal-based research.
- *Current Research:* Biology, molecular biology, and pathogenesis of animal lentiviral infections including visna-maedi (sheep), caprine encephalitis-arthritis virus, and feline lentivirus as models of human AIDS; etiology and pathogenesis of enteric viral and bacterial infections of laboratory rodents; investigation of animal models of neurologic disease including hereditary spinal muscular atrophy and cerebellar ataxia; studies of aging changes in the central nervous system in nonhuman primates; Borna virus infection; fish as environmental monitors; hepatic toxicology and carcinogenesis in fish; evaluation of animal and in vitro models for carcinogenesis risk assessments; development of an SPF nonhuman primate colony; inherited deficiency of complement in dogs; canine, murine, and primate models of benign prostatic hyperplasia; use of animals in development of interventional radiologic techniques; animal models of radioimmunotherapy in oncology; pathologic changes associated with aging in hamsters; development of ingestible telemetric temperature probes; bone integration in surgical hip replacement procedures; development of insulin pump therapy for diabetes mellitus.

NIST Technology Update

National Institute of Standards & Technology
(Formerly the National Bureau of Standards)
U.S. Department of Commerce, Gaithersburg, MD 20899

Non-Toxic Acids are the Basis for a New Class of Cements

A new family of non-aqueous dental cements have been developed based on non-toxic dimer and trimer acids. They can be used in temporary filings, liners, and as a foundation for other restorative materials. The new patented formulations, developed by Dr. Joseph M. Antonucci in the NIST Dental and Medical Materials Research Group, use a dimer and/or a trimer acid derived from the partial polymerization of simple unsaturated fatty acids. These liquids can be mixed with a variety of basic powders used in restorative materials such as zinc oxide and calcium hydroxide. When mixed with powders, the bulky, flexible, hydrophobic nature of the dimer and trimer acids with their relatively low carboxylic acid content produce cements that are tough, low shrinking, water resistant, hydrolytically stable, and nonirritating. These new materials can be replacements for the eugenol cements that are mechanically and hydrolytically weak.

FOR ADDITIONAL INFORMATION: For information on the new non-aqueous dental cements, contact: Dr. Joseph M. Antonucci, NIST, A143 Polymers Bldg., Gaithersburg, MD. 20899; telephone: (301)975-6794.

NASA Tech Brief
National Aeronautics and Space Administration
Lyndon B. Johnson Space Center, Houston, Texas

Biomedical Telectrodes

Compact transmitters would eliminate the need for wires to monitors.

Biomedical telectrodes have been proposed for the transmission of physiological measurements to monitoring equipment. A biomedical telectrode would be a small electronic package containing a sensing device — for example, a pair of electrodes in contact with the body, a single electrode with terminals for wire connections to electrodes elsewhere on the body, or a thermometer. The package (see Figure 1) would also contain signal-conditioning circuitry to process the signals picked up by the sensing devices, a small radio transmitter, and a small battery. The design of the biomedical telectrode would take advantage of the recent advances in the fabrication of integrated circuits and the technologies of batteries and sensors.

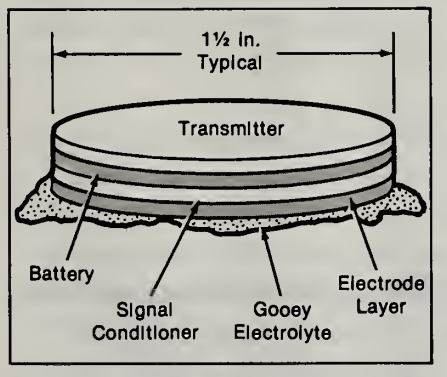

Figure 1. A **Biomedical Telectrode** would be a small electronic package that could be attached to the patient in a manner similar to that of a small adhesive bandage.

The principal advantages of biomedical telectrodes are that they would be relatively unobtrusive and that they would allow the patient (or animal subject under investigation) to move freely, without risk of entanglement in wires connected to monitoring equipment, and without fear of accidental disconnection of wires. These features would be especially beneficial to patients undergoing electrocardiographic monitoring in intensive-care units in hospitals; they would eliminate the accidental disconnections that occur when patients roll over wire electrode connections and pull them out while sleeping. They would also eliminate the nuisance of coping with wire connections while dressing and going to the toilet.

The design of the signal-conditioning integrated circuit in a biomedical telectrode would depend on the signal to be measured. The power supply would be designed so that the device would not be activated until attached to the patient and would be deactivated when detached. The telectrode would transmit at a fixed frequency. If a set of telectrodes were to be used on a patient, each would transmit at a different frequency. A label on the telectrode package would state the type of internal circuitry (or the type of signal to be sensed and transmitted) and the frequency of the transmitter.

This work was done by C.K. Shepherd of Lockheed Engineering and Sciences Co. for **Johnson Space Center.**
MSC-21501/TN

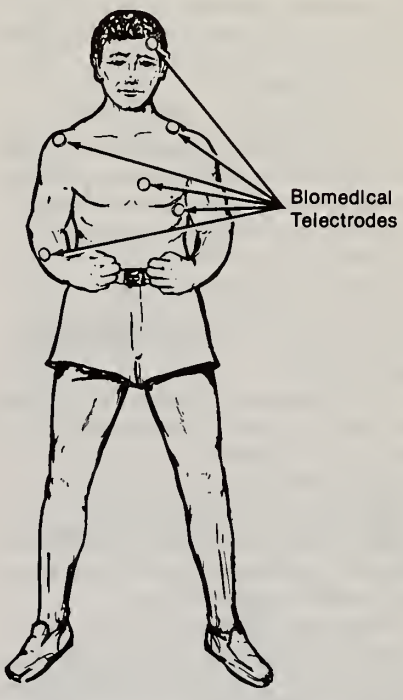

Figure 2. A **Patient Wearing Biomedical Telectrodes** could move freely, without risk of breaking or entangling wire connections.

FOR ADDITIONAL INFORMATION: *Contact: Director, Technology Transfer Division, P.O. Box 8757, BWI Airport, MD 21240; (301) 621-0100 Ext. 241*
REFER TO THE NUMBER LISTED AT THE END OF THIS ARTICLE

NASA Tech Brief
National Aeronautics and Space Administration
Marshall Space Flight Center, Alabama

Cleaning Animals' Cages With Little Water

Freezing and thawing may save energy and time.

A proposed freeze/thaw method for cleaning animals' cages would require little extra weight and consume little power and water. The cleaning concept was developed for maintaining experimental rat cages on extended space missions. It is adaptable as well to similar use on Earth. The proposed method would reduce cleaning time. It would make use of such already available facilities as refrigerator, glove box, and autoclave.

Each cage has a wire-mesh floor through which rat feces and urine pass into a litter pan. Some of the waste gradually accumulates on the wire-mesh floor and adheres to it. From time to time, it is necessary to replace the dirty floor with a clean one from storage. Because the feces adhere strongly to the dirty floor, the conventional practice has been to clean the dirty floor with a blast of steam.

In the new cleaning method, the attendant would first place the dirty floor in a bag, then in a freezer at a temperature of −80 °C. After waiting long enough for equilibration at the low temperature, the attendant would remove the bagged floor, place it in a glove box, and cut a hole in the bag to admit warm, humid air.

Water vapor would enter the microscopic pores of the feces, condensing in the pores and on the floor as liquid water and ice (see figure). The combination of the formation of ice crystals and hydrolysis by condensed water would weaken the adhesive bonds within the feces and between the feces and the floor. The attendant would then remove the loosened feces by blasting them with air while vibrating the floor or by applying an expanding foam.

It may be necessary to heat the floor (possibly in an autoclave) to remove solidified lipids. However, water would probably not be needed. A degreaser and/or disinfectant could be included in the foaming agent or added to the bag in the glove box.

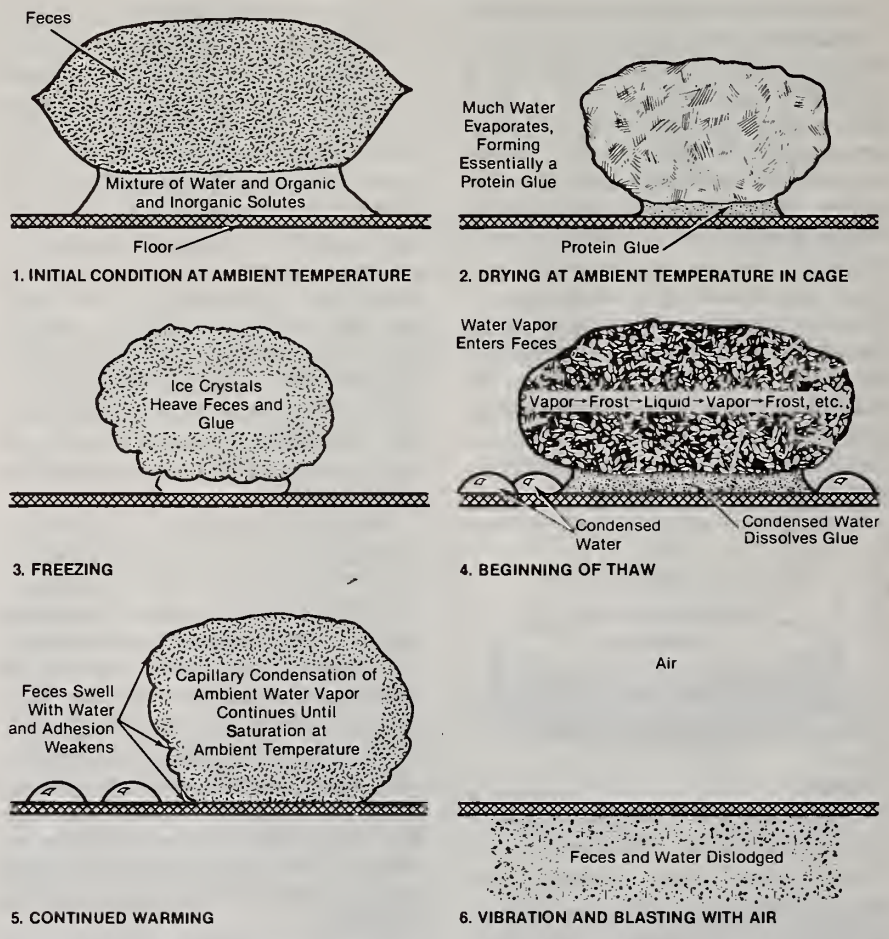
Feces
Mixture of Water and Organic and Inorganic Solutes
Floor
1. INITIAL CONDITION AT AMBIENT TEMPERATURE
Much Water Evaporates, Forming Essentially a Protein Glue
Protein Glue
2. DRYING AT AMBIENT TEMPERATURE IN CAGE
Ice Crystals Heave Feces and Glue
3. FREEZING
Water Vapor Enters Feces
Vapor→Frost→Liquid→Vapor→Frost, etc.
Condensed Water
Condensed Water Dissolves Glue
4. BEGINNING OF THAW
Feces Swell With Water and Adhesion Weakens
Capillary Condensation of Ambient Water Vapor Continues Until Saturation at Ambient Temperature
5. CONTINUED WARMING
Air
Feces and Water Dislodged
6. VIBRATION AND BLASTING WITH AIR

Rat Waste Adheres to the steel-wire-mesh floor of a cage. The feces are removed by the loosening action of a freezing-and-thawing process, followed by a blast of air.

This work was done by Benjamin J. Harman of The Boeing Co. for **Marshall Space Flight Center.**
MFS-28275/TN

FOR ADDITIONAL INFORMATION: *Contact: Director, Technology Transfer Division, P.O. Box 8757, BWI Airport, MD 21240; (301) 621-0100 Ext. 241*
REFER TO THE NUMBER LISTED AT THE END OF THIS ARTICLE

Department of Energy

Technology Application

Oak Ridge National Laboratories

Radiolabeling Technique for Early Cancer Detection

Researchers in the Nuclear Medicine Group of ORNL's Health and Safety Research Division have developed a new radiolabeling technique that may provide a safe and an effective method for the early diagnosis and treatment of cancer. This technique exploits the immune system's ability to produce antibodies that target specific proteins produced by cancer cells. It is an improvement over previous techniques for radiolabeling antibodies because the radiolabel (radioactive iodine) remains firmly bound to the antibody.

By chemically binding a radioactive isotope to these special antibodies, the ORNL team has produced new compounds that can carry radioactive isotopes through the bloodstream to a malignant tumor (Fig. 1). In this way, researchers can locate a tumor by using special imaging devices (radioimmunodetection) or, by using a different isotope, destroy cancerous cells (radioimmunotherapy). These compounds can locate a primary tumor early, before it has had time to spread the seeds of cancer throughout the rest of the body.

In the conventional procedure, radioactive iodine (^{123}I or ^{131}I) is attached to the amino acid tyrosine, which is a part of the antibody. However, using conventionally radioiodinated antibodies for cancer diagnosis or treatment has the drawback of in vivo deiodination (the release of iodine from the labeled antibodies injected into the body). Two problems are caused by in vivo deiodination: the therapeutic in vivo half-life for the radiolabeled antibody is reduced, and unwanted, potentially cancer-causing radioactive

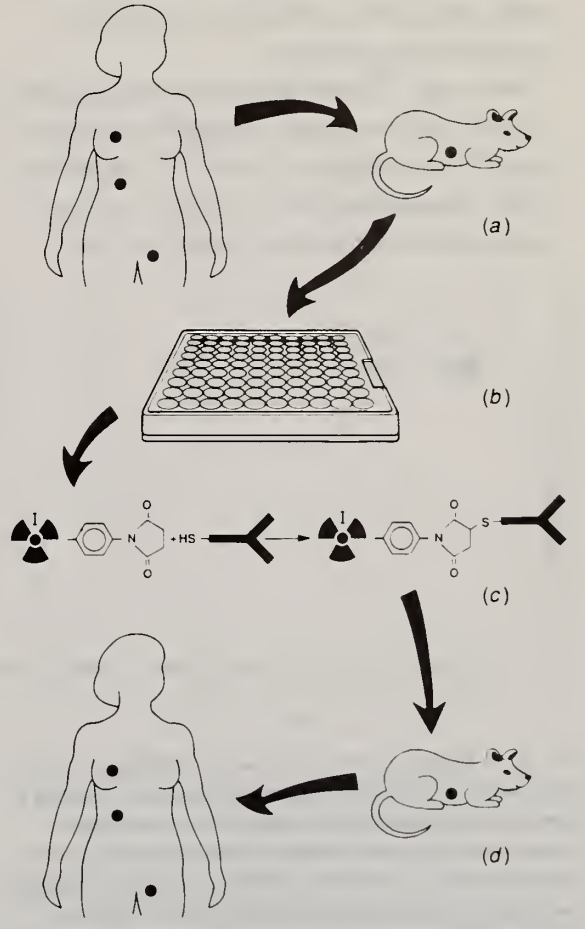

Fig. 1. Steps involved in the preparation of radiolabeled antibody for immunodetection and therapy of cancer. *(a)* Tumor cells from a cancer patient are injected into a mouse; the mouse produces antibodies specific to antigens produced by the cancer cells. *(b)* The antibody-producing cells are cloned and produce more antibodies. *(c)* Antibodies from the cloned cells can be labeled with radioactive iodine by means of the ORNL technique. *(d)* The labeled antibodies carry the isotope to the cancer site, initially in test animals and then, if successful, in human cancer patients.

iodine becomes trapped in the thyroid or stomach, resulting in an increased exposure to radiation.

The technique developed at ORNL minimizes deiodination. The researchers designed and synthesized a new radiolabeled maleimide agent (an organic compound containing nitrogen, hydrogen, and oxygen), which can be covalently attached to a benzene ring (phenyl) that includes a stably bound ^{125}I atom. The new imaging agent, called iodophenylmaleimide, can be prepared using an iodine-reactive mercury acetate maleimide kit developed at ORNL. This imaging agent has a strong affinity for the sulfhydryl (thiol) group that is naturally or artificially attached to an antibody.

Although ^{125}I was selected for experimental reasons, the new agent could also be labeled with ^{123}I for diagnosis or with ^{131}I for therapy. Other radioisotopes that could be used with modifications of functional groups on the maleimide agent are indium-111 (^{111}In), yttrium-90 (^{90}Y), and rhenium-188 (^{188}Re).

A preliminary study carried out at the University of Michigan, using nude mice implanted with melanoma and colon tumors, showed that the ORNL maleimide agent can label antibodies that seek out these types of cancer cells and that in vivo deiodination of the labeled antibody is insignificant (Fig. 2). Studies done with rats at ORNL compared the performance of the ^{125}I-maleimide-labeled antibody with the performance of conventionally prepared (^{131}I-tyrosine-linked) antibody and confirmed that using the ORNL agent results in less release and therefore less thyroid uptake of the radioactive iodine.

U.S. Patent Number 4,735,792, "Radioiodinated Maleimides and Use as Agents for Radiolabeling Antibodies," has been granted for this technology.

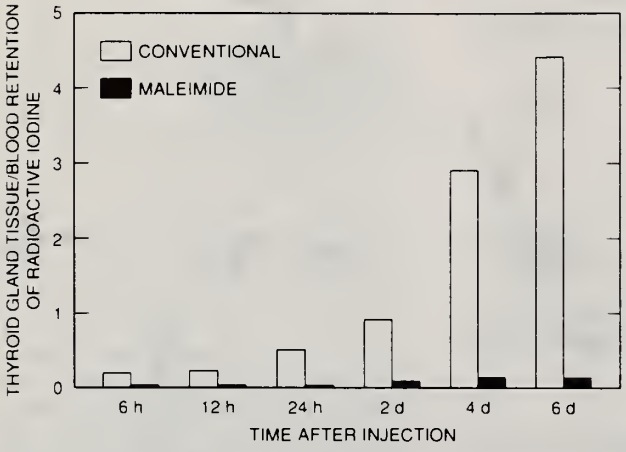

Fig. 2. In studies at the University of Michigan using nude mice, the maleimide-labeled antibody resulted in dramatically lower iodine uptake in thyroid gland tissue compared with iodine uptake from use of the same amount of antibody labeled by the conventional technique using tyrosine linkage. The low thyroid uptake indicates a relatively high in vivo stability of the ORNL-developed agent, iodophenylmaleimide.

P. C. Srivastava, "New Radiolabeling Technique May Aid Early Cancer Detection," *Oak Ridge National Laboratory Review* **21**(1), 34-5 (1988).

P. C. Srivastava, "Radioiodinated Maleimides and Use as Agents for Radiolabeling Antibodies," U.S. Patent 4,735,792 (1988).

P. C. Srivastava et al., "Evaluation of N-(p-[^{125}I]iodophenyl)maleimide for Labeling Monoclonal Antibodies," pp. 296-97 in *Seventh International Symposium on Radiopharmaceutical Chemistry Abstracts*, University of Groningen, the Netherlands, 1988.

Additional information:

Office of Technology Applications
Oak Ridge National Laboratory
P.O. Box 2008
Oak Ridge, TN 37831-6257
(815) 574-4192

Natural Resources Technology & Engineering

0199 Fractal Geometry Harnessed to Aid Mining Petroleum Work

0200 Very-Long-Baseline Interferometry Using Cheap Satellites—Celestial radiation below 25 MHz, heretofore inaccessible, could yield new insights.

Sandia National Laboratory

Fractal Geometry Harnessed to Aid Mining Petroleum Work

A newly emerging branch of mathematics - fractal geometry - may permit more accurate prediction of geological factors useful to mining, petroleum extraction, construction, and other industries, according to a Sandia National Laboratories scientist.

Such information might include predictions of the flow rates of fluids in the deeply buried, fractured rock of an oil and gas reservoir. Or it could include calculations of rock strength prior to construction work.

Sandia Geologist Stephen R. Brown says the application of fractal geometry to geology can be valuable: in relating laboratory-scale work to real-world studies; in improving predictions of mechanical rock properties; and in making more accurate calculations of fluid flow through natural fractures.

Fractal geometry expresses randomness and irregularity of form with nearly the same ease with which Euclidian geometry describes straight lines, rectangles, curves, and regular shapes. Thus, fractal geometry can be used to mathematically describe random objects. This might include the shape of the earth's surface, irregular coastlines, river tributaries, clouds, and other complex patterns, such as those now being investigated by Brown at Sandia.

Fractal geometry has revealed that small parts of many natural objects are often similar to the whole object when seen through changes of scale - as in the changing of magnification in a microscope. For this reason, a numeric description - called the fractal dimension - can be used to create an acceptable imitation of a surface mathematically.

This makes it possible, for example, to conduct mathematical experiments on important properties of fractures in rocks. Examples might be the compressibility of a fracture (referred to as normal stiffness) or the ability of fluid to flow through a fracture.

A member of Sandia's Geomechanics Division, Brown is continuing work on fractals he started several years ago with Professor Christopher Scholz and others at Columbia University.

At Columbia, Brown and Scholz built a device to measure fracture surfaces in the field and convert the roughness information into a graphic representation. After reviewing field and laboratory results at that time, the two concluded that "geometrical similarity" of fracture surfaces exists for a wide range of lengths. Since then, work by Brown and others in fractal geometry has confirmed this similarity on scales from 10 millionths of a meter to features the size of the San Andreas fault.

In two case studies to support his points, Brown described the effects that the roughness of a fracture surface and the fit, or match, of opposing fracture surfaces have on the solutions to certain geologic problems. In case, he studied these variables as they relate to the closure of the fracture under pressure. In another, he analyzed fluid flow through the fractures.

In the case of fluid flow, Brown compared calculations using fractals with more commonly used, highly idealized calculations, which assume the fracture walls are smooth, parallel surfaces. When the distance between the fracture surfaces was large, the calculated difference between the two methods was small. But as the surfaces are pressed together, calculations using fractals became significantly more accurate.

Browns' most recent work suggests that several properties of fractures (including compressibility and resistance to fluid flow) are independent of sample size - provided that the adjacent fracture surfaces are closely matched. In many cases this means that properties determined from laboratory specimens can be applied to the evaluation of large-scale problems in the field.

FOR ADDITIONAL INFORMATION: Public Information Division, Code 3161, Department of Energy, Sandia National Laboratories, Albuquerque, NM 87185-5800; (505)844-4207.

NASA Tech Brief
National Aeronautics and
Space Administration

Very-Long-Baseline Interferometry Using Cheap Satellites

Celestial radiation below 25 MHz, heretofore inaccessible, could yield new insights.

A report discusses the feasibility of an array of small satellites that would be deployed in a high orbit around the Earth to monitor celestial radio sources at frequencies less than 25 MHz. The objective is to make a high-angular-resolution map of such sources over the entire sky by use of very-long-baseline interferometry (VLBI).

At present, this part of the celestial radio spectrum is essentially unexplored because it is hidden from terrestrial antennas by the ionosphere most of the time and subject to interference by terrestrial sources.

The satellites would be built cheaply in "get-away-special" canisters ("GAS cans") similar to those developed for carrying small experiments aboard the Space Shuttle. (Alternative launching craft would have to be used, however, because the Space Shuttle cannot deploy such canisters in sufficiently high orbits.) Because the multiple-satellite array would be an aperture-synthesis array of many elements, it would have inherent protective redundancy. Thus, the success of the project would not be threatened by the failure of a few satellites. This feature would relax the requirements for long-term reliability, thereby helping to keep the cost low.

The main technical discussion is contained in nine chapters. Chapter I introduces the concept of the VLBI mission and describes the 2-day workshop-type conference at which the subjects of the other chapters were discussed. Chapter II describes the scientific motivation, including a list of questions regarding the radio spectrum that might be answered by data from the VLBI array.

Chapter III discusses technical requirements and problems involved in observation at various frequencies. Topics include the ionospheric critical frequency, interstellar and interplanetary scattering, radiation from auroras, the range of angular sizes of sources, and the large number of detectable sources. There is also a brief discussion of the cost.

Chapter IV describes the "GAS-can" concept and the standard configuration of an emerging series of small, inexpensive satellites designed to be launched in improved "GAS cans". Chapter V presents some of the engineering considerations. These include engineering tradeoffs that depend on the altitude of the orbit, the inclination of the orbit, alternative launching vehicles and organizations, the number of elements in the array, and keeping track of the changing relative positions of elements in the array.

Chapter VI describes some of the radio equipment likely to be carried aboard the satellite, including various kinds of antennas and receiving electronics. Chapter VII discusses the requirements for telemetry and ground support equipment. Chapter VIII outlines topics that would have to be studied further to arrive at a satisfactory design. Chapter IX presents some additional topics to be studied and some conclusions, the major one of which is that there appears to be no insurmountable obstacle to the deployment of the multiple-satellite VLBI array.

Following Chapter IX is a brief list of references. There are also three appendixes: one on vibrations and stability of a satellite, one on the application of magnetic torquers, and one on the separation of coorbiting satellites that is caused by differences in atmospheric drag.

This work was done by M.J. Mahoney, D.L. Jones, T.B.H. Kuiper, and R.A. Preston of Caltech for **NASA's Jet Propulsion Laboratory**. *"Low Frequency VLBI in Space Using 'GAS-Can' Satellites."*
NPO-17488/TN

FOR ADDITIONAL INFORMATION: *Contact: Director, Technology Transfer Division, P.O. Box 8757, BWI Airport, MD 21240; (301) 621-0100 Ext. 241*
REFER TO THE NUMBER LISTED AT THE END OF THIS ARTICLE

Physical Sciences

0201 Algorithm Estimates Microwave Water-Vapor Delay—Accuracy equals or exceeds that of conventional linear algorithms.

0202 Algorithm for Hypersonic Flow in Chemical Equilibrium—An improved shock-capturing scheme is mathematically stable. (Licensing Opportunity)

0203 Hollow-Cathode Source Generates Plasma—Exposure to air and moisture does not degrade performance

0204 Survey of Cooling Techniques—Methods of maintaining electronics at the best operating temperatures are reviewed.

Software

0205 Fluid Properties of Lennard-Jones Mixtures

0206 Gaussian-Beam Laser-Resonator Program—Radii of laser beams are calculated as functions of position.

Testing & Instrumentation

0207 Digital Count Rate Meter with Logarithmic Scale (Licensing Opportunity)

0208 Digital/Optical Conversion Module (Licensing Opportunity)

0209 HRXRP-5 High-Resolution X-Ray Microprobe

0210 Standard Method for Radiation Tests of Liquids—Three vials are used.

Other Items of Interest

0158 Mechanical Device Traces Parabolas—Continuous curves are generated and points located with ease.

0159 Ozone/Ultraviolet-Photo-Oxidation Reactor—Hydrazines are precessed more thoroughly into harmless substances.

NASA Tech Brief
National Aeronautics and Space Administration
NASA's Jet Propulsion Laboratory, Pasadena, California

Algorithm Estimates Microwave Water-Vapor Delay

Accuracy equals or exceeds that of conventional linear algorithms.

The "profile" algorithm is an improved algorithm that uses water-vapor-radiometer data to produce estimates of microwave delays caused by water vapor in the troposphere. Unlike conventional linear algorithms, it does not require site-specific and weather-dependent empirical parameters other than standard meteorological data, latitude, and altitude for use in conjunction with published standard atmospheric data.

A water-vapor radiometer measures the brightness temperature along a line of sight at frequencies close to the 22.2-GHz resonance of water. These temperatures depend on the distributions of kinetic temperature, pressure, water vapor, and liquid water along this line of sight. The microwave wet-path delay depends on the distributions of water vapor and kinetic temperature along the line of sight. The problem is to estimate the wet-path delay from the brightness temperatures without detailed knowledge of the actual line-of-sight distributions of relevant quantities.

The basic premise of the profile algorithm is that the wet-path delay is approximated closely by the solution to a simplified version of the nonlinear delay problem and can be generated numerically from each radiometer observation and simultaneous meteorological data. The algorithm first chooses various simple vertical distributions of water vapor and liquid and inserts them in a mathematical model of emission by the atmosphere at the radiometric wavelengths. When it finds a distribution for which the output of the model matches the radiometric observations, it uses this distribution in an integration along the desired line of sight to obtain the delay.

It is assumed that the vertical distribution of relative humidity can be represented adequately by the two-piece linear function shown in the figure. At the surface, the relative humidity is measured conventionally. The relative-humidity profile is then approximated by connecting the two endpoints by straight lines to the relative humidity at an altitude of 3 km. This relative humidity is adjusted by the algorithm and used to estimate the trial vapor distributions via standard-atmosphere temperature and pressure profiles calibrated to the temperature and pressure measured at the surface.

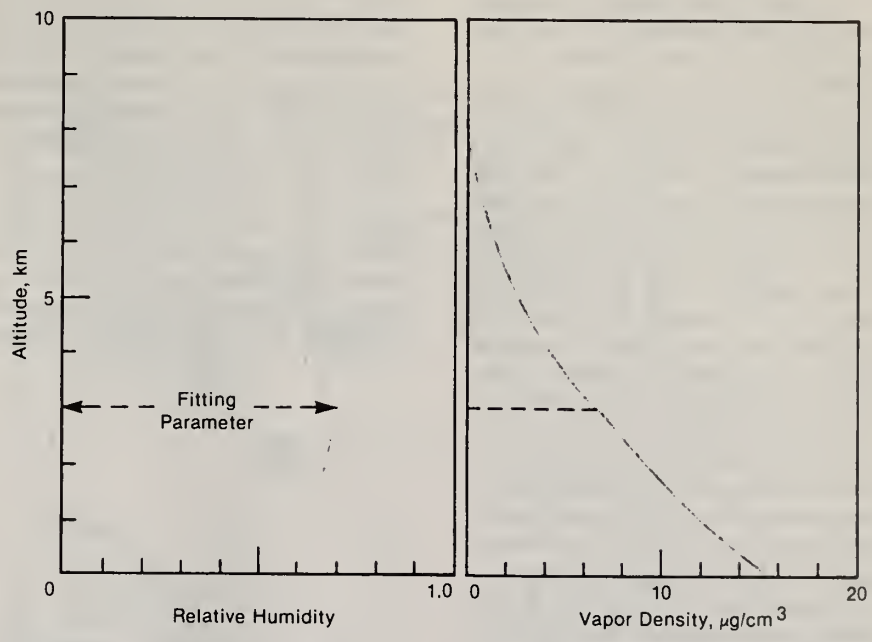

The **Vertical Distribution of Relative Humidity** is represented by a two-piece linear profile with one arbitrary fitting parameter. Once this parameter is chosen, the relative-humidity distribution is used in conjunction with standard temperature and pressure distributions to obtain the water-vapor-density distribution.

The emission model accounts for the continuum emission from droplets of water by assuming that the density of liquid water is proportional to the saturation water-vapor density as set by the temperature and pressure at each point. The algorithm tries different constants of proportionality until it obtains a fit.

The intrinsic accuracy of the profile algorithm, excluding uncertainties in radiometer data and the emission model, has been estimated with the help of archival radiosonde data. The annual root-mean-square errors for a wide range of sites average 1.8 mm in clear weather, 2.2 mm in cloudy weather, and 1.9 mm overall. In clear weather, the accuracy of the profile algorithm is comparable to the best that can be obtained from conventional linear algorithms; in cloudy weather, the profile algorithm offers a 35-percent improvement.

This work was done by Steven E. Robinson of Caltech for **NASA's Jet Propulsion Laboratory**.
NPO-17267/TN

FOR ADDITIONAL INFORMATION: *Contact: Director, Technology Transfer Division, P.O. Box 8757, BWI Airport, MD 21240; (301) 621-0100 Ext. 241*
REFER TO THE NUMBER LISTED AT THE END OF THIS ARTICLE

NASA Tech Brief
National Aeronautics and Space Administration
Ames Research Center, Moffett Field, California

Licensing Opportunity

Algorithm for Hypersonic Flow in Chemical Equilibrium

An improved shock-capturing scheme is mathematically stable.

An implicit, finite-difference, shock-capturing algorithm calculates inviscid, hypersonic flows in chemical equilibrium. The algorithm is an intermediate product of continuing efforts to understand flows of air and other gases about blunt bodies where ideal-gas conditions do not apply. The shock-capturing scheme was chosen over a shock-fitting scheme because shock-fitting schemes tend to be less flexible and computationally more expensive. Although it is more difficult to make into a computer program, the implicit formulation was chosen because it overcomes the limitation on mathematical stability encountered in explicit formulations.

For the dynamical portion of the problem, the Euler equations are written in conservation-law form in a Cartesian coordinate system (x, y) for two-dimensional or axisymmetric flow. These equations are reformulated in terms of a generalized, equispaced coordinate system (ξ, η) that can be related via a Jacobian transformation to a curvilinear coordinate system that conforms to the body in the flow field. An equation of state is derived to relate the total energy density to the pressure and the kinetic-energy density. The temperature, pressure, and density are related via the thermally perfect equation of state.

The part of the algorithm devoted to the foregoing equations is similar in its basic form to the approximate-factorization algorithm of Beam and Warming. The differences that correspond to the spatial derivatives are calculated via a flux-splitting technique, in which matrices and vectors that express the various coordinate transformations and flow variables are split into upstream- and downstream-propagating parts. These give rise to backward- and forward-difference approximations. The major advantage of this approach is that the resulting algorithm is naturally stable and can capture strong shocks without the help of artificial-dissipation terms to damp out spurious numerical oscillations.

For the chemical portion of the problem, the equilibrium state of the gas at each point in the computational grid is determined by minimizing the local Gibbs free energy, subject to the local conservation of molecules, atoms, ions, and total enthalpy.

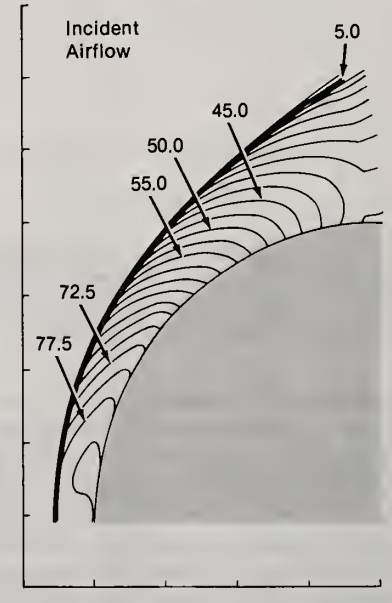

Normalized Temperatures as computed by the algorithm for the flow around a hemisphere are plotted on isothermal lines in half of a meridional plane.

The minimization is performed by the technique of Lagrange multipliers. The Newton-Raphson technique is used to find the updated values of these multipliers and of the temperature and the number densities of the species.

The algorithm was tested with a Mach-20 flow of air over a hemisphere at free-stream conditions of pressure corresponding to an altitude of 20 km and a temperature of 216.7 K (see figure). The calculated pressures, temperatures, and densities were generally within a few percent of previously published results.

This work was done by Grant Palmer of **Ames Reseach Center**. *Further information may be found in AIAA Paper No. 87-1580, "An Implicit Flux-Split Algorithm to Calculate Hypersonic Flowfields in Chemical Equilibrium."*

Copies may be purchased [prepayment required] from AIAA Technical Information Service Library, 555 West 57th Street, New York, New York 10019, Telephone No. (212) 247-6500.

Inquiries concerning rights for the commercial use of this invention should be addressed to the Patent Counsel, Ames Research Center. Refer to ARC-12140/TN.

Ames Research Ctr.
Technology Utilization Officer: Laurance Milov
Mail Code 223-3
Moffett Field, CA 94035
(415) 694-4044
Patent Counsel:
Darrell G. Brekke
Mail Code 200-11
Moffett Field, CA 94035
(415) 694-5104

FOR ADDITIONAL INFORMATION: *Contact: Director, Technology Transfer Division, P.O. Box 8757, BWI Airport, MD 21240; (301) 621-0100 Ext. 241*
REFER TO THE NUMBER LISTED AT THE END OF THIS ARTICLE

NASA Tech Brief
National Aeronautics and Space Administration
NASA's Jet Propulsion Laboratory, Pasadena, California

Hollow-Cathode Source Generates Plasma

Exposure to air and moisture does not degrade performance.

A device generates an argon, krypton, or xenon plasma via thermionic emission and electrical discharge within a hollow cathode and ejects the plasma into the surrounding vacuum. The device goes from a cold start up to full operation in less than 5 s after the initial application of power. It can be exposed to moist air between operations without significant degradation of its starting and running characteristics. Designed for the neutralization of static electrical charges on spacecraft, the device might be modified for use as a source of plasma in laboratory experiments or industrial processes.

The source includes an emitter tube within the hollow cathode barrel and a keeper electrode just outside the orifice at the end of the barrel (see figure). A flow of the working gas is established within the barrel, and a starting potential of 300 to 400 V is applied, causing the cathode barrel to act as an anode with respect to the emitter tube. Initially, the working gas breaks down electrically in a glow discharge to the end of the emitter tube. Bombardment by ions from the discharge heats the end of the tube to thermionic temperatures within the short starting time. (The much larger heat capacity of the cathode barrel prevents the barrel from heating significantly during the starting process.)

The emitter tube then begins to emit electrons, and the discharge changes from a glow to an arc. In this condition, the device is considered to be "on" and acts as a stable source of dense plasma. The arc discharge is sustained at the lower barrel/emitter potential of about 55 V. The discharge consumes about 350 W during start-up and about 100 W during steady operation.

Flows of plasma containing either predominantly electron or predominantly ion currents are extracted through the orifice in the cathode by applying positive or negative bias, respectively, to the keeper electrode. Electron currents from 20 mA to 6 A and ion currents up to 352 μA have been demonstrated. Ambipolar diffusion ensures that a plasma will be drawn from the cathode at keeper biases up to a few tens of volts.

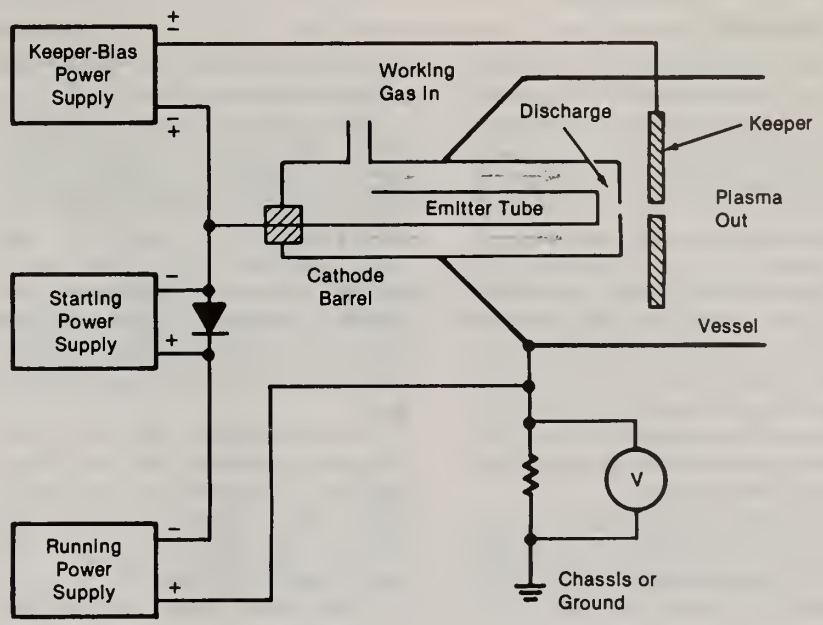

Plasma Is Generated by an electrical discharge in the cathode barrel that sustains and is aided by thermionic emission from the emitter tube. The emitter tube does not depend on rare-earth oxides, which would make it vulnerable to contamination by exposure to the atmosphere.

The tip of the emitter tube is optimized for the minimum heat capacity (for rapid startup and low consumption of power) consistent with adequate mechanical strength. The emitter tube is made of pure tantalum, which can be exposed to humid air, then placed in a vacuum again and restarted with no adverse effects. Because this tube is not impregnated (as many cathode tubes are) with rare-earth oxides to lower its electron work function, there is no need to take the customary precautions to prevent contamination of the oxides by exposure to the atmosphere.

The dimensions (e.g., orifice diameter 1.00 mm) and separation (1.83 mm) of the emitter tube and the cathode barrel are chosen so that the stagnation pressure of the working gas is in the proper range [about 2 torr (270 Pa)] for a minimum-potential glow discharge. The rate of flow of the gas is chosen to yield this pressure.

This work was done by W. D. Deininger, G. Aston, and L. C. Pless of Caltech for **NASA's Jet Propulsion Laboratory**. *NPO-16992/TN*

FOR ADDITIONAL INFORMATION: *Contact: Director, Technology Transfer Division, P.O. Box 8757, BWI Airport, MD 21240; (301) 621-0100 Ext. 241*
REFER TO THE NUMBER LISTED AT THE END OF THIS ARTICLE

NASA Tech Brief
National Aeronautics and
Space Administration

Survey of Cooling Techniques

Methods of maintaining electronics at the best operating temperatures are reviewed.

A paper surveys cooling techniques for electronic components and sensors that must be kept at temperatures ranging from thousandths of a kelvin to room temperature. The paper discusses the characteristics of the various coolers in terms of ground and space applications, cooling capacity, reliability, and temperature range. It discusses briefly the cooling of conventional electronic circuitry operating a few degrees above the environmental temperature by natural or forced convection of air or liquid. At greater length, it discusses the passive and active refrigeration of "cold" electronic circuitry operating below the environmental temperature.

The simplest and most reliable cooler is a passive radiator. Radiators are seldom used at temperatures below 100 K when the heat load is more than 100 mW because the radiative area required becomes too large.

Other passive coolers depend on such stored cryogens as helium or nitrogen in solid or liquid form. As in melting in an old-fashioned ice box, vaporization or sublimation of the cryogen removes heat. The useful life of a stored-cryogen cooler depends on how quickly the cryogen becomes exhausted, if it cannot be replenished. The paper includes a table of operating temperatures and boiloff rates of common cryogens.

The Joule-Thomson refrigerators are half passive and half active. They cool by expansion of high-pressure gases through nozzles. They can be made very small. However, they depend on constant supplies of gas at high pressures.

Active coolers (closed-cycle refrigerators) are machines that require work to transfer heat from devices to hotter reservoirs. In household refrigerators, the work is done by electric motors. Commercial thermoelectric coolers in cascade can attain temperatures of about 170 K. Cryocoolers, which are fairly well developed, can cool to about 4 K.

Cooling below 10 K is best performed by a closed-cycle Joule-Thomson refrigerator or a magnetic refrigerator, which involves changing the magnetic field in a salt. Below 1 K, either $^3He/^4He$ dilution refrigeration or adiabatic demagnetization can be used.

This work was done by Chung K. Chan of Caltech for **NASA's Jet Propulsion Laboratory**. *"Survey of Cooling Techniques for Electronic and Sensor Devices."*
NPO-17457/TN

FOR ADDITIONAL INFORMATION: *Contact: Director, Technology Transfer Division, P.O. Box 8757, BWI Airport, MD 21240; (301) 621-0100 Ext. 241*
REFER TO THE NUMBER LISTED AT THE END OF THIS ARTICLE

NIST Technology Update

National Institute of Standards & Technology
(Formerly the National Bureau of Standards)
U.S. Department of Commerce, Gaithersburg, MD 20899

Fluid Properties of Lennard-Jones Mixtures

The design of chemical process unit operations equipment requires detailed knowledge of the thermophysical properties of fluids and mixtures, often based on mathematical models of their properties and behavior. Many emerging technologies, such as enhanced oil recovery and biotechnology, typically involve materials and fluids not well represented in the current database or which are used in areas of fluid behavior difficult or impossible to study in the laboratory. Computerized models of these systems often benefit from comparison to a model of an idealized mixture. NIST has simulated an idealized mixture (one that obeys the Lennard-Jones intermolecular potential function and has a size ratio of 2:1) over a broad range of temperatures, composition, and energy ratios, and has published the data to be used as a point of comparison for similar real-fluid models.

FOR ADDITIONAL INFORMATION: A report of this work, *Properties of Lennard-Jones Mixtures at Various Temperatures and Energy Ratios with a Size Ratio of Two* (TN 1331), is available from NTIS, Springfield, VA 22161; (703)487-4600.

NTIS order number: PB89-235204NAC
Price code: A19

Gaussian-Beam Laser-Resonator Program

Radii of laser beams are calculated as functions of position.

In designing a laser cavity, the engineer is frequently concerned with more than the stability of the resonator. Other considerations include the sizes of the beam at various optical surfaces within the resonator and the performance of intraresonator line-narrowing or other optical elements. Laser resonators obey the laws of Gaussian beam propagation, not geometric optics. The Gaussian Beam Laser Resonator Program models laser resonators by use of Gaussian-beam-propagation techniques. It can be used to determine the radii of beams as functions of position in laser resonators.

The algorithm used in the Gaussian Beam Resonator Program has three major components. First, the ray-transfer matrix for the laser resonator must be calculated. Next, the initial parameters of the beam are calculated. These parameters are the stability of the beam, the radius and location of the waist of the beam in the input element of the resonator, and the curvature of the wavefront and radius of the beam at the input surface of the first element of the resonator. Finally the propagation of the beam through the optical elements is computed.

The optical elements that can be modeled are parallel plates, lenses, mirrors, dummy surfaces, and gradient-index (GRIN) lenses. A gradient-index lens is a good approximation of a laser rod operating under a thermal load. The optical system may contain up to 50 elements. In addition to the internal beam elements, the optical system may contain elements external to the resonator.

The Gaussian Beam Resonator program was written in Microsoft FORTRAN (Version 4.01). It was developed for the IBM PS/2 80-071 microcomputer and has been implemented on an IBM PC compatible under MS DOS 3.21. The program was developed in 1988 and requires approximately 95K bytes to operate.

This program was written by Patricia L. Cross, Clayton H. Bair, and Norman Barnes of **Langley Research Center.**
LAR-14080/TN

FOR ADDITIONAL INFORMATION

CONTACT:
COSMIC®
112 Barrow Hall
University of Georgia
Athens, GA 30602
(404) 542-3265

Department of Energy

Technology Application

Idaho National Engineering Laboratory

Digital Count Rate Meter with Logarithmic Scale

A digital logarithmic count rate meter is an instrument that is used to process nuclear pulses for the purpose of providing a display or record of the average number of detected events occurring per selected time interval. It provides a calculation of the Logarithm of the average count rate to obtain a high accuracy with a wide dynamic range (5 decades) for the displayed count rate value. The use of a microprocessor allows very low count rates (less than 1 per second) to be measured using a running average method thus avoiding the usual analog problems associated with long integration of averaging times. For critical response time alarm functions, a digital rate of change, independent of and usually shorter than the main averaging time, is easily implemented. A single chip microprocesser with integral memory and BASIC language is used to keep costs low. The device provides faster response time and wider dynamic range. It avoids the longer integration response time of analog counters. Applications include gamma, beta, alpha, count-rate meters used for monitoring and controlling radioactive and nuclear processes.

FOR ADDITIONAL INFORMATION: Contact Robert R. Campbell, Idaho National Engineering Laboratory, P.O. Box 4000, Idaho Falls, ID 83403 (208)526-0997. Refer to DOE/INEL-044TN.

Department of Energy

Technology Application

Idaho National Engineering Laboratory

Digital/Optical Conversion Module

The digital/optical conversion module allows an analog-parametric electrometer to interface through an optical link with a mass spectrometer computer-controlled data-acquisition system. The analog output signal of the mass spectrometer is converted to a digitized form which is compatible for computer analysis. The optical link reduces background electromagnetic interference and increases sensitivity and resolution of isotopic mass spectrometric analysis. The device has general application to mass spectrometers where high resolution and sensitivity is needed.

FOR ADDITIONAL INFORMATION: Contact Robert R. Campbell, Idaho National Engineering Laboratory, P.O. Box 4000 Idaho Falls, ID 83403 (208)526-0997. Refer to DOE/INEL-043TN.

Oak Ridge National Laboratories

HRXRP-5 High-Resolution X-Ray Microprobe

A new high-resolution X-ray microprobe, the HRXRP-5, has been developed at the Oak Ridge Y-12 Plant. The HRXRP-5 produces high-resolution color images of the distributions of chemical elements in metals, ceramics, and composites, as well as in biological and geological materials (Fig. 1). It uses a highly collimated, intense X-ray beam as a fluorescence probe. A typical analysis with HRXRP-5 is carried out in air with little or no sample preparation and is fast enough to maintain a high sample throughput.

During an analysis, a highly collimated X-ray beam impinges upon the sample surface, causing specific elemental fluorescence. The fluorescent X rays are captured with a solid-state detector and then separated by energy to identify each element present in the analysis volume. This analysis is repeated up to 40,000 times per sample by translating the sample in a grid pattern normal to the incident X-ray beam. Elemental spatial distributions are displayed on a graphics workstation as color, grey-scale, or color topographic images.

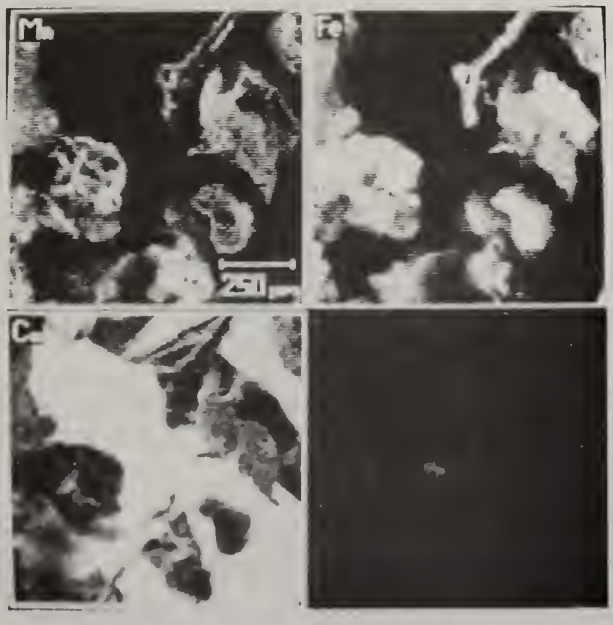

Fig. 1. Elemental distribution in a malachite ore. These grey scale images show separate element distributions in a higher-contrast format than the color composite (see cover). Comparisons between the two formats facilitate feature location and characterization.

The HRXRP-5 fills a technological gap between high-resolution electron-beam microprobes and low-resolution X-ray beam devices. With the X-ray microprobe, analyses are carried out in air, whereas electron-beam microprobes require a high vacuum. Unlike electron beams, which are limited to the near surface, X-ray beams can penetrate up to 40 μm beneath the surface, depending on the material analyzed. In addition, the low peak-to-background ratio inherent in X-ray beam instruments results in greater sensitivity than electron-beam instruments. Because electrical conductivity is not required, the specimens do not need to be coated with a thin film of conducting substance. Thus, nondestructive tests can be carried out on ceramics and biological materials in addition to metals and alloys.

The HRXRP-5 occupies a unique position in the field of X-ray beam-induced X-ray fluorescence instrumentation because of its high resolution and speed. The unique features of the HRXRP-5 are its high-brilliance, laboratory-based X-ray source combined with a tightly coupled collimation system consisting of extremely fine-bore glass capillary tubing. The source is a microfocus X-ray tube with a 10-μm focal spot operated at 22 W power.

The end of the capillary tube is placed only a few millimeters from the focal spot of the X-ray tube by means of a unique coupling system that

uses an O-ring fitting to maintain the vacuum inside the X-ray tube. X rays emanating from the focal spot are transmitted down the glass capillary tubing by total external reflection from the smooth capillary walls with an intensity loss proportional to length of the tubing rather than to the square of the distance, as in conventional X-ray collimation using metal pinholes. A spatial resolution of nearly 5 μm is obtained routinely with the HRXRP-5. Typical scans resulting in 5 μm spatial resolution require from a few minutes to about 1 h (compared to the many hours to several days required for other instruments using laboratory sources of X rays).

D. A. Carpenter et al., "A Scanning X-Ray Microprobe with Glass Capillary Collimation, pp. 391-93 in *Microbeam Analysis—88*, ed. D. E. Newbury, San Francisco Press, 1988.

Additional information:

Office of Technology Applications
Oak Ridge National Laboratory
P.O. Box 2008
Oak Ridge, TN 37831-6257
(815) 574-4192

NASA Tech Brief
National Aeronautics and Space Administration
NASA's Jet Propulsion Laboratory, Pasadena, California

Standard Method for Radiation Tests of Liquids

Three vials are used.

A simple procedure provides a standard method for radiation tests of liquids. It assures identical handling and dosage so that data from different test laboratories can be compared reliably. Developed for measuring properties of liquids for use in radiation-resistant liquid-dielectric capacitors, the procedure can be used for any of a variety of liquids proposed for use in the high-radiation environment — in x-ray and particle-accelerating machines and nuclear reactors, for example.

A pair of glass vials, joined by a frangible neck and equipped with valves, is used (see figure). A third vial is also used. It is filled with a control specimen and not irradiated. A technician first opens valve A, valve B, and the vacuum valve to pull contaminants from the vials. The vacuum valve and valve B are then closed and the filling valve opened to transfer the specimen liquid to vial A.

Next, the vacuum and filling valves are closed while valve A is left open and valve B is opened. The technician then irradiates the vials. The gas given off by the liquid in vial A as a result of chemical reactions stimulated by the radiation is collected in vial B. When irradiation is complete, the technician closes valves A and B, then breaks the joint to separate the vials.

The irradiated liquid in vial A is tested for such properties as viscosity, dielectric strength, and dielectric constant. The gas in vial B is analyzed in a mass spectrometer to identify its constituents.

This work was done by Frank L. Bouquet and Robert B. Somoano of Caltech for **NASA's Jet Propulsion Laboratory**.

NPO-16840/TN

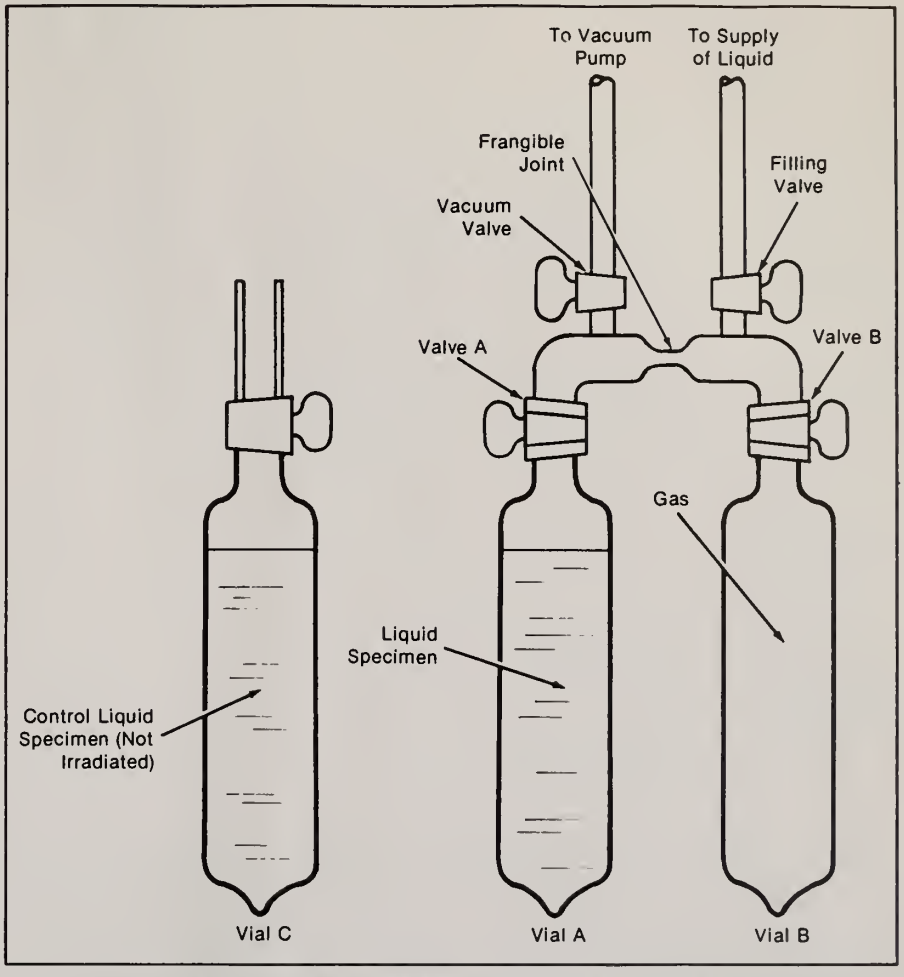

The **Twin-Vial Portion of the Testing Apparatus** provides for standardized handling and irradiation of the liquid specimen. Vials A and B are readily separated so that each can be subjected to different tests.

FOR ADDITIONAL INFORMATION: *Contact: Director, Technology Transfer Division, P.O. Box 8757, BWI Airport, MD 21240; (301) 621-0100 Ext. 241*

REFER TO THE NUMBER LISTED AT THE END OF THIS ARTICLE

Transportation & Components

0211 Digital Video Measurements of Wing Deflections in a Wind Tunnel—Solid-state cameras and a computer-controlled image-acquisition system measure deformations of wind-tunnel models.

NASA Tech Brief
National Aeronautics and Space Administration
Langley Research Center, Hampton, Virginia

Digital Video Measurements of Wing Deflections in a Wind Tunnel

Solid-state cameras and a computer-controlled image-acquisition system measure deformations of wind-tunnel models.

The dynamic pressure of the National Transonic Facility (NTF) is greater than three times that of other transonic wind tunnels and can cause wingtip deflections of several centimeters. A number of techniques have been suggested to measure these deflections. A photogrammetric approach was chosen because of its inherent rapid recording of data on the entire object field.

Video cameras were used instead of film cameras to acquire data because the cameras must be housed within the cryogenic, high-pressure plenum of the facility and are, therefore, inaccessible for the exchange of photographic film. The digital video model-deformation (VMD) system includes solid-state-array cameras and a digital image-acquisition system controlled by a personal computer. It is an improved version of an earlier VMD system that included high-resolution-tube cameras. The new system eliminates both the vibration-induced distortion associated with tube cameras and the manual processing of video hardcopy images necessary in the earlier version.

An AT-class personal computer controls two commercially available image-capture boards ganged to capture simultaneously two video images, each 752 picture elements wide and 480 picture elements high, in one-thirtieth of a second. The video images are digitized into 256 gray levels. The figure is a block diagram of the system.

The ability to interact conveniently with image files and processing algorithms is important in the developmental stage. The current system incorporates the flexibility of a popular operating system (DOS) and higher-level programming languages (e.g., C and BASIC) to facilitate the development of code. Commercially available software written in C enables a personal computer to digitize, process, display, and store video images. The video images, which are stored as DOS files, can be randomly read with code written by the user in either compiled BASIC or C for such operations as the computation of centroids. This technique, in addition to specifying the required algorithms, also details methods for calibrating both the solid-state sensors and the imaging lenses.

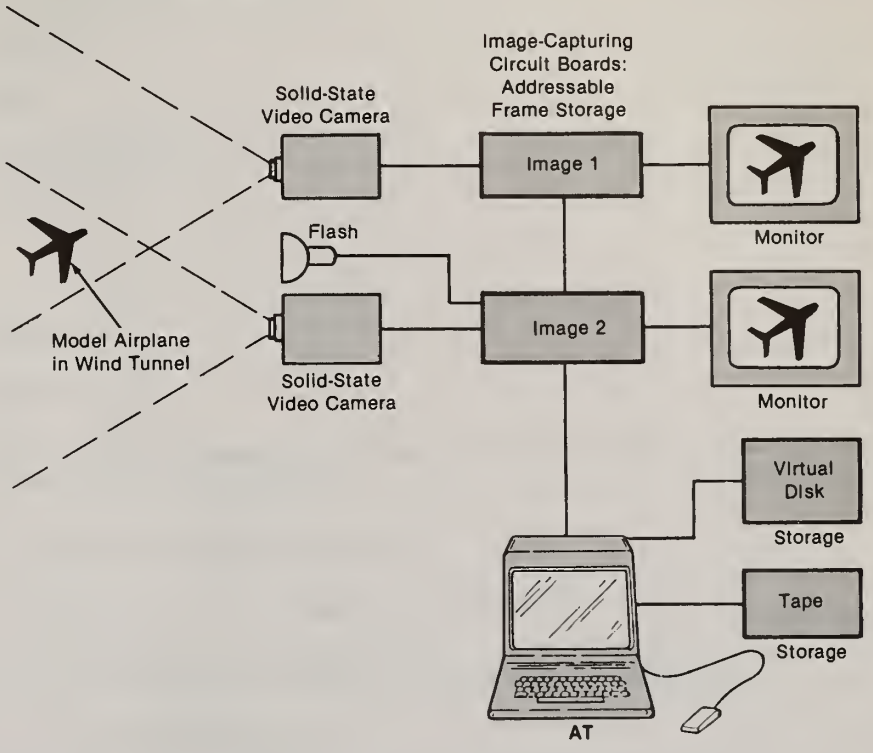

A **Computer Controls Two Image-Capturing Boards** used for triangulation measurements of deflection of the model.

Tests were conducted at the NTF to establish the best-case accuracy of the digital VMD system. These tests were conducted without flow to avoid operational constraints and uncertainties in the effects of flows as well as to enable independent verification of measurements. The accuracy of the system was shown to be about 5 mils (0.13 mm) root mean square under best-case conditions over a test wing that had a semispan of 26.5 in. (67.3 cm). The accuracy of the system for the measurement of controlled single-point deflections is less than 2 mils (0.05 mm). Although this particular application was restricted to remote measurements of wing deflections in a wind tunnel, the calibration and software procedures would be generally useful to anyone attempting highly accurate remote measurements by use of charge-coupled-devices or charge-injection-device solid-state cameras.

This work was done by Alpheus W. Burner, Walter L. Snow, William K. Goad, and Brooks A. Childers of **Langley Research Center.**
LAR-13917/TN

FOR ADDITIONAL INFORMATION: *Contact: Director, Technology Transfer Division, P O. Box 8757. BWI Airport, MD 21240; (301) 621-0100 Ext. 241*
REFER TO THE NUMBER LISTED AT THE END OF THIS ARTICLE

U.S. DEPARTMENT OF COMMERCE
National Technical Information Service
Springfield, VA 22161

NTIS ORDER FORM

Use this form ONLY to order reports designated as available from NTIS.

TELEPHONE ORDERS (703) 487-4650 FAX (703) 321-8547 TELEX 89-9405

For Subscription Questions
(703) 487-4630

For Tracing an Order
(703) 487-4660

For Editorial Questions
(703) 487-4805

Postage:
NTIS uses First Class Delivery, or equivalent service, on all shipping. For information about one day RUSH ordering, call (800) 336-4700 or (703) 487-4700.

NTIS PRICE SCHEDULE *

This schedule converts into actual prices the price codes cited in those Tech Notes having a report available from NTIS.

Price Code	*Price*
A01	$8.00
A02	11.00
A03	15.00
A04 through A05	17.00
A06 through A09	23.00
A10 through A13	31.00
A14 through A17	39.00
A18 through A21	45.00
A22 through A25	53.00
A99	Contact NTIS for price

These prices are for customers in United States, Canada, and Mexico. Other addresses should write for the price listing, number PR-360-4.

Prices effective January 1, 1990

† Purchase Order Service: There is a $7.50 charge for this service. It is restricted to customers in the United States, Canada, and Mexico. A late payment charge will be applied to all billings more than 30 days overdue.

If your address lable on this Tech Notes is NOT correct, call the NTIS Subscriptions Department on (703) 487-4630.

1 ADDRESS INFORMATION

Last Name .....

Title .....

Company/Organization .....

Address .....

.....

City/State/ZIP .....

Telephone Number .....

2 METHOD OF PAYMENT

☐ Charge my NTIS Deposit Account .... – .....

☐ Check/Money order enclosed payable to NTIS for $ .....

☐ Purchase order **ADD $7.50 per order** (see below for restrictions)†

Purchase order number .....

Charge my ☐ American Express ☐ VISA ☐ MasterCard

Account Number. ..... Exp. .....

Signature .....
(Required to validate order)

3 ORDER SELECTION (Use only for reports stated as available from NTIS)

NTIS Order Number	*Price**	*Quantity*	*Total Price*
..... /NAC	.....	.....	.....
..... /NAC	.....	.....	.....
..... /NAC	.....	.....	.....
..... /NAC	.....	.....	.....
..... /NAC	.....	.....	.....
		Handling fee	$3.00
		Total	.....

U.S. DEPARTMENT OF COMMERCE
National Technical Information Service
Springfield, VA 22161

NTIS ORDER FORM

Use this form ONLY to order reports designated as available from NTIS.

TELEPHONE ORDERS (703) 487-4650 FAX (703) 321-8547 TELEX 89-9405

For Subscription Questions
(703) 487-4630

For Tracing an Order
(703) 487-4660

For Editorial Questions
(703) 487-4805

Postage:
NTIS uses First Class Delivery, or equivalent service, on all shipping. For information about one day RUSH ordering, call (800) 336-4700 or (703) 487-4700.

NTIS PRICE SCHEDULE *

This schedule converts into actual prices the price codes cited in those Tech Notes having a report available from NTIS.

Price Code	*Price*
A01	$8.00
A02	11.00
A03	15.00
A04 through A05	17.00
A06 through A09	23.00
A10 through A13	31.00
A14 through A17	39.00
A18 through A21	45.00
A22 through A25	53.00
A99	Contact NTIS for price

These prices are for customers in United States, Canada, and Mexico. Other addresses should write for the price listing, number PR-360-4.

Prices effective January 1, 1990

Purchase Order Service: There is a $7.50 charge for this service. It is restricted to customers in the United States, Canada, and Mexico. A late payment charge will be applied to all billings more than 30 days overdue.

If your address lable on this Tech Notes is NOT correct, call the NTIS Subscriptions Department on (703) 487-4630.

1 ADDRESS INFORMATION

Last Name .....

Title .....

Company/Organization .....

Address .....

.....

City/State/ZIP .....

Telephone Number .....

2 METHOD OF PAYMENT

☐ Charge my NTIS Deposit Account .... – .....

☐ Check/Money order enclosed payable to NTIS for $ .....

☐ Purchase order **ADD $7.50 per order** (see below for restrictions)†

Purchase order number .....

Charge my ☐ American Express ☐ VISA ☐ MasterCard

Account Number. ..... Exp. .....

Signature .....
(Required to validate order)

3 ORDER SELECTION (Use only for reports stated as available from NTIS)

NTIS Order Number	*Price**	*Quantity*	*Total Price*
..... /NAC	.....	.....	.....
..... /NAC	.....	.....	.....
..... /NAC	.....	.....	.....
..... /NAC	.....	.....	.....
..... /NAC	.....	.....	.....
		Handling fee	$3.00
		Total	.....

U.S. DEPARTMENT OF COMMERCE
National Technical Information Service
Springfield, VA 22161

NTIS ORDER FORM

Use this form ONLY to order reports designated as available from NTIS.

TELEPHONE ORDERS (703) 487-4650 FAX (703) 321-8547 TELEX 89-9405

For Subscription Questions
(703) 487-4630

For Tracing an Order
(703) 487-4660

For Editorial Questions
(703) 487-4805

Postage:
NTIS uses First Class Delivery, or equivalent service, on all shipping. For information about one day RUSH ordering, call (800) 336-4700 or (703) 487-4700.

NTIS PRICE SCHEDULE *

This schedule converts into actual prices the price codes cited in those Tech Notes having a report available from NTIS.

Price Code	*Price*
A01	$8.00
A02	11.00
A03	15.00
A04 through A05	17.00
A06 through A09	23.00
A10 through A13	31.00
A14 through A17	39.00
A18 through A21	45.00
A22 through A25	53.00
A99	Contact NTIS for price

These prices are for customers in United States, Canada, and Mexico. Other addresses should write for the price listing, number PR-360-4.

Prices effective January 1, 1990

Purchase Order Service: There is a $7.50 charge for this service. It is restricted to customers in the United States, Canada, and Mexico. A late payment charge will be applied to all billings more than 30 days overdue.

If your address lable on this Tech Notes is NOT correct, call the NTIS Subscriptions Department on (703) 487-4630.

1 ADDRESS INFORMATION

Last Name .....

Title .....

Company/Organization .....

Address .....

.....

City/State/ZIP .....

Telephone Number .....

2 METHOD OF PAYMENT

☐ Charge my NTIS Deposit Account .... – .....

☐ Check/Money order enclosed payable to NTIS for $ .....

☐ Purchase order **ADD $7.50 per order** (see below for restrictions)†

Purchase order number .....

Charge my ☐ American Express ☐ VISA ☐ MasterCard

Account Number. ..... Exp. .....

Signature .....
(Required to validate order)

3 ORDER SELECTION (Use only for reports stated as available from NTIS)

NTIS Order Number	*Price**	*Quantity*	*Total Price*
...../NAC	.....	.....	.....
...../NAC	.....	.....	.....
...../NAC	.....	.....	.....
...../NAC	.....	.....	.....
...../NAC	.....	.....	.....
	Handling fee		$3.00
	Total		.....

- Agriculture & Food
- Computers
- Electrotechnology
- Energy
- Engineering
- Environmental Science & Technology
- Manufacturing, Machinery, & Tools
- Materials
- Medicine & Biology
- Natural Resources Technology & Engineering
- Physical Sciences
- Transportation & Components

Route To:

PENN STATE UNIVERSITY LIBRARIES
A0000720101 74

EPARTMENT OF COMMERCE
al Technical Information Service
ld, Va. 22161
L BUSINESS
or Private Use, $300

AN EQUAL OPPORTUNITY EMPLOYER

BULK RATE
POSTAGE & FEES PAID
NTIS
Permit No. G-292